ISSN number 0971 - 9709

# The Journal of Indian Geophysical Union

AN OPEN ACCESS BIMONTHLY JOURNAL OF IGU

Volume 20, Issue 3 | May 2016

## EDITORIAL OFFICE


Indian Geophysical Union, NGRI Campus, Uppal Road, Hyderabad- 500 007
Telephone: +91 -40-27012799; 23434631; Telefax:+91-04-27171564
E. mail: jigu1963@gmail.com, website: www.j-igu.in


The Open Access Journal with six issues in a year publishes articles covering
Solid Earth Geosciences; Marine Geosciences; and Atmospheric, Space and Planetary Sciences.

## Annual Subscription

Individual Rs. 1000 per issue and Institutional Rs. 3500 for four issues (from 2017 onwards, six issues Rs.5000/-)

Payments should be sent by DD drawn in favour of "The Treasurer, Indian Geophysical Union", payable at Hyderabad, Money Transfer/NEFT/RTGS (Inter-Bank Transfer), Treasurer, Indian Geophysical Union, State Bank of Hyderabad, Habsiguda Branch, Habsiguda, Uppal Road, Hyderabad- 500 007
A/C: 52191021424, IFSC Code: SBHY0020087, MICR Code: 500004020, SWIFT Code: SBHYINBB028.

For correspondence, please contact, Hon. Secretary, Indian Geophysical Union, NGRI Campus, Uppal Road, Hyderabad - 500 007, India; Email: igu123@gmail.com; Ph: 040 27012799

# CONTENTS

# Editorial - May 2016

After bringing out March/April issue some significant developments changed the structure of JIGU. As planned the outgoing editorial team succeeded in bringing out two special volumes; both of them have been released during GBM of IGU held on 15$^{th}$ March. As promised we succeeded in making the journal a cited journal under a new category introduced by Thomson Reuters (TR). The *Emerging Sources Citation Index* (ESCI) accreditation from 2016, is a major positive step to enhance visibility of JIGU (*http://wokinfo.com/products_tools/multidisciplinary/esci/*). This development should encourage researchers to contribute quality articles, as their studies would be available for international scientific community through TR website. The journal has dedicated website, **www.j-igu.in**, where contributors and readers can down load details pertaining to publication norms, contents of old and present articles and titles of forthcoming. To facilitate faster publication of peer reviewed and selected articles, journal has been converted as bimonthly in place of quarterly. Because of this change, for the first time this May issue has come out.

As I agreed to serve as Chief Editor for a further period of two years stating from 1$^{st}$ April it is my bounden duty to thank each and every member of outgoing team for their help and support in strengthening JIGU. I seek their continued support to JIGU. The incoming editorial board has a bigger task on their hands. Every member of the incoming board is requested to take interest in reviewing articles, motivating their colleagues and wards to contribute articles to the journal. It is essential for us to fight our natural resistance to change. We need to figure out what needs to be done. We need to find out what no longer needs to be done, and then take steps to stop doing it. As doing more with less drained my energies completely during earlier term of two years, I urge my colleagues to do more by doing differently. Such a change needs setting aside ego hassles and extending support to one another believing others are as good as you. In nut shell work smarter, perpetually adjust, refine, innovate and adapt.

JIGU is every one`s property and it can safely grow and blossom only when scientific community extends support. IGU award winners have moral obligation to strengthen JIGU. In spite of repeated requests only 10% of award winners have contributed articles. It is for those who have shut their ears and eyes to our pleadings to change their attitude and perception. Whatsoever a great man does, the same is done by others as well. Whatever standard he sets, the world follows. Since the award winners are identified as great they are requested not to set wrong standards to be copied by others, quoting precedence. Let my genuine appeals be not construed as irresponsible.

**Request to authors:**

One of the conclusions I've reached as I've grown older and, I hope, wiser is that...less is usually more. In other words, when given the opportunity to simplify your life...take it. I compare it to pruning a tree. By removing the excess branches, the tree has more energy to bear beautiful blossoms and healthy fruit. Such an approach has become essential in structuring individual issues of JIGU. Compared to March-April issue we have half the number of articles in May issue. Such a reduction is also essential in size of the articles. Many times authors prefer to have number of tables, figures and in addition to narration of details given both in the tables and figures, increasing number of pages. A good article with focus on main theme and derived results in about 8 to 10 pages can serve better compared to a longer version. Contributors are requested to focus on methodology and results.

**Poster presentations during IGU annual conventions and the necessity to introduce Virtual Poster Showcases (VPS)**

We have long been advocating that IGU caters to the needs of students and research scholars. Unfortunately, due to various limitations poster presentations by students are crammed in to a two hour session. These sessions neither satiate the thirst of inquisitive student/young researcher nor allows senior scientists to interact properly with the students. In place of this unhealthy compressed poster presentation, a new program of online student poster sessions-- The Virtual Poster Showcase (VPS) (started by American Geophysical Union-AGU) can enhance students' confidence and career skills.

Students generally need to attend an in-person conference to present a poster, but only a tiny percentage of them do. The American Geosciences Institute (AGI) estimates that there are 38,000 undergraduate geoscience students in 2-year and 4-year programs in the United States and 65,000 to 100,000 undergraduates in non-U.S. programs (according to the AGI's "Status of Geoscience Workforce 2014" report). Yet a look at the annual conference programs of the leading geoscience societies (including IGU) shows that with a few exceptions, the number of posters presented by undergraduate students is less than 100, which leaves a significant gap.

VPS can facilitate the building of skills to develop and present a poster and to review science. AGU leads a group of societies committed to growing and developing the global talent pool. AGU believes that every undergraduate student doing research, whether field/lab based or literature based, should have the opportunity to present a poster. The Virtual Poster Showcase (VPS) achieves that goal by offering a platform that allows any faculty to couple research with a poster presentation opportunity.

A Virtual Poster Showcase takes place in phases. Students first register in the online platform and submit an abstract in one of five divisions: Earth sciences, ocean sciences, atmospheric sciences, planetary sciences, and environmental sciences. Graduate students submit abstracts by division and also choose a discipline. VPS does not require membership in a professional society. Showcase abstracts, starting with those from 2016, will become part of a database, which will allow each student to have a citable abstract from the poster presentation. As soon as a student receives a notification that his or her abstract has been accepted, the student can submit the poster about the research as well as a link to a video explaining the work. Students can access online guidelines for writing an abstract, creating a poster (including maximum dimensions), and making a video by visiting IGU website.

After the phase of uploading posters and videos ends, students need to be encouraged to participate in the peer evaluation phase, during which they view and judge couple of other students' posters. Students use the platform to pose questions and receive feedback, as well as to score the posters using a rubric (A rubric is an easily applicable form of authentic assessment).

All students who participate in a showcase become eligible to receive a certificate of participation after they complete the peer evaluation phase of the event. Students who presented highly ranked posters receive other recognition as well.

Since IGU entered in to an MOU with AGU for effective co-operation in propagating earth system sciences and as JIGU editorial advisory committee comprises at least 3 eminent US scientists who have close links with AGU, IGU management can seek needed guidance from AGU through these 3 advisors for introduction of VPS during forthcoming annual convention at ISM, Dhanbad. Such an initiative strengthens IGU's resolve to encourage students/ research scholars.

**Better Tools to Build Better Climate Models**

Developing, maintaining, and enhancing a predictive climate model demand enormous human and computing resources. Decades' worth of observational data must be compiled, vetted, and integrated into a database. Parameters and variables must be identified and built into algorithms that simulate physical processes. Massive calculations can then convert past observations into predictions of the future. To determine the accuracy of predictions, results are validated by comparing them to present-day observations. As new data are fed to the model and scientific understanding of climate systems evolves, new information gets built into the model, and the testing and validation continue. One of the most resource-intensive aspects of climate modeling is the creation of a system for calibrating climate models, where model simulations are used to validate model output against observational data sets that span the globe. It is called a "climate model test bed." Such test bed environments typically evaluate each component of the model in isolation, using a skeleton framework that makes the module behave as if it were functioning within the larger program. To calibrate the model against regional observational data sets, uncertainty quantification techniques assess the accuracy of predictions, given the limitations inherent in the input information. If model developers could compare test bed output to observational measurements as the output was being generated, the comparison could facilitate aligning the model with the observed data. This capability could eliminate some of the more tedious activities associated with model development and evaluation.

If successful, the capability could accelerate the development of climate sub-model components, such as atmosphere, land, ocean, and sea ice. Researchers from five Department of Energy (DOE) laboratories of USA are currently developing this real-time comparison capability. If successful, the capability could accelerate the development of climate sub-model components, such as atmosphere, land, ocean, and sea ice. It could also improve the process by which the sub-models are integrated with each other to form the resulting coupled Earth system climate model.

The prototype test bed team is now under the banner of the newly formed Accelerated Climate Modeling for Energy (ACME) project, under the auspices of the U.S. Department of Energy's Office of Science. Under ACME, the team will continue its efforts to deliver an advanced model development, testing, and execution workflow and data infrastructure production test bed for DOE climate and energy research needs. The team anticipates rolling out the test bed by end of 2016 for ACME use.

**https://eos.org/project-updates/better-tools-to-build-better-climate-models**

Let us wish for its success to put at rest various anomalies in different models that are creating bottle necks.

**In this issue**

The present issue has 8 research publications, in addition to editorial and news and views. Out of which the last two are categorised as research notes. Author and title details are listed in the Contents Table. More specific information may please be extracted by going through the individual papers.

New Editorial board solicits continued support from scientific community.

**P.R.Reddy**

J. Ind. Geophys. Union ( May 2016 )
**v.20, no.3, pp: 309-315**

# Estimation of gas hydrate saturation using model based acoustic impedance inversion from Mahanadi offshore basin

**Uma Shankar*[1], Debjani Bhowmick[2] and Kalachand Sain[3]**

[1]Department of Geophysics, Institute of Science, Banaras Hindu University, Varanasi-221005
[2]CMPDI (HQ), Kanke Road, Rachi-834008
[3]CSIR-National Geophysical Research Institute, Uppal Road, Hyderabad – 500007
*Corresponding Author : umashankar_ngri@yahoo.com

**ABSTRACT**

The bottom simulating reflector (BSR), observed on seismic section in the Mahanadi offshore basin indicates the presence of gas hydrates. Gas hydrate saturation is estimated from electrical resistivity log based on Archie's empirical relation and/or from sonic velocity log using rock physics modeling approach at the vertical log position. The lateral and vertical extent of gas hydrates saturation over a larger area is obtained by post-stack impedance inversion of seismic data constrained by well log data. The inverted velocity coupled with rock physics modeling provides the estimation of gas hydrate saturation. The present study suggests that average gas hydrate saturation along a seismic line passing through site NGHP-01-19 in the Mahanadi Basin is about 3%. Gas hydrate saturation directly measured from the pressure cores, is found to be 2.4% at site NGHP-01-19, showing close correspondence with the estimation.

**Key words:** Gas hydrate, Acoustic velocity, Acoustic impedance inversion, Gas hydrate saturation.

## INTRODUCTION

The Mahanadi (MN) Basin is a major sedimentary Basin of the east coast of India Figure 1. The MN Basin is characterized by thick accumulation (8-10 km) of sediments (Collett et al., 2008). Sediment input to the Bay of Bengal is dominated by the Ganges-Brahmaputra river system, which drains much of the Himalayas. The resulting sediment influx has built the Bengal Fan, the world's largest sediment accumulation. The sediment reaches to a maximum thickness of over 22 km on the Bangladesh shelf (Curray and Munasinghe, 1991). Various seismic indicators of the occurrences of gas hydrates were identified on multichannel seismic (MCS) data in the central and deeper parts of the MN Basin (Collett et al., 2008, Prakash et al., 2010, Sain and Gupta, 2012, Shankar and Riedel, 2014). These include bottom-simulating reflectors (BSRs), enhanced reflections below the BSR, channelized (cut-and-fill) deposition and seismic chimneys, faults, slumps/slides and sedimentary ridges (Bastia, 2006). The BSR occurs from about 200 to less than 300 meter below seafloor (mbsf) on MCS data in the central part of the basin (Shankar and Riedel, 2014). However, strong BSR could not be identified at some profiles, the top of the high-reflectivity band is interpreted to represent the base of the gas hydrate stability zone (BGHSZ) with free gas accumulations below, causing very high reflectivity (Collett et al., 2008; Shankar and Riedel, 2014). The overall sediment flux that is received in the MN Basin is mainly from the Mahanadi, Brahmani, Baitarani and Dhamara rivers system with a sediment load to the basin on the order of $7.1\times 10^{9}$ kg/yr (Subramanian, 1978) and total organic carbon (TOC) to be more than 1.5% (Collett et al., 2008; Sain and Gupta, 2012), which favors the formation of gas hydrates in this region. The MN Basin is also characterized by bathymetry, sediment thickness and geothermal gradient ranging from 40-55 ºC/km (Sain et al., 2011).

The MN Basin was studied using high resolution MCS data (Bastia, 2006; Bastia et al., 2010a, b; Prakash et al., 2010; Shankar and Riedel, 2014) for the investigation of hydrocarbon prospect and gas hydrate occurrences. The area was also investigated using deep drilling by the Directorate General of Hydrocarbon (DGH) under the Indian National Gas Hydrate Program (NGHP) Expedition-01 (Collett et al., 2008).The NGHP Expedition-01 was completed successfully in the continental margins of India in April to June 2006 and gas hydrate samples were recovered by drilling and coring from sites NGHP-01-08, 09, 18 and 19 in the MN Basin. The in situ temperature measured at site NGHP-01-19 in the MN Basin shows the geothermal gradient of 52 ºC/km (Collett et al., 2008) and the BSR depth of 205 mbsf (Collett et al., 2008; Shankar and Riedel, 2014). The 2D high resolution MCS data, which is used here reveals flat BSR that coincides with the BGHSZ followed by very high reflectivity (Collett et al., 2008; Shankar and Riedel, 2014). The interpreted BGHSZ is in good correspondence with the geothermal modeling of BGHSZ performed by Shankar and Riedel (2014).

Seismic data provides important information about the general geology of the area. However, extraction of physical properties information such as velocity, porosity, density etc. is a great challenge. The seismic inversion is a powerful tool for estimating detailed characteristics of the reservoir (Kumar et al., 2016). Different seismic inversion

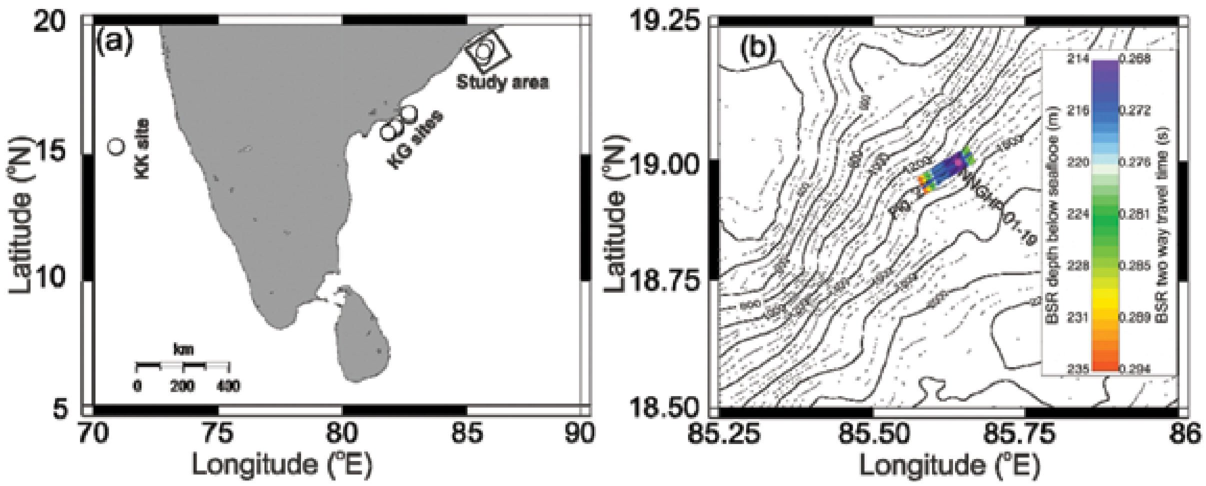


**Figure 1.** (**a**) Study area map in the Mahanadi Basin shown in box. (**b**) Bathymetry map of the Mahanadi Basin targeted during the drilling and coring of Indian National Gas Hydrate Drilling Expedition-01. Drilling sites are shown with black dots. The location of 2-D MCS line is shown with bold blue line passing through NGHP-01-19 site. The BSR depth below seafloor in meters and two way travel time below seafloor in seconds are also shown.

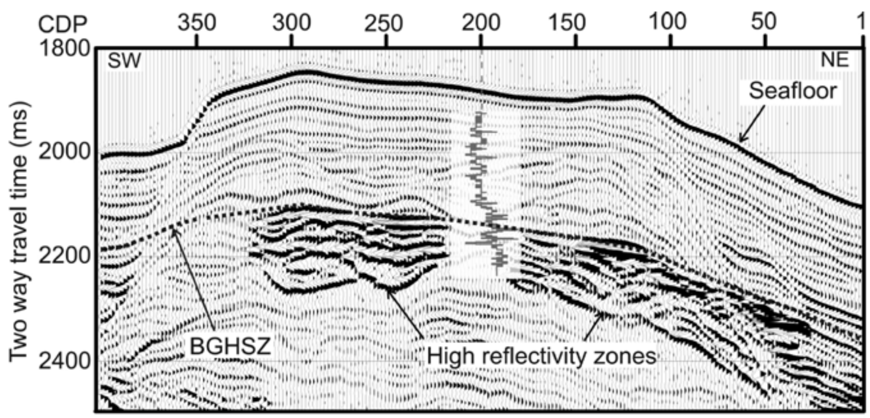


**Figure 2.** Sonic P-wave velocity log is overlain on seismic section crossing the Site NGHP-01-19, which was drilled in a gap between two similar channelized free-gas accumulations in order to safely obtain core and down hole log data from both above and below the expected BGHSZ (Collett et al., 2008). Top of the high reflectivity zone interpreted as BGHSZ. Dotted blue line represents the modeled BGHSZ (Shankar and Riedel, 2014).

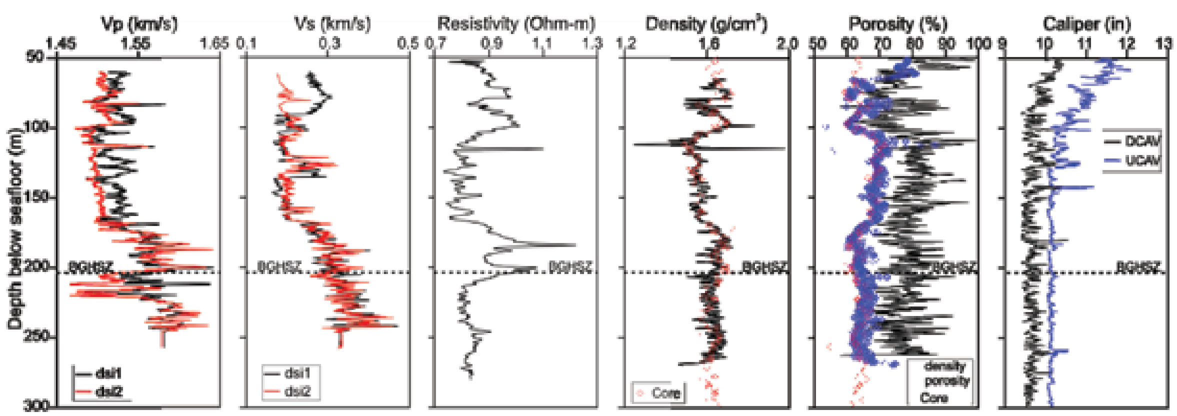


**Figure 3.** Suite of logs from site NGHP-01-19, including the sonic P and S-wave velocity, electrical resistivity, bulk density (RHOB), neutron porosity and caliper (DCAV, UCAV). Open red squares show density, porosity values measured from core samples and open blue squares are porosity derived from density log superimposed on the corresponding log curve. The BGHSZ is highlighted by the dotted black line.

methods are used commercially to derive detailed reservoir properties such as the lithology and fluid properties in combination with well log data and prior knowledge of geology (Riedel and Shankar, 2012). Model based acoustic impedance inversion was applied on stacked seismic data constrained by log data to derive physical properties of gas hydrate bearing sediments (Lu and McMechan, 2002; Dai et al., 2008; Wang et al., 2006; Riedel and Shankar, 2012; Shankar, 2016). To appraise the areal extent of gas hydrate in the MN Basin, gas hydrate saturation is estimated from physical properties derived from the acoustic impedance inversion coupled with rock physics modeling.

## Seismic and log data

The high resolution 2-D seismic stacked data was made available to the NGHP from the Reliance Industries Limited for scientific research (Collett et al., 2008). The seismic data was also previously used for defining geophysical drilling targets and site selection for the NGHP Expedition-01. The BSR and BSR-like features have been identified on seismic data (Shankar and Riedel, 2014), and Figure 2 shows a SW-NE oriented section crossing the site NGHP-01-19, which was drilled at ~1422 m water depth (Collett et al., 2008). The BSR was estimated at a depth of 205 mbsf (0.125 s TWT) using a constant velocity of 1610 m/s for the entire sediment column above the BGHSZ (Collett et al., 2008). The site NGHP-01-19 was drilled up to depth of only 300 mbsf between two anomalous high reflective zones. Presence of bright reflectivity zones beneath the BGHSZ indicates likely presence of free gas zones Figure 2.

Four sites were drilled in the MN Basin, and extensive Logging-While-Drilling (LWD)/Measurement-While-Drilling (MWD) data were acquired at site NGHP-01-08 and 09 without coring. The Site NGHP-01-18 was only cored and wire-line logged, and suits of logs were acquired at Site NGHP-01-19 to measure the physical properties of gas hydrate-bearing sediments. Site NGHP-01-19 was continuously cored up to 305 mbsf (Collett et al., 2008). At site NGHP-01-19, the gas hydrate is unevenly distributed in very thin layers and lies just above interpreted BGHSZ (Collett et al., 2008). Gas hydrate was found at 177-204 mbsf and maximum gas hydrate saturation was found to be 2.4% of pore space at a depth 193.5 mbsf at site NGHP-01-19A by pressure core measurement. Gas hydrate found at depth interval of 177-204 mbsf with maximum gas hydrate saturation of 10%. Hydrate saturation percentage was estimated from electrical resistivity log and pore-water chlorinity data (Collett et al., 2008; Shankar and Riedel, 2014).

Figure 3 shows the suite of logs at site NGHP-01-19. Wire-line logging with the dipole sonic imager (DSI) tools was utilized to measure the P- and S-wave velocities. Two run of DSI tools (DSI1 and DSI2) are shown in Figure 3 with different colors. The sonic velocity log shows an increasing trend of P- and S-wave velocities with depth, and the maximum velocity is observed just above the BSR at ~205 mbsf Figure 3. A sudden drop in P-wave velocity to ~1.53 km/s is observed just below the BGHSZ and the velocity again increases up to 1.63 km/s Figure 3. Resistivity log consistent with the P-wave velocity log trend and relatively high resistivity zone maximum up to ~1.2 ohm-m (165-185 m) is observed. But no visible gas hydrate samples were recovered from the site NGHP-01-19. However, the IR camera has identified a steady decrease in temperature with depth measured on the core liner above 205 mbsf. This is interpreted as the indication of gas hydrate disseminated in the formation above BGHSZ (Collett et al., 2008, Shankar and Riedel, 2014). Density and porosity measurements of core samples are superimposed on the corresponding logs. Density log matches reasonably well with the measured core despite the irregular hole size. The porosity calculated from density log shows good correspondence with the porosity measured from the core samples, indicating a precise measurement of density log data Figure 3. The neutron porosity log showing consistently higher than the measured core porosity is because of the influence of mineral-bound water in these clay dominated sediments (Collett et al., 2008) Figure 3. The shallow zone of the log above 60 mbsf cannot be used, as the caliper log shows a much enlarged hole near the seafloor.

## Material and methods

Acoustic impedance provides rock properties information and has been used to describe rock types. Rock properties information has also been used as direct hydrocarbon indicator (Latimer et al., 2000). Model based acoustic impedance inversion can be used to derive acoustic impedance variation based on seismic data and low frequency impedance information obtained from well logs (Lindseth, 1979). In this study we performed post-stack impedance inversion along a seismic section in the MN Basin. The model based acoustic impedance inversion is based on perturbation of a low frequency P-impedance model until the synthetic traces matches the observed seismic data. This method is based on the convolution of a seismic wavelet with the earth's reflectivity (Lu and Mcmechan, 2002) as:

$$S_t = [W_t * R_t] \qquad \text{...........(i)}$$

where $S_t$ is the seismic trace, $W_t$ is the seismic wavelet and $R_t$ is the reflectivity.

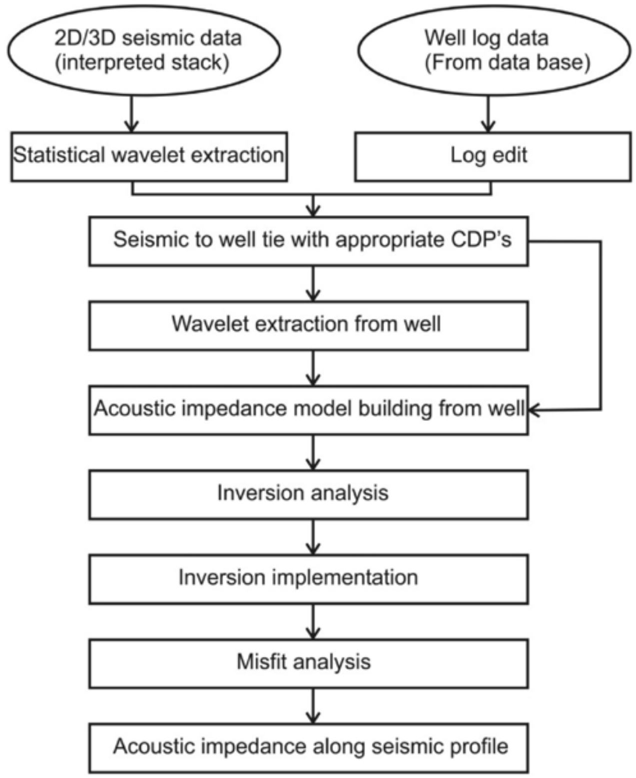


**Figure 4.** Post stack model-based acoustic impedance inversion simplified flow chart.

The zero-offset P-wave reflectivity $R_t$, is related to the acoustic impedance Z of the earth as:

$$R_t = \frac{Z_{t+1} - Z_t}{Z_{t+1} + Z_t} \qquad \text{...........(ii)}$$

where $Z_t = \rho v_t$ is the impedance of the $t^{th}$ layer ($\rho$ is density and $v_t$ is P-wave velocity of the $t^{th}$ layer), and $Z_{t+1}$ is the impedance of the underlying layer. We can invert equation (ii) for the P-impedance by recursive method.

$$Z_{t+i} = Z_t \left[ \frac{1+R_t}{1-R_t} \right] \qquad \text{...........(iii)}$$

From equation (iii) we can effectively transform reflection seismic traces to P-impedance. However, all inversion algorithms suffer from the non-uniqueness problem. This means that there is more than one possible geological model, consistent with the seismic data. In practice, this problem is handled by using geological constraints, provided by well logs. Gas hydrate saturation can be estimated from acoustic impedance of seismic data computed using different post-stack impedance inversion techniques such as: model-based, sparse spike and band limited inversion (Lu and Mcmechan, 2002; Dai et al., 2008; Riedel and Shankar, 2012; Shankar, 2016). Model -based post- stack inversion is used (Russell and Hampson, 1991) for computation of acoustic impedance from seismic data. Figure 4 shows the detail flow chart of the model based acoustic impedance analysis and inversion. In this study an effective medium model on inverted P-wave velocity is applied to obtain gas hydrate saturations. The modeled P-wave velocities of gas hydrate bearing sediments assumes the pore-filling form of gas hydrate, as it affects only the P-wave velocity (Singha et al., 2014).

Following the analysis at well location, the model based inversion was performed using the extracted wavelet from the seismic stacked data and a low frequency initial model with prior geological information such as the reservoir geometry. This can be done by interpretation of geological features on seismic section. In this study, two horizons were interpreted on the basis of prominent amplitudes and characteristics such as the sea floor and BSR. A low frequency initial acoustic impedance model was computed from the P-wave impedance log at well position and extrapolated along the seismic line. Figure 5a shows the acoustic impedance initial model along the seismic line. The P-wave impedance along the line interpolated from the well NGHP-01-19 shows increasing impedance with depth. Simultaneously, the inverted P-wave velocity obtained at the well location and extrapolated along the seismic line crossing the well NGHP-01-19 is shown in Figure 5b.

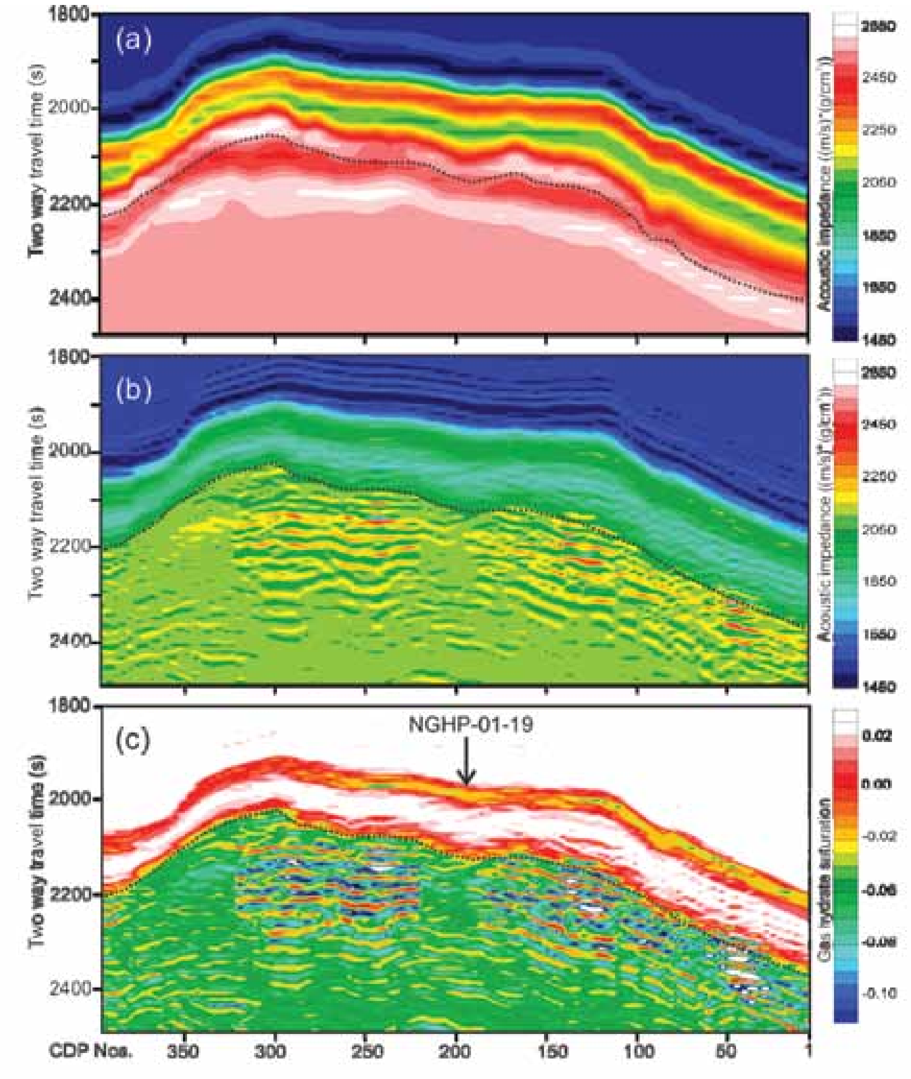


**Figure 5.** (**a**) Initial model for model based acoustic impedance inversion of 2D multi-channel seismic data, (**b**) Result from model based P-impedance inversion of the stacked volume along 2D seismic profile crossing well NGHP-01-19. Color-code shows inverted P- impedance in ((m/s) × (g/cc)), (**c**) Estimated gas hydrate saturation along 2D seismic profile using effective medium rock physics model on inverted velocity. The well location is marked with arrow. Black dotted curve shows the BGHSZ.

## RESULTS AND DISCUSSION

The acoustic impedance is calculated by model-based inversion constrained by well logs data at site NGHP-01-19 passing through the seismic line. The inversion of the hydrates region uses the interpreted information from seafloor, BSR and key reflectors to build structural model and to control the low frequency part of the model. To calculate impedance, the density and velocity logs were used along with low frequency (15 Hz) initial model.

Well-to-seismic correlation provides an efficient way to establish hydrate events on seismic data and for the calibration of gas hydrate estimation using an appropriate model. A well-based, zero-offset synthetic seismogram is created and compared with the post-stack seismic traces at the well location. The first step of seismic inversion is to correlate the well with the seismic stacked data, in which events recorded on the well log are correlated with the events recorded on the seismic data. To start a well to seismic tie, synthetic traces are generated to correlate with the recorded seismic traces. A suitable wavelet is extracted from the observed seismic data. The post-stack impedance inversion analysis is performed at the well location NGHP-01-19 to evaluate the accuracy of the inversion and to calculate an amplitude scaling factor between the seismic data and the impedance at the well site. The P-impedance inverted from single trace at the well location, and then a synthetic trace generated using this impedance and the extracted P-wavelet is compared with the extracted trace from the seismic data at well location.

To estimate gas hydrate saturation along the seismic line, physical parameters required are velocity, porosity and density. Density estimated simply by dividing inverted impedance by inverted velocity. Porosity estimated from the derived density along the seismic line from density porosity relationship $\phi = (\rho_g - \rho_b)/(\rho_g - \rho_w)$. Where $\rho_b$ is the formation bulk density of the medium, $\rho_w$ is the density of pore water which is 1030 kg/m$^3$ and $\rho_g$ is the average grain density equal to 2750 kg/m$^3$ measured in the core moisture and density analysis. The porosity estimation using this method is tested at well log site NGHP-01-19. The inverted P-wave velocity was then translated into the saturation of gas hydrate by invoking the effective medium rock physics theory to the time/depth varying porosity-profile and assumed mineralogical mix (Shankar and Riedel, 2011; Shankar and Riedel, 2013; Shankar et al., 2013). The saturation of gas hydrate estimated along the SW-NE trending seismic profile shows as high as 3.0% of the pore space Figure 5c.

## CONCLUSIONS

The impedance was calculated from the stacked seismic data using a post-stack model-based acoustic impedance inversion method. The gas hydrate saturation derived from the model-based acoustic impedance coupled with rock physics modelling, varies up to 3.0% of the pore space along the seismic line. The gas hydrate saturation (2.4% of the pore) directly measured from the recovered core shows close correspondence with the estimated values at drilling site NGHP-01-19. Estimation of this kind of saturation of gas hydrates provides a quick idea of the areal extent of gas hydrate along a seismic line.

## ACKNOWLEDGEMENTS

We thank the gas hydrate science team of National Gas Hydrate Expedition 01 (NGHP-01) and crew members. The Director of CSIR-National Geophysical Research Institute (NGRI), Hyderabad is thanked for encouragement and support. In addition, U Shankar is grateful to the Indo-US Science and Technology Forum (IUSSTF), Govt. of India, New Delhi for the Indo-US Fellowship-2013. This is a contribution to the SHORE Project under the 12th Five Year Plan of CSIR-NGRI.

## Compliance with Ethical Standards

The authors declare that they have no conflict of interest and adhere to copyright norms.

## REFERENCES

Bastia, R., 2006. An overview of Indian sedimentary basins with special focus on emerging east coast deepwater frontiers. The Leading Edge, v.25, no.7, pp: 818–829.

Bastia, R., Radhakrishna, M., Srinivas, T., Nayak, S., Nathaniel, D.M., and Biswal, T.K., 2010a. Structural and tectonic interpretation of geophysical data along the Eastern Continental Margin of India with special reference to the deepwater petroliferous basins. Journal of Asian Earth Sciences, v.39, pp: 608–619.

Bastia, R., Radhakrishna, M., Das, S., Kale, A.S., and Catuneanu, O., 2010b. Delineation of the 85ºE ridge and its structure in the Mahanadi Offshore Basin, Eastern Continental Margin of India (ECMI), from seismic reflection imaging. Marine and Petroleum Geology, v.27, no.9, pp: 1841–1848.

Curray, J.R., and Munasinghe, T., 1991. Origin of the Rajmahal Traps and the 85ºE Ridge: preliminary reconstructions of the trace of the Crozet hotspot. Geology., v.19, no.12, pp: 1237–1240.

Collett, T.S., Riedel, M., Cochran, J.R., Boswell, R., Presley, J., Kumar, P., Sathe, A.V., Sethi, A., Lall, M., Sibal, V. and NGHP Expedition 01 Scientists, 2008.National Gas Hydrate Program Expedition 01 initial reports. Directorate General of Hydrocarbons, New Delhi.

Dai, J., Snyder, F., Gillespie, D., Koesoemadinata, A., and Dutta, N., 2008. Exploration for gas hydrates in the deepwater, northern Gulf of Mexico: Part I, A seismic approach based on geologic model, inversion, and rock physics principles. Marine and Petroleum Geology, v.25, no.9, pp: 830–844.

Kumar, R., Das, B., Chatterjee, R., and Sain, K., 2016. A Methodology of Porosity Estimation from Inversion of Post-Stack Seismic Data. Journal of Natural Gas Science and Engineering, v.28, pp: 356–364.

Latimer, R.B., Davison, R., and Riel, P.V., 2000. An interpreter's guide to understanding and working with seismic-derived acoustic impedance data. The Leading Edge, v.19, no.3, pp: 242–256.

Lindseth, R.O., 1979. Synthetic sonic logs – A process for stratigraphic interpretation. Geophysics, v.44, no.1, pp: 3–26.

Lu, S., and McMechan, G.A., 2002. Estimation of gas hydrate and free gas saturation, concentration, and distribution from seismic data. Geophysics, v.67, no.2, pp: 582–593.

Prakash, A., Samanta, B. G., and Singh, N.P., 2010. A seismic study to investigate the prospect of gas hydrate in Mahanadi deep water basin, northeastern continental margin of India. Marine Geophysical Researches, v.31, no.4, pp: 253–262.

Russell, B., and Hampson, D., 1991. Comparisons of post stack inversion methods: 61stAnnual International Meeting, SEG, Expanded Abstracts v.10, pp: 876–878.

Riedel, M., and Shankar, U., 2012. Combining acoustic impedance and seismic similarity for robust gas hydrate concentration estimate – A case study from Krishna Godavari Basin, East coast of India. Marine and Petroleum Geology, v.36, no.1, pp: 35–49.

Sain, K., Rajesh, V., Satyavani, N., Subbarao, K.V., and C. Subrahmanyan. 2011. Gas hydrates stability thickness map along the Indian continental margin. Marine and Petroleum Geology, v.28, no.10, pp: 1779–1786.

Sain K., and Gupta, H.K., 2012. Gas hydrates in India: Potential and Development. Gondwana Research, v.22, no.2, pp: 645–657.

Singha, D.K., Chatterjee, R., Sen, M.K., and Sain, K., 2014. Pore pressure prediction in gas-hydrate bearing sediments of Krishna-Godavari basin, India. Marine Geology., v.357, pp: 1–11.

Subramanian, V., 1978. Input by Indian rivers into the world oceans. Proc. Indian Acad. Sci. Sect. A: Earth Planetary Science, v.87, no.7, pp: 77–88.

Shankar, U., and Riedel, M., 2011. Gas hydrate saturation in the Krishna-Godavari basin from P-wave velocity and electrical resistivity logs. Marine and Petroleum Geology, v.28, no.10, pp: 1768–1778.

Shankar, U., and Riedel, M., 2013. Heat flow and gas hydrate saturation estimates from Andaman Sea, India. Marine and Petroleum Geology, v.43, pp: 434–449.

Shankar, U., Gupta D.K., Bhowmick, D., and Sain, K., 2013. Gas hydrate and free gas saturations using rock physics modeling at site NGHP-01-05 and 07 in the Krishna Godavari Basin, Eastern Indian Margin. Journal of Petroleum Science and Engineering, v.106, pp: 62–70.

Shankar, U., and Riedel, M., 2014. Assessment of gas hydrate saturation in marine sediments from resistivity and P-wave velocity log measurements in the Mahanadi basin, India. Marine and Petroleum Geology, v.58, part A, pp: 265–277.

Shankar, U., 2016. Gas hydrate saturation from seismic data constrained by log data in the Krishna-Godavari Basin. Journal of Petroleum Exploration and Production Technology., DOI 10.1007/s13202-015-0170-1., v.6, no.1, pp: 13–23.

Wang, X., Wu, S., Xu, N., and Zhang, G., 2006. Estimation of gas hydrate saturation using constrained sparse spike inversion: Case study from the Northern South China Sea. Terrestrial of Atmospheric Oceanic Science, v.17, no.4, pp: 799–813.

J. Ind. Geophys. Union ( May 2016 )
**v.20, no.3, pp: 316-324**

# Global Seismic Temporal Pattern and Enhanced Seismicity Since 2000

**B. K. Rastogi and Jyoti Sharma***

Institute of Seismological Research (ISR), Department of Science and Technology
Government of Gujarat, Village - Raisan, Gandhinagar, Gujarat - 382009, India
*Corresponding Author: jyotisharmaiitkgp@gmail.com

**ABSTRACT**

Temporal pattern of global seismicity indicates temporal clustering of large earthquakes ($M_w \geq 8.2$) followed by relative quiescence (stress shadow). It is a characteristic seismic pattern along the plate boundaries. Clustering of the largest earthquakes during 1950s to 1960s followed by the extended period of low-moment release until 2003 and then again heightened moment release since 2004 has been observed, which represents a seismic temporal pattern of 50 years period. Similarly, the Alpine-Himalaya-Andaman-Sumatra (AHAS) belt and stable Indian Peninsular region have showed repeated temporal pattern of high and low seismicity. In the AHAS belt, seismicity was high during 1897 to 1916, low during 1917 to 1933, high again during 1934 to 1951, low again during 1952-1999 and since 2000 onwards seismicity has again enhanced. It has been observed that when there were no great earthquakes in Himalaya, the Peninsular India experienced, during that period, more number of $M \geq 6$ earthquakes.

**Key words:** Seismicity, Clustering, Quiescence, Temporal pattern.

## INTRODUCTION

Earthquakes do not occur randomly in space and time; on this assumption, temporal and spatial seismicity patterns have been studied by various researchers (Benioff, 1951, 1954; Davies and Brune, 1971; Mogi, 1974, 1979; Evison, 1982; Kagan and Jackson, 1991; Pacheco and Sykes, 1992; Bufe, 1997; Bufe and Perkins, 2005), and have observed that the study of seismic pattern is very much essential to understand the phenomenon of great earthquake preparation. Many researchers including Evison (1982), Bowman et al., (1998) Jaume and Sykes (1999), Bufe and Perkins (2005) have reported the changes in seismicity over a wider region before the occurrence of a major event. Further, most of the space-time pattern seismic studies are mainly concentrated on seismic quiescence, accelerating seismic energy/moment release and migration of seismicity. The present study is also focused on the temporal pattern of energy release of globally recorded strong earthquakes of $M_w \geq 8.2$, and accelerated seismicity and seismic moment release before the occurrence of a great earthquake.

In the present study, we have considered the globally recorded large earthquakes since 1900 of $M_w \geq 8.2$, which contribute the maximum moment to the accelerating seismic moment, and it is observed that the $M_w \geq 8.2$ earthquakes are the most influencing to the rate of moment release, directly or indirectly. Also, it has been observed that worldwide rate of occurrence of smaller earthquakes ($M < 7$) does not change systematically over time (Pacheco and Sykes, 1992, Bufe and Perkins, 2005). Hence, our present study is based on the large earthquakes of $M_w \geq 8.2$ for global seismicity study. Moreover, we have observed that the great earthquakes of $M_w \geq 9.0$ are preceded by quiescence or relatively lower seismicity of $M_w \geq 8.2$ earthquakes. Hence, $M_w \geq 8.2$ earthquakes can be considered as precursor to great or mega earthquake, and it can be considered as partially reoccurrence temporal pattern of high and relatively low seismicity.

Globally, rate of release of seismic moment has seen a sudden rise after 2004 Sumatra earthquake ($M_w$ 9.3, Tsai et al., 2005) that still continues, and which may be considered as a precursor to the next great earthquake, similar to 1960 Chile earthquake ($M_w$ 9.5, Kanamori and Anderson, 1975). The 1952 Kamchatka earthquake can be considered as a precursor to the great 1960 Chile earthquake. Moreover, similar kind of seismic pattern has also been observed at regional and local scale. The Alpine-Himalaya-Andaman-Sumatra (AHAS) belt and stable Indian Peninsula has also observed alternative temporal pattern of relatively low and high seismicity for $M \geq 7.7$ and $M \geq 6.0$, respectively.

### Earthquake data and Catalogue Preparation

Pacheco and Sykes (1992) have provided the high quality homogeneous seismic-moment catalogue for large magnitude ($M \geq 7.0$) and shallow depth ($z \leq 70$ km) earthquakes for the period 1900-1989. Hence, in the present study Pacheco–Sykes catalogue of $M_w \geq 8.2$ earthquakes has been considered for the period 1900 -1989, and from 1989 onwards Global Centroid Moment Tensor (GCMT) catalogue (Dziewonski et al., 1981, 2001; Ekstörm et al., 2012). In the present study, for 1960 Chile earthquake we have considered the Kanamori and Anderson (1975) estimated seismic moment ($M_o$) of 2000

**Table 1.** Extended Pacheco-Sykes catalog of earthquakes $M_w \geq 8.2$, 1900 - 2014. Pacheco-Sykes catalog from 1900-1989, and from 1989 onwards using GCMT catalog.

| EQ Nos. | Date YYYY-MM-DD | Origin Time Hr:Mn | Lat (°) | Long (°) | Depth (km) | $Mo \times 10^{20}$ (Nm) | $M_w$ | Location |
|---|---|---|---|---|---|---|---|---|
| 1 | 1905-07-09 | 09:40 | 49.0 | 99.0 | 35 | 55.0 | 8.5 | Mangolia |
| 2 | 1905-07-23 | 02:46 | 49.0 | 97.0 | 35 | 50.0 | 8.4 | Mangolia |
| 3 | 1906-01-31 | 15:36 | 01.0 | -81.3 | 33 | 80.0 | 8.6 | Colombia-Ecuador |
| 4 | 1906-08-17 | 00:40 | -33.0 | -72.0 | 33 | 66.0 | 8.5 | Chile |
| 5 | 1917-06-26 | 05:49 | -15.5 | -173.0 | 33 | 70.0 | 8.5 | Tonga Islands |
| 6 | 1918-08-15 | 12:18 | 05.7 | 123.5 | 33 | 25.0 | 8.2 | Philippines |
| 7 | 1918-09-07 | 17:16 | 45.5 | 151.5 | 33 | 22.0 | 8.2 | Kurile Islands |
| 8 | 1919-04-30 | 07:17 | -19.0 | -172.5 | 33 | 27.1 | 8.3 | Tonga Islands |
| 9 | 1920-12-16 | 12:05 | 36.6 | 105.4 | 33 | 30.0 | 8.3 | Kansu, China |
| 10 | 1922-11-11 | 04:32 | -28.5 | -70.0 | 33 | 140.0 | 8.7 | Chile |
| 11 | 1923-02-03 | 16:01 | 54.0 | 161.0 | 33 | 70.0 | 8.5 | Kamchatka |
| 12 | 1924-06-26 | 01:37 | -55.0 | 158.4 | 33 | 30.2 | 8.3 | Macquarie Ridge |
| 13 | 1933-03-02 | 17:30 | 39.3 | 144.5 | 30 | 43.0 | 8.4 | Japan |
| 14 | 1938-02-01 | 19:04 | -05.5 | 131.5 | 40 | 52.0 | 8.4 | Banda Sea |
| 15 | 1943-04-06 | 00:00 | -31.0 | -71.3 | 20 | 25.0 | 8.2 | Chile |
| 16 | 1950-08-15 | 14:09 | 28.7 | 96.6 | 30 | 95.0 | 8.6 | Assam |
| 17 | 1952-11-04 | 16:58 | 52.8 | 159.5 | 33 | 350.0 | 9.0 | Kamchatka |
| 18 | 1957-03-09 | 14:22 | 51.6 | -175.4 | 33 | 100.0 | 8.6 | Aleutian Islands |
| 19 | 1958-11-06 | 22:58 | 44.4 | 148.5 | 32 | 44.0 | 8.4 | Kuril Islands |
| 20 | 1960-05-21 | 10:02 | -37.2 | -73.0 | 33 | 20.0 | 8.2 | Chile |
| 21 | 1960-05-22 | 19:11 | -38.2 | -73.5 | 32 | 2000.0 | **9.5*** | Chile |
| 22 | 1963-10-13 | 05:17 | 44.9 | 149.6 | 40 | 75.0 | 8.6 | Kuril Islands |
| 23 | 1964-03-28 | 03:36 | 61.1 | -147.6 | 30 | 750.0 | 9.2 | Alaska |
| 24 | 1965-01-24 | 00:11 | -02.4 | 126.0 | 23 | 24.0 | 8.2 | Banda Sea |
| 25 | 1965-02-04 | 05:01 | 51.3 | 178.6 | 35 | 140.0 | 8.7 | Aleutian Islands |
| 26 | 1966-10-17 | 21:41 | -10.9 | -78.8 | 21 | 20.0 | 8.2 | Peru |
| 27 | 1968-05-16 | 00:48 | 40.9 | 143.4 | 35 | 28.0 | 8.3 | Tokachi-oki, Japan |
| 28 | 1969-08-11 | 21:27 | 43.6 | 147.2 | 30 | 22.0 | 8.2 | Kurile Islands |
| 29 | 1977-08-19 | 06:08 | -11.1 | 118.5 | 23 | 24.0 | 8.2 | Indonesia |
| 30 | 1979-12-12 | 07:59 | 01.6 | -79.4 | 24 | 29.0 | 8.3 | Colombia-Ecuador |
| 31 | 1989-05-23 | 10:54 | -52.3 | 160.6 | 50 | 24.0 | 8.2 | Macquarie Ridge |
| 32 | 1994-10-04 | 13:23 | 43.6 | 147.6 | 68 | 30.0 | 8.3 | Kuril Islands |
| 33 | 1996-02-17 | 06:00 | -0.7 | 136.6 | 15 | 24.0 | 8.2 | Irian, Indonesia |
| 34 | 2001-06-23 | 20:34 | -17.3 | -72.7 | 30 | 47.0 | 8.4 | Peru |
| 35 | 2003-09-25 | 19:50 | 41.8 | 143.9 | 27 | 30.5 | 8.3 | Hokkaido, Japan |
| 36 | 2004-12-26 | 05:08 | 03.3 | 96.0 | 30 | 1200.0 | **9.3**** | Sumatra |
| 37 | 2005-03-28 | 16:09 | 2.1 | 97.1 | 30 | 105.0 | 8.6 | Sumatra |
| 38 | 2006-11-15 | 11:14 | 46.6 | 153.3 | 10 | 35.1 | 8.3 | Kuril Islands |
| 39 | 2007-09-12 | 11:10 | -04.4 | 101.4 | 34 | 67.1 | 8.5 | Sumatra |
| 40 | 2010-02-27 | 06:34 | -36.1 | -72.9 | 22 | 186.0 | 8.8 | Chile |
| 41 | 2011-03-11 | 05:46 | 38.3 | 142.4 | 29 | 531.0 | 9.1 | Honshu, Japan |
| 42 | 2012-04-11 | 08:39 | 02.2 | 92.8 | 40 | 89.6 | 8.6 | Sumatra |
| 43 | 2012-04-11 | 10:43 | 0.8 | 92.3 | 53.7 | 25.3 | 8.2 | Sumatra |
| 44 | 2013-05-24 | 05:45 | 54.6 | 153.8 | **611.4#** | 39.5 | 8.3 | Sea of Okhotsk |
| 45 | 2014-04-01 | 23:47 | -19.6 | -70.8 | 20.1 | 23.5 | **8.2$** | Chile |

* EQ no. 21 (1960 Chile earthquake) $M_w$ is consider after Kanamori and Anderson (1975), and Bufe and Perkins (2005).

** EQ no. 36 (2004 Sumatra earthquake) $M_w$ is consider after Tsai et al., (2005), and Stein and Okal (2007).

\# EQ no. 44 (2013 Sea of Okhotsk) is a deep earthquake.

$ EQ no. 45 (2014 Chile earthquake) Hypocentral parameters, Moment magnitude ($M_w$) and Seismic Moment ($M_o$) are considered from USGS report.

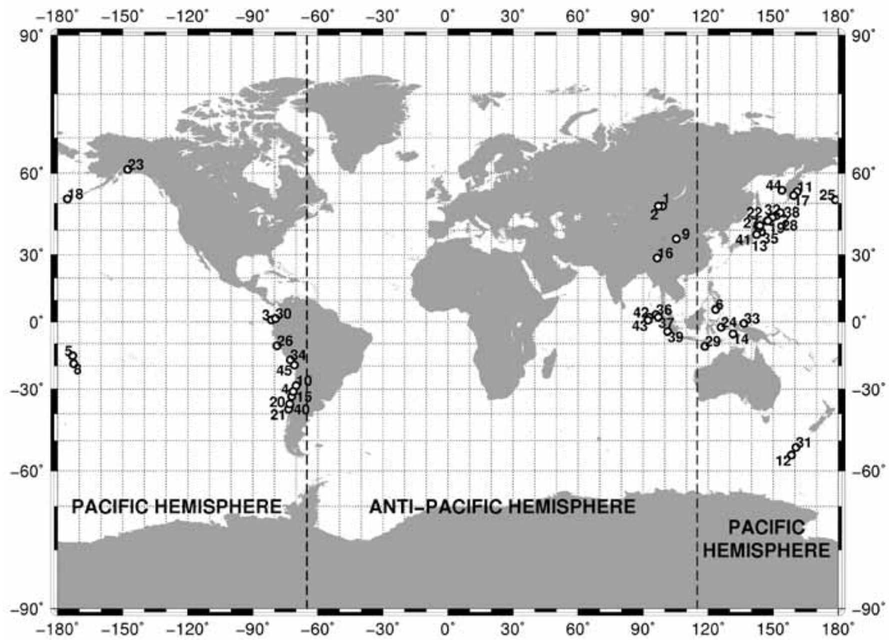


**Figure 1.** Global distribution of $M_w \geq 8.2$ earthquakes as a function of latitude and longitude by using catalogue provided in Table 1. The great earthquakes are represented here by earthquake (EQ) numbers provided in Table1.

$\times 10^{20}$ Nm and $M_w = 9.5$. Cifuentes and Silver (1989) and Pacheco and Sykes (1992) estimate of $M_w = 9.6$ and $M_o = 3200 \times 10^{20}$ Nm were not considered. Also, for the 2004 Sumatra earthquake, Tsai et al., (2005) and Stein and Okal (2007) estimated values, $M_w = 9.3$ and $M_o = 1200 \times 10^{20}$ Nm were used in the present study. Further, seismic moment provided in the Pacheco and Sykes (1992) catalogue is converted into $M_w$ using Hanks and Kanamori (1979) relation, $M_w = (\log (M_o) - 9.05)/1.5$ ($M_o$ is in Nm) for global seismicity analysis. The spatial distribution of the globally recorded larger events (Mw ≥ 8.2) that dominate the history of the moment release and used in the present study are represented in Figure 1 and tabulated in Table 1. Further the earthquakes (M ≥ 7.7) distribution for the AHAS belt provided by the Hamada (1981) and Gupta (1992) has been updated using USGS catalogue as listed in Table 2.

## Clustering, Quiescence, and Migration

To understand earthquakes occurrence as non-random, non-linear and coherent system, we have used the catalogue of large earthquakes at global and regional scale. The globally recorded $M_w \geq 8.2$ earthquakes catalogue is further studied to observe the temporal and spatial pattern. The alternative temporal pattern of enhanced seismic activity and quiescence has been observed for $M_w \geq 8.2$ earthquakes as shown in Figure 2a by decadal plot of earthquake records. Also the moment release by great earthquakes per decade is represented in Figure 2b and cumulative accumulation of seismic moment of $M_w \geq 8.2$ earthquakes in Figure 2c. The high moment release is noticed during 1950s to 1960s followed by extended period of low moment release until 1999 and again heightened moment release has been observed since 2000 as shown in Figures 2b and 2c. The period of 1950 to 1999 represents one complete seismic pattern of clustering and quiescence of great earthquakes. Further, on analysing the recent records of $M_w \geq 8.2$ earthquakes, it has been observed that the 34% of the total seismic moment since 1900 has been released during the decades of 2000s and 2010s (2010 decade includes data up to 2015). Hence the recent accelerated seismic moment can be compared with 1950-1960 accelerated seismic moment release as shown in Figure 2a. The rate of seismic moment release was accelerated after the 1952 Kamchatka earthquake ($M_w$ 9.0) and continued till the occurrence of 20th century greatest 1960 Chile earthquake ($M_w$ 9.5). However, no great earthquake of $M_w \geq 9.0$ was observed before the 1952 Kamchatka earthquake. Hence, 1952-1962 decade represents clustering of great earthquakes ($M_w \geq 9.0$), and includes 1952 Kamchatka, 1960 Chile and 1962 Alaska earthquakes. Similar observation of clustering of large earthquakes before the occurrence of great earthquake and quiescence (stress shadow) has been reported by Bufe and Perkins (2005). They have reported the seismic pattern of clustering and quiescence by using Monte-Carlo simulation technique to determine probabilities of random occurrence. Monte-Carlo simulations of random occurrence provided the probability of temporal clustering

**Table 2.** Earthquakes of Mw ≥ 7.7 in Alpine-Himalaya-Andaman-Sumatra belt during 1991 - 2014 using USGS catalog.

| EQ Nos. | Date YYYY-MM-DD | Origin Time Hr:Mn:Sec | Lat.(°) | Long.(°) | Depth (Km) | Mw | Location |
|---|---|---|---|---|---|---|---|
| 1 | 1992-12-12 | 05:29:26 | -8.5 | 121.9 | 28 | 7.8 | Indonesia |
| 2 | 1994-06-02 | 18:17:34 | -10.5 | 112.8 | 18 | 7.8 | Java,Indonesia |
| 3 | 1996-01-01 | 08:05:11 | 0.7 | 119.9 | 24 | 7.9 | Minahassa Peninsula, Sulawesi |
| 4 | 1998-11-29 | 14:10:32 | -2.1 | 124.9 | 33 | 7.7 | Ceram Sea |
| 5 | 1999-09-20 | 17:47:18 | 23.8 | 121.0 | 33 | 7.7 | Taiwan |
| 6 | 2000-06-04 | 16:28:26 | -4.7 | 102.1 | 33 | 7.9 | Sumatra,Indonesia |
| 7 | 2000-06-18 | 14:44:13 | -13.8 | 97.5 | 10 | 7.9 | South Indian Ocean |
| 8 | 2001-01-26 | 03:16:41 | 23.4 | 70.2 | 16 | 7.7 | Kachchh,Gujarat,India |
| 9 | 2001-11-14 | 09:26:10 | 40.0 | 90.5 | 10 | 7.8 | Qinghai,China |
| 10 | 2004-12-26 | 00:58:53 | 3.3 | 96.0 | 30 | 9.3 | Sumatra,Indonesia |
| 11 | 2005-03-28 | 16:09:37 | 2.1 | 97.2 | 30 | 8.6 | Sumatra,Indonesia |
| 12 | 2006-07-17 | 08:19:27 | -9.3 | 107.4 | 20 | 7.7 | Java,Indonesia |
| 13 | 2007-09-12 | 23:49:04 | -2.6 | 100.8 | 35 | 7.9 | Kepulauan Mentawai Region,Indonesia |
| 14 | 2007-09-12 | 11:10:27 | -4.4 | 101.4 | 34 | 8.5 | Sumatra,Indonesia |
| 15 | 2008-05-12 | 06:28:02 | 31.0 | 103.3 | 19 | 7.9 | Sichuan,China |
| 16 | 2010-04-06 | 22:15:02 | 2.4 | 97.5 | 31 | 7.8 | Sumatra,Indonesia |
| 17 | 2010-10-25 | 14:42:22 | -3.5 | 100.1 | 20 | 7.8 | Kepulauan Mentawai Region,Indonesia |
| 18 | 2012-04-11 | 10:43:11 | 0.8 | 92.5 | 25 | 8.2 | Sumatra,Indonesia |
| 19 | 2012-04-11 | 08:38:37 | 2.3 | 93.1 | 20 | 8.6 | Sumatra,Indonesia |
| 20 | 2013-04-16 | 10:44:21 | 28.1 | 62.1 | 82 | 7.7 | Iran -Pakistan Border Region |
| 21 | 2013-09-24 | 11:29:47 | 26.9 | 65.5 | 15 | 7.7 | Awaran, Pakistan |
| 22 | 2015-04-25 | 06:11:25 | 28.2 | 84.7 | 8 | 7.8 | Lamjung, Nepal |

in a 12-yr period (1952–1964) of the three greatest ($M_w \geq 9.0$) earthquakes as 4%. Also they have provided 0.5% probability of quiescence of $M_w \geq 8.4$ earthquakes for a period of 36 yrs (after 1964), and this quiescence period is called as global stress shadow. Mogi (1969), Sykes and Jaume (1990), Bufe and Varnes (1993), Sobolev and Tyupkin (1999), and Bufe and Perkins (2005) have also reported the clustering of large earthquakes before the occurrence of great earthquakes. Moreover, Kagan and Jackson (1991) have also provided the statistical results on existence of large-scale temporal earthquake clustering and quiescence. The observed global moment release pattern (clustering of large earthquakes, with acceleration before and deceleration after the mainshock) suggests that Earth, over many decades, may also respond as a coherent, non random, nonlinear system of stress redistribution.

Further, we have also observed high and low seismic moment release alternatively in pacific and anti-pacific hemispheres as shown in Figure 3. In 1960's decade, Pacific hemisphere has only seen the seismic moment release through great earthquakes. While on the contrary, in 2000's decade anti-pacific hemisphere has seen the maximum moment release (see Figure 3). On comparing the seismic moment release in the pacific and anti-pacific hemispheres, we have observed that during 1950-1970, 97% of the seismic moment released in the pacific hemisphere, with a dominating 1960 Chile earthquake, which itself contributes 84% of the total moment released. Only 1950 Assam earthquake ($M_w$ 8.6) contributed to the anti-pacific moment release. While since 2000 we have seen equal number of great earthquakes in both the hemispheres with 63% of moment release in anti-pacific hemisphere (see Figure 3). The 2004 Sumatra earthquake (Mw 9.3) itself contributes 51% of the total moment released during 2000-2015. This increase in global-moment release rate in both the Pacific and anti-Pacific hemispheres may be related to the recent changes in moment of inertia and shape of the earth (Cox and Chao, 2002). Dickey et al., (2002) attribute the observed increase to subpolar glacial melting and mass shifts in the oceans. Also, Bufe and Perkins (2005) urge for the concept that if global seismic cycle is valid, then the global cycle durations will be shorter than the recurrence times of most individual great earthquakes, because not all the global potential seismic moment or energy is released

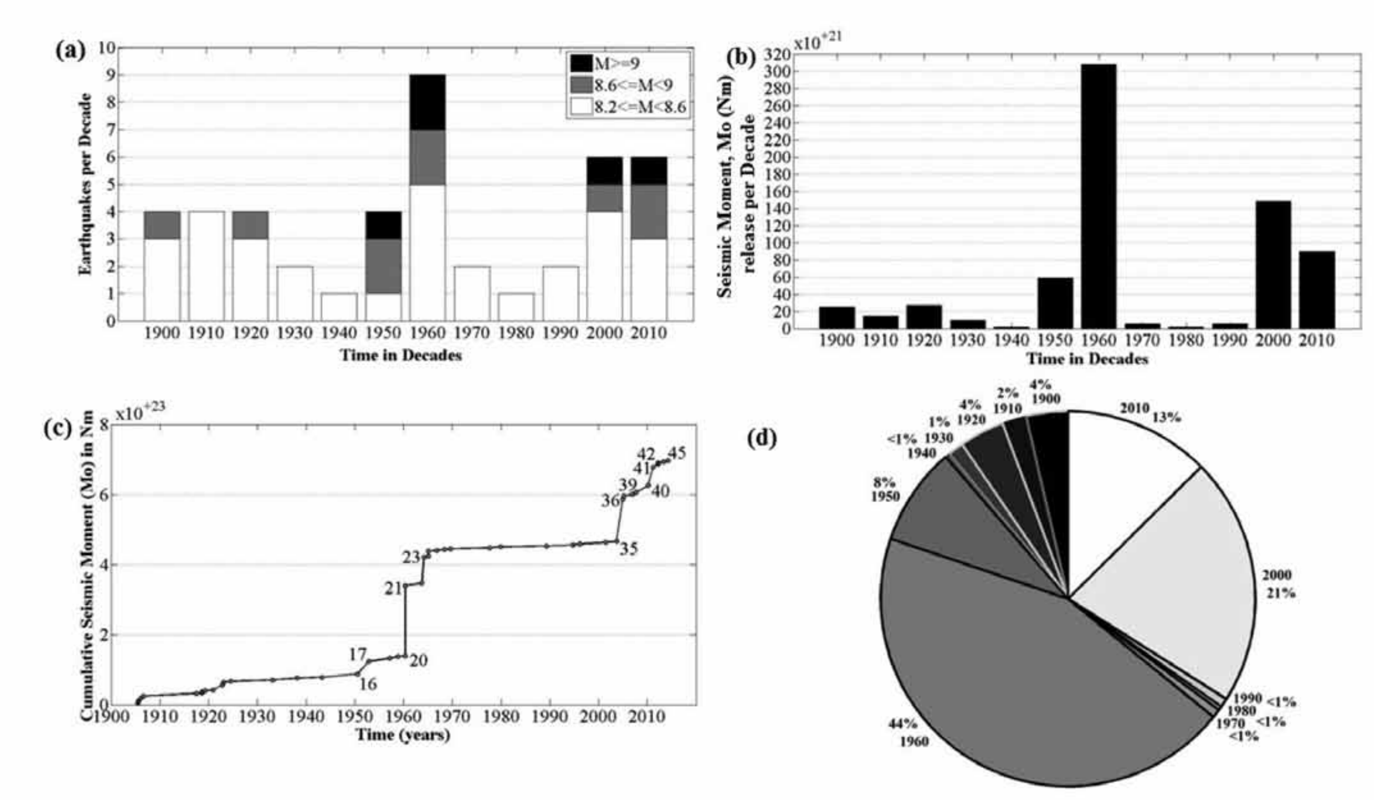


**Figure 2.** Plot showing (a) Decadal histogram illustrating temporal clustering of global great earthquakes of $M_w \geq 9.0$ (black), $M_w \geq 8.6$ (black+gray), and $M_w \geq 8.2$ (black+gray+white).The bar for the decade 2010 represents earthquakes of the first 4.5 yrs, (b) Decadal histogram illustrating seismic moment, $M_o$ (Nm) release of $M_w \geq 8.2$ earthquakes by using catalogue presented in Table 1, (c) Cumulative global seismic moment release, 1900–2014, for $M_w \geq 8.2$ earthquakes by using catalogue presented in Table 1, and (d) Seismic moment release per decade (in percentage of total moment release in 114.5yrs) decade wise of earthquakes $M_w \geq 8.2$.

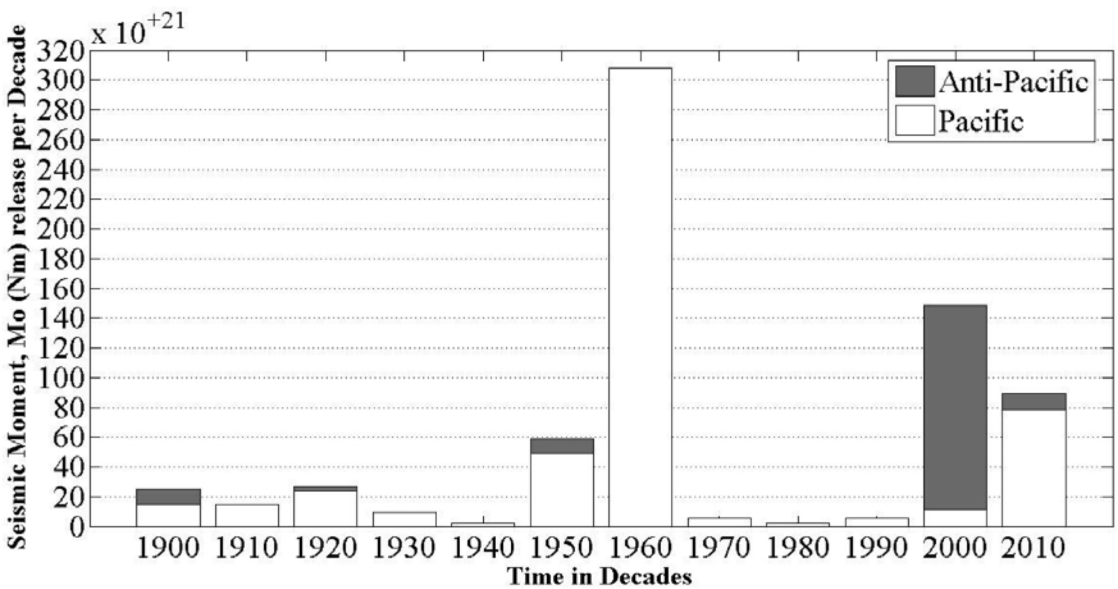


**Figure 3.** Decadal histogram illustrating seismic moment, $M_o$ (Nm) release of $M_w \geq 8.2$ earthquakes in Pacific and Anti-Pacific hemisphere using catalogue presented in Table 1.

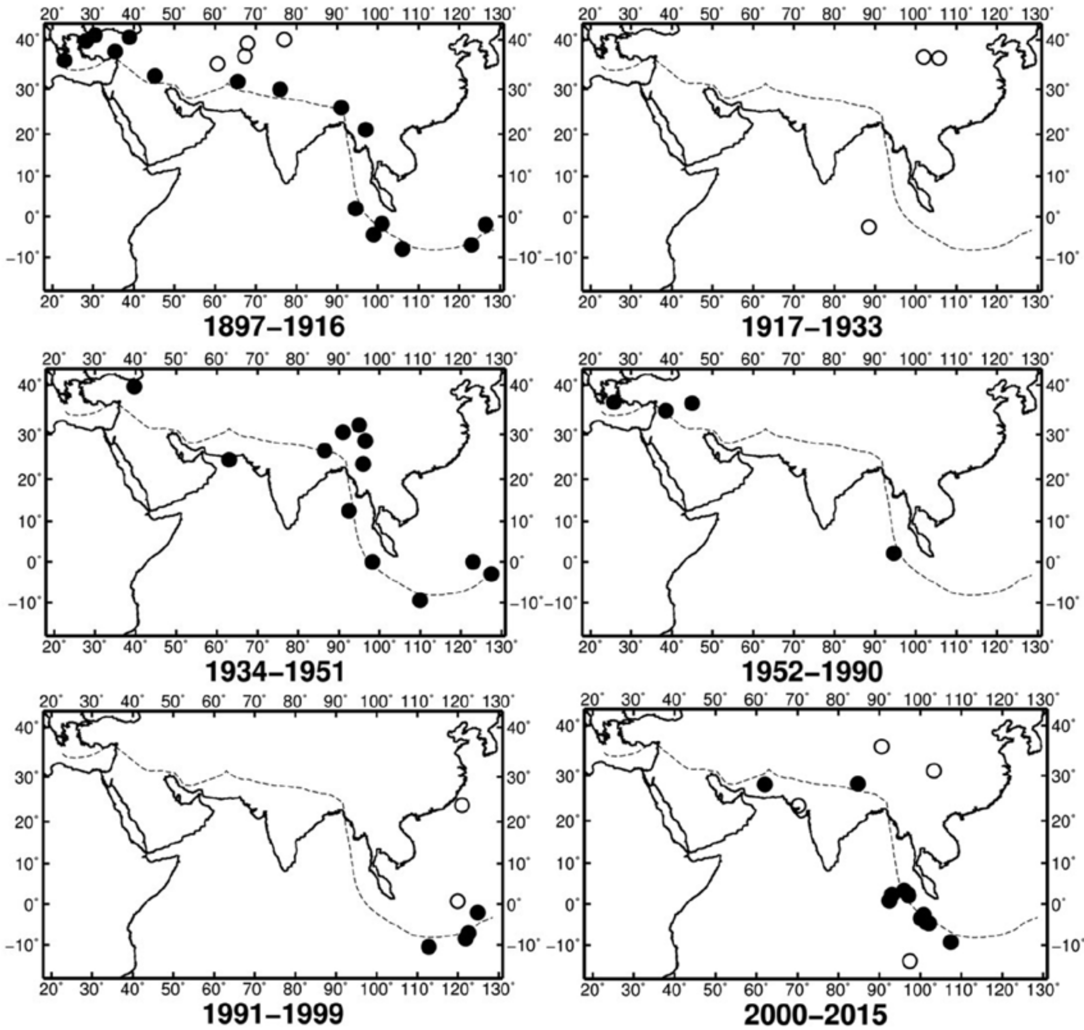


**Figure 4.** Seismic temporal pattern in the Alpine-Himalaya-Andaman-Sumatra belt for shallow earthquakes of focal depth 100 km and M≥7.7 (up to 1981 after Hamada, 1981 and later on modified till 1990 by Gupta, 1992). Subsequently, after 1990 USGS catalogue has been used (refer Table 2). Solid and open circles represent M≥7.7 earthquakes. Open circles indicate epicenters away from the belt.

in a single cycle. Besides this Romanowicz (1993) provided a different category of global seismic pattern, representing alternating temporal pattern of toroidal (strike-slip) and poloidal (thrust or normal) energy release. The period of high moment release during 1950-1960 and 2010-2014 corresponds to the poloidal seismic pattern, while 1965-2003 represents the lower-moment toroidal seismic pattern.

The similar kind of repeated alternative temporal pattern of low and high seismicity has also been observed for the AHAS and stable Indian Peninsular region (see Figure 4). The high seismicity has been observed for AHAS belt during 1897-1916, 1934-1951 and since 2000. While, low seismicity was observed for 1917-1933 and 1952-1999. The present observation for the AHAS and stable Indian Peninsular region is based on the M ≥ 7.7 earthquakes. Also, around the same period 1965-1999, rest of the world has also seen low seismicity. Hamada (1981) and Gupta (1992) have also reported the alternative temporal pattern of clustering and quiescence for M ≥ 7.7 earthquakes for the AHAS region. Contradictory to this, stable Indian peninsular region was active during 1965-1999 with large number of earthquakes of M ≥ 5.0, as shown in Figure 5. It has also been observed that during the periods when there are no great earthquakes in the Himalaya, the Peninsular India has seen more number of M ≥ 5 earthquakes (see Figure 5). Since 1960s Peninsular India has unusually experienced a large number of M ≥ 5 earthquakes. It may be explained on the basis of long range migration of the strain energy between the mechanically coupled fault systems in the continental interior, on the basis of Liu et al., (2011) explanation for the North China. Liu et al., (2011) have observed the similar pattern of

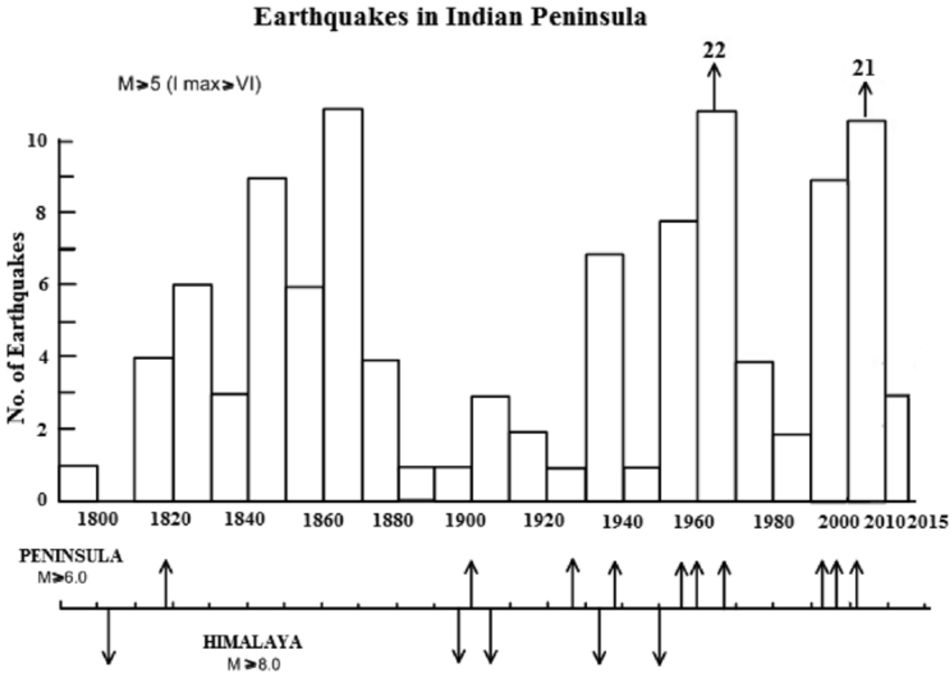


**Figure 5.** During the shadow periods when M8 earthquakes are absent in Himalaya (lowermost part), earthquakes are more in SCR India and vice-versa.

migration for earthquakes of M ≥ 4.0 in North China region. They have proposed a simple conceptual model for intra-continental earthquakes, in which slow tectonic loading in mid-continents is accommodated collectively by a complex system of interacting faults, each of which can be active for a short period after a long dormancy, and the resulting large earthquakes are episodic and spatially migrating. However, since 2000 AHAS Belt and its nearby regions again have seen many large earthquakes of $M_w$ ≥ 7.7 including 2004 Andaman-Sumatra ($M_w$ 9.3), 2013 Iran ($M_w$ 7.7) and 2015 Nepal ($M_w$ 7.8), which may be possibly indicating enhanced seismicity in AHAS Belt for M ≥ 7.7 earthquakes. The pattern of high and low seismicity in AHAS Belt is similar to the global seismicity pattern, including enhanced seismicity since 2000.

The similar kinds of seismicity temporal pattern have also been reported by many other earth scientists (Mogi, 1969; Evison, 1982; Wyss and Habermann, 1988; Sornette and Sornette, 1990; Sykes and Jaume, 1990; Bufe and Varnes, 1993; Sornette and Sammis, 1995; Sobolev and Tyupkin, 1999; Bowman and King, 2001; Bufe and Perkins, 2005) for different source zones around the world. Mogi (1969) has explained the enhanced seismicity on the basis of "doughnut pattern", according to which increased seismicity during a certain period before the occurrence of strong earthquake concentrates around the periphery of the future earthquake rupture zone. The rupture zone of the oncoming earthquake remains relatively quiet. Wyss and Habermann (1988) have also reported the precursory quiescence, lasting for months or years before the occurrence of large earthquakes. Bufe and Varnes (1993) have observed accelerating seismic moment release within a broader area around the epicentre of a future earthquake. Sobolev and Tyupkin (1999) have also reported the similar findings by using region-time-length (RTL) method. Bowman et al., (1998); Jaume and Sykes (1999) and Simpson and Reasenberg (1994) also supported the change in seismicity over a wider zone before the occurrence of a major event. Moreover, on the basis of Evison (1982), and Bowman and King (2001) observations, occurrence of large earthquake can be identified on the basis of increased seismicity and increase in stress level around the seismic active zone; large seismically active region indicates the large magnitude earthquake. On the basis of Evison (1982), swarms of special pattern in time and space may indicate a precursory signal to an impending large earthquake. Based on the earthquake swarm hypothesis of Evison (1982), Gupta and Singh (1986) tested the precursory phenomena of the 1984 Cachar earthquake (M5.8, USGS) and made a forecast of the August 6, 1988 Manipur-Burma border earthquake (M 7.2). The 1988 earthquake occurred within the stipulated time and space window and they claimed it to be a successful forecast (Gupta and Singh, 1989). Hence, all precursory studies based on seismic rate changes and acceleration of seismic activity prior to large earthquake can be considered as a decisive phenomenon in understanding the Earth as coherent, non-random and non-linear system of stress redistribution.

## Earthquake triggering and Temporal pattern of Seismicity

The mechanism behind the global triggering of earthquakes, and following a specific seismic pattern can be explained on the basis of following assumptions/possibilities: (1) Large or global scale processes take place in the lithosphere (Barenblatt et al., 1983; Press and Allen 1995); (2) Propagation of viscoelastic deformation in the asthenosphere (Piersanti et al., 1995; Pollitz et al., 1998); (3) Stress transfer from great slow earthquakes migrating along the base of the seismogenic zone along plate margins (Bufe and Perkins 2005); (4) Redistribution of mass in the hydrosphere or mantle (Cox and Chao 2002; Dickey et al., 2002); (5) Long range correlation of complex non linear hierarchical dynamical systems (Kelis–Borok, 1990, 2002; Sornette and Sammis, 1995; Turcotte et al., 2000), for example, the lithosphere can be considered as a complex hierarchical-dynamical system where strong earthquakes are critical phenomenon; (6) Quasi-static changes in fault properties or pore pressure induced by transient dynamic stresses of seismic waves or free oscillations of the earth generated by distant great earthquakes (Bufe and Perkins 2005). (7) Attainment of a global tectonic state of self-organized criticality.

## CONCLUSIONS

The present study provides some facts to elucidate that the large earthquakes do not occur randomly in space and time. They generally follow a specific pattern.

The present study also provides underlying physics behind the earthquake temporal pattern that can be incorporated into seismic hazard analysis.

The present study helps in illustrating the existing seismicity scenario of the World in general and AHAS belt and stable Indian Peninsular region in particular.

The great earthquakes ($M_w \geq 8.2$) follow a specific pattern of quiescence (stress shadow) and clustering globally. In our study, we have observed two such temporal patterns during the periods of 1925-1965 and 1966-2015 (still continue).

The AHAS belt has seen repeated alternative temporal pattern of high and low seismicity for large earthquakes ($M_w \geq 7.7$). The AHAS belt has seen low seismicity during the periods, 1917-1933 and 1952-1999 and high seismicity during 1897-1916, 1934-1951 and 2000-2015 (still continue). The AHAS belt represents the similar temporal pattern of high and low seismicity, almost during the same period as observed globally.

The stable Indian Peninsular region has also seen the seismic pattern of low and high, but reversely. When seismicity is high in Himalaya region, Peninsula has observed low seismicity and vice-versa.

The present day scenario is showing enhanced seismicity, globally as well as in AHAS region. In future, it may lead to the occurrence of another great earthquake like 1960 Chile ($M_w$ 9.5).

The seismicity modifies or high seismicity is observed with a clustering of great earthquakes before the major event and stress shadows follow great earthquakes.

The evolution pattern of cumulative seismic moment prior to the occurrence of great earthquake can be used as an additional tool for seismic hazard assessment, besides the duration of our current seismic record is not representing a complete cycle of large earthquakes.

## ACKNOWLEDGEMENTS

The authors are grateful to their organization for support of this research. The authors are thankful to the USGS, USA and Global Centroid-Moment-Tensor (CMT) Project resource persons; Prof. Göran Ekström, Prof. Meredith Nettles and Prof. Adam Dziewonski for earthquake catalogues. The authors are also thankful to Dr. J. R. Kayal and an anonymous reviewer for their useful comments and suggestions in improving the quality of the manuscript.

## Compliance with Ethical Standards

The authors declare that they have no conflict of interest and adhere to copyright norms.

## REFERENCES

Barenblatt, G.I., Keilis-Borok, V.I., and Monin, A.S., 1983. Filtration model of earthquake sequence, Dokl. Akad. Nauk. SSSR, v.269, no.4, pp: 831-834.

Benioff, V.H., 1951. Global strain accumulation and release as revealed by great earthquakes, Bull. Geol. Soc. Am., v.62, pp: 331–338.

Benioff, V.H., 1954. Evidence for world-strain readjustment following the Kamchatka earthquake of 4 November 1952, Bull. Geol. Soc. Am., v.65, pp: 1332–1333.

Bowman, D.D., and King, G.C.P., 2001. Accelerating seismicity and stress accumulation before large earthquakes, Geophys. Res. Lett., doi:10.1029/2001GL013022., v.28, pp: 4039-4042.

Bowman, D.D., Ouillon, G., Sammis, C.G., Sornette, A., and Sornette, D., 1998. An observational test of the critical earthquake concept, J. Geophys. Res.,v.103, no.B10, pp: 24359-24372.

Bufe, C.G., 1997. 1924–1994: evidence for a global moment release sequence, EOS Trans., Am. Geoph. Un., v.78, pp: F476.

Bufe, C.G., and Varnes, D. J., 1993. Predictive modeling of the seismic cycle of the Great San Francisco Bay region, J. Geophys. Res., doi:10.1029/93JB00357., v.98, pp: 9871–9883.

Bufe, C.G., and Perkins, D.M., 2005. Evidence for a Global Seismic-Moment Release Sequence, Bull. Seism. Soc. Am., v.95, no.3, pp: 833–843.

Cifuentes, I., and Silver, P., 1989. Low-frequency source characteristics of the Great 1960 Chilean earthquake, J. Geophys. Res., v.94, pp: 643–663.

Cox, C., and Chao, B. F., 2002. Detection of large-scale mass redistribution in the terrestrial system since 1998. Science, v.297, pp: 831-833.

Davies, G., and Brune, J., 1971.Regional and global fault slip rates from seismicity, Nature Phys. Sci., v.229, pp: 101-107.

Dickey, J.O., Marcus, S.L., Viron, Ode and Fukumori, I., 2002. Recent earth oblateness variations: unraveling climate and postglacial rebound effects, Science, v.298, pp: 1975-1977.

Dziewonski, A.M., Chou T-A and Woodhouse, J.H., 1981. Determination of earthquakes source parameters from waveform data for studies of global and regional seismicity, J. Geophys. Res., v.86, pp: 2825-2852.

Dziewonski, A.M., Ekstrom, G., and Maternovskaya, N.N., 2001. Centroid-moment tensor solutions for April-June 2000, Phys. Earth Planet. Inter., v.123, pp: 1-14.

Ekström G., Nettles M. and Dziewonski A.M., 2012. The global CMT project 2004-2010, centroid moment tensors for 13,017 earthquakes, Phys. Earth Planet. Inter., v.200-201, pp: 1-9.

Evison, F.F., 1982. Generalised precursory swarm hypothesis, J. Phys. Earth., v.30, pp: 155-170.

Gupta, H.K., 1992. Earthquake prediction related studies in India. Curr. Sci., v.62, no.1 and 2, pp: 257-263.

Gupta, H.K., and Singh, H.N., 1986. Seismicity of northeast India region. Part II: Earthquake swarm precursory to moderate magnitude to great earthquakes, J. Geol. Soc. India, v.28, pp: 367-406.

Gupta, H.K., and Singh, H.N., 1989. Precursory to moderate magnitude to great earthquakes in northeast India region, Tectonophysics, v.167, pp: 255-298.

Hamada, K., 1981. Current research in Earthquake Prediction, Development in Earth and Planetary Sciences, Part 2, (Ed. T. Rikitake) Centre for Academic Publications, Japan, pp: 221.

Hanks, T.C., and Kanamori, H., 1979. A moment magnitude scale, J. Geophys. Res., v.84, pp: 2348-2350.

Jaume, S.C., and Sykes, L.R., 1999. Evolving towards a critical point: a review of accelerating seismic moment/energy release rate prior to large and great earthquakes, PAGEOPH., doi:10.1007/s000266., v.155, pp: 279-305.

Kagan, Y.Y., and Jackson, D.D., 1991. Long-term earthquake clustering, Geophys. J. Int., v.104, pp: 117-133.

Kanamori, H., and Anderson, D.L., 1975. Theoretical basis of some empirical relations in seismology, Bull. Seismo. Soc. Am., v.65, pp: 1073-1095.

Keilis-Borok, V.I., 1990. The lithosphere of the Earth as a nonlinear system with implications for earthquake prediction, Rev. Geophys., v.28, no.1, pp: 19-34.

Keilis-Borok, VI, 2002. Earthquake prediction: state-of-the-art and emerging possibilities, Annual Rev. Earth Planet. Sci., v.30, pp: 1-33.

Liu, M., Stein, S., and Wang, H., 2011. 2000 years of migrating earthquakes in North China: How earthquakes in midcontinents differ from those at plate boundaries, Lithosphere, doi:10.1130/L129.1., v.3, no.2, pp: 128-132.

Mogi, K., 1969. Some features of the recent seismic activity in and near Japan: 2. Activity before and after great earthquakes, Bull. Earthquake Res. Inst., Univ. Tokyo, v.47, pp: 395–417.

Mogi, K., 1974. Active periods in the world's chief seismic belts, Tectonophysics, v.22, pp: 265–282.

Mogi, K., 1979. Global variation of seismic activity, Tectonophysics,v.57, pp: 43–50.

Pacheco, J.F. and Sykes, L.R. 1992. Seismic moment catalog of large shallow earthquakes, 1900 to 1989, Bull. Seism. Soc. Am., v.82, pp: 1306-1349.

Piersanti, A., Spada, G., Sabadini, R., and Bonafede, M., 1995. Global postseismic deformation, Geophys. J. Int., v.120, pp: 544–566.

Pollitz, F.F., Burgmann, R., and Romanowicz, B., 1998. Viscosity of oceanic asthenosphere inferred from remote triggering of earthquakes, Science, v.280, pp: 1245–1249.

Press, F., and Allen, C., 1995. Patterns of seismic release in the southern California region, J. Geophys. Res., v.100, no.B4, pp: 6421-6430.

Romanowicz, B., 1993. Spatiotemporal patterns in the energy release of great earthquakes, Science, v.260, pp: 1923-1926.

Simpson, R.W., and Reasenberg, P.A., 1994. Prof. Pap, U. S. Geol. Surv., Washington D.C., v.1550-F, pp: 55-89.

Sobolev, G.A., and Tyupkin, Y.S., 1999. Precursory phases, seismicity precursors, and earthquake prediction in Kamchatka, J. Volcano Seismo., v.20, pp: 615–627.

Sornette, A., and Sornette, D., 1990. Earthquake rupture as a critical point: Consequences for telluric precursors, Tectonophysics., doi:10.1016/0040-1951(90)90298-M., v.179, pp: 327–334.

Sornette, D., and Sammis, C.G., 1995. Complex critical exponents from renormalization group theory of earthquakes: Implications for earthquake predictions. J. Phys. I., doi:10.1051/jp1:1995154., v.5, pp: 607-619.

Stein, S., and Okal E.A., 2007. Ultralong Period Seismic Study of the December 2004 Indian Ocean Earthquake and Implications for Regional Tectonics and the Subduction Process, Bull. Seism. Soc. Am., doi:10.1785/0120050617., v.97, no.1A, pp: S279–S295.

Sykes, L.R., and Jaume S., 1990. Seismic activity on neighboring faults as a long term precursor to large earthquakes in the San Francisco Bay area, Nature, doi:10.1038 /348595a0., v.348, pp: 595–599.

Tsai, V.C., Nettles, M., Ekström. G, and Dziewonski, A.M., 2005. Multiple CMT source analysis of the 2004 Sumatra earthquake, Geophys. Res. Letts., doi:10.1029/2005 GL023813., v.17, pp: L17304.

Turcotte, D.L., Newman, W.I., and Gabrielov, A., 2000. A statistical physics approach to earthquakes, In Geocomplexity and the Physics of Earthquakes, Am. Geophy. Un., Washington D.C.

Wyss, M., and Habermann, R.E., 1988. Precursory seismic quiescence, PAGEOPH., doi:10.1007/BF00879001., v.126, pp: 319-332.

J. Ind. Geophys. Union ( May 2016 )
**v.20, no.3, pp: 325-333**

# A statistical study of TEC anomalies induced by major earthquakes occurred around Indian Subcontinent

**Devbrat Pundhir*[1,3], Birbal Singh[1], O. P. Singh[2] and Saral Kumar Gupta[3]**

[1]Department of Electronics & Communication Engineering, R. B. S. Engineering Technical Campus, Bichpuri, Agra, India-283105
[2]Department of Physics, R. B. S. Engineering Technical Campus, Bichpuri, Agra, India-283105
[3]Department of Physics, Banasthali Vidyapith, Banasthali, Rajasthan, India-304022
*Corresponding Author: devbratpundhir@gmail.com

**ABSTRACT**

The GPS based TEC measurements have been in progress at Bichpuri, Agra station (27.2° N, 78° E) in India since 1 April 2006 using a dual frequency GPS-receiver. In the present paper, we analyze the TEC data for the period of April-September 2013 to examine the anomalous variations as precursors corresponding to some major earthquakes (M > 6) that occurred during this period in the Indian subcontinent. We processed the data using well known mean (m) and standard deviation around the mean (σ) criterion to see the anomalous variations as precursors in the form of enhancements above the upper limit (m + σ). Then we found the correlation coefficients between magnitude of earthquakes and precursory days and average TEC enhancement, respectively. We found significant correlation coefficients in the two cases. Finally, we tested the null hypothesis for pairs, which have the maximum and minimum values of correlation coefficients. In this way, the precursory days and corresponding TEC anomalies are fixed for the earthquakes. The concepts of E × B drift mechanism and Global Electric Circuit (GEC) are invoked to explain the ionospheric precursors of earthquakes.

**Key words**: Multiple earthquakes; GPS-TEC; correlation coefficients; null hypothesis; E × B drift; Global Electric Circuit (GEC) .

## INTRODUCTION

In the recent past, several researchers have studied GPS-TEC anomalies related to earthquakes and their results have shown unusual precursors as enhancements or depletions in TEC prior to the earthquakes (Calais and Minster, 1995; Liu et al., 2000, 2001, 2002, 2004a, b, 2008, 2009; Pulinets et al., 2007; Dautermann et al., 2007, Zhao et al., 2008). Reviews on early studies have been presented by Pulinets (2004) and Pulinets and Boyarchuk (2004) and on recent studies by Pulinets and Davidenko (2014). Generally, it has been found that such ionospheric precursors show a temporal variation by occurring not only on a single day but on few different days prior to the main shock. For example Liu et al., (2001) analyzed the GPS based TEC data prior to occurrence of Chi-Chi earthquake and found significant precursors on 1, 3 and 4 days prior to the occurrence of earthquake (M = 7.7). Similarly, Liu et al., (2004a) examined pre-earthquake ionospheric data of GPS-TEC and identified the precursors on different days in the interval of 1-5 days prior to the earthquakes. Recently, Kon et al., (2011) analyzed global ionospheric maps (GIMs) data for 12 years to see the effect of earthquakes. They found that the ionospheric anomalies occurred on different days in the interval of 1-5 days before the occurrence of all earthquakes. More recently, Pundhir et al., (2014) have examined the effect of a major earthquake on GPS-TEC observed at Agra station (27.2° N, 78° E) and found the precursory period of 1-9 days prior to the main shock.

While intermittent appearance of anomalies before the major shock is normally interpreted in terms of processes in the earthquake preparation zone and resulting electric field penetration in the ionosphere (Pulinets, 2004), there is a possibility that some of the anomalies might be caused by other factors as well. For example, there are evidences that magnetic storm induced electric field may penetrate the ionosphere and magnetosphere at low latitudes a few days late and play useful role in ionospheric dynamics (Jain et al., 1977; Lakshmi et al., 1983, 1997). It is also known that day to day variability in $foF_2$, which is not related to any solar geophysical phenomenon is also very large at low latitudes. Other factors influencing the ionospheric precursors may include volcanic activities, nuclear explosions, and dust storms ,which may cause drop of atmospheric conductivity (what is equivalent to the column resistance increase) leading to increase in earth-ionosphere potential and appearance of local positive TEC anomalies (Pulinets and Davidenko, 2014). In order to reach a definite conclusion of whether the ionospheric anomalies are produced by earthquakes or by other factors, it is worthwhile to examine them by carrying out extensive correlation studies and significant statistical tests.

In the present paper, we consider five major earthquakes (M > 6) which occurred in Indian subcontinent between

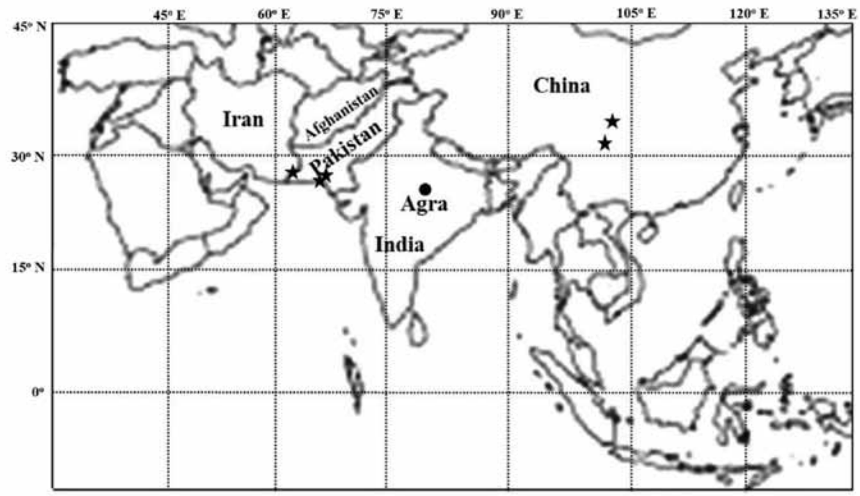


**Figure 1.** The map of India and its surrounding countries indicating the epicenters of earthquakes (by star). The solid circle shows the location of TEC observing station Agra in India.

**Table 1.** Details of Major Earthquakes during the period of April to September 2013 in neighbouring countries around India.

| Sl. No. | Date of Earthquake | Time (UT) | Lat. (deg.) | Long. (deg.) | Depth (km) | Magnitude | Region | Radius of Influence Zone (km) |
|---|---|---|---|---|---|---|---|---|
| 1 | 16/04/2013 | 10:44:11 | 28.0°N | 62.1°E | 46 | 7.8 | Pakistan-Iran Border | 2259.4 |
| 2 | 20/04/2013 | 00:02:48 | 30.2°N | 103.0°E | 29 | 6.6 | Sichuan, China | 688.7 |
| 3 | 21/07/2013 | 23:45:56 | 34.5°N | 104.2°E | 10 | 6.2 | Gansu, China | 463.4 |
| 4 | 24/09/2013 | 11:29:48 | 27.0°N | 65.7°E | 10 | 7.4 | Pakistan | 1520.5 |
| 5 | 28/09/2013 | 07:34:10 | 27.2°N | 65.9°E | 20 | 6.8 | Pakistan | 839.5 |

April and September 2013, and examine the effect of these earthquakes on TEC data observed at Agra station. Initially, we ascertain their character as precursors by applying mean and standard deviation criterion and then calculate the correlation coefficients between magnitude of earthquakes, precursory days, and average TEC enhancements to confirm ionospheric precursors of earthquakes. Finally, we test our results by applying null hypothesis.

## Experimental setup and method of analysis

The experimental setup used for TEC measurements at Agra station is similar to that used by our group earlier (Singh et al., 2009). The GPS receiver and antenna are placed in the seismo-electromagnetic and space research laboratory in the Faculty of Engineering building at Bichpuri Campus of our college and round the clock observations are taken. Bichpuri is located in rural area about 12 km west of Agra city where local electrical and electromagnetic disturbances are extremely low. We have used the well-developed statistical $\sigma$ criterion to analyze the TEC data for the months of April, July and September 2013 (in which the major earthquakes occurred) to find the anomalous variation in data and also calculate the corresponding mean and standard deviation for each month separately. Further, we have calculated the sum ($m + \sigma$) and difference ($m - \sigma$) of mean and standard deviation, respectively. Then, we have found the correlation coefficients between magnitude of earthquakes and precursory days, and between magnitude of earthquakes and average enhancement of TEC data, respectively. Finally, we have tested the null hypothesis using 't' test for the pairs, which have shown the maximum positive and maximum negative correlation coefficients.

## RESULTS AND DISCUSSION

Figure 1 shows the map of Indian subcontinent in which the stars indicate the location of earthquakes and solid circle indicates the location of observing station Agra (27.2° N, 78° E). The details of these earthquakes are mentioned in Table 1. Details include the days of occurrence, magnitudes, depths (km), locations (Latitude and Longitude in degrees), radius of influence zone (km) and distances from the Agra station (km). The details of the earthquake data have been taken from United States Geological Survey (USGS) website www.earthquake.usgs.gov.in. The radius of influence zone is calculated by using the expression $R = 10^{0.43M}$, where M is the magnitude of the earthquake (Dobrovolsky et al., 1979). Although these earthquakes have occurred far away from the observing station Agra, at least two of them cover the observing station very well through large radii of influence zone (> 1000 km). However, the effect of smaller earthquakes (7 > M > 6) on the ionosphere considered here cannot be ruled out because there are several satellite based observations showing large ionospheric perturbation zones ranging between ± 5° to ± 30° longitudes around the epicenters of the earthquakes (Galperin et al., 1992; Molchanov et al., 1993; Sorokin and Chmyrev, 1999). In the light of these results the consideration of all the earthquakes including those of M = 6.2, 6.6, and 6.8 in this paper is highly justified. To support our selection of earthquakes, it may be mentioned that many researchers have investigated the earthquakes of even moderate and low magnitudes that are far away from the observing stations (> 1000 km). For example, Dabas et al., (2007) have presented the variations of $foF_2$ and TEC data observed at Delhi station in relation to earthquakes, which occurred in the North-East countries around India. In a similar way, Singh et al., (2012) have also investigated $foF_2$ variations using the multi-instruments at Varanasi and Delhi stations to see the effect of earthquakes varying in magnitude between 5 and 7.5 on Richter scale. Most of the earthquakes have occurred in China, Myanmar, Indonesia and Japan. Zhao et al., (2008) and Liu et al., (2010) have also found that the ionospheric anomalies may extend to adjacent region around the epicenter. By adjacent region, they possibly mean the large perturbation zones, as stated above. We have also seen the variations of geomagnetic parameters such as Dst index and ∑Kp for each case separately for which data have been taken from the website http://omniweb.gsfc.nasa.gov/form/dx1.html. We can see from Table 1 that all the earthquakes have shallow focal depths except one of them. The earthquake with 46 km focal depth has not been ignored as this earthquake is of relatively large magnitude (M = 7.8). Two of the earthquakes occurred in the month of April, one in July, and rest of the two in September, 2013.

The top two panels of Figure 2 show the day to day variation of GPS-TEC for the month of April 2013, as observed at Agra station. Here, the vertical-TEC is shown in blue colour and the corresponding sum (m + σ) and difference (m – σ) are shown in red and green colours respectively. The days of occurrence of the two earthquakes are shown by solid black stars. The variation of Dst and ∑Kp Indices are shown in bottom two panels respectively, for the period under consideration. The major enhancements in the data can be seen clearly on 9, 16 and 29 April. Since Agra station lies between the epicenters of the two earthquakes under consideration the influence of both the earthquakes on TEC enhancements on 9 and 16 April cannot be ruled out, although the effect of larger earthquake of magnitude M = 7.8 is expected to be more than that of the smaller magnitude earthquake because of varying influence zone. Here, we consider two separate cases for each of the two earthquakes causing the enhancements in TEC over Agra station and hence, as shown in table 2, the precursory periods for the earthquake of magnitude M = 7.8 will be 0 and 7 days, whereas those for the earthquake of magnitude M = 6.6 will be 4 and 11 days. It may be seen from bottom two panels of Figure 2 that these periods are magnetically quiet and hence the ionospheric perturbations may be caused solely due to earthquakes. The enhancement on 29 April may be due to isolated geomagnetic storm on 24 April (∑Kp > 30). The minor depletions and enhancements have also been seen throughout the month but they are insignificant.

Figure 3 (top two panels) shows the variations of GPS-TEC for the month of July 2013 and the bottom two panels show the variation of Dst and ∑Kp data. The other descriptions are same as mentioned in preceding Figure. From table 1 and Figure 3 it may be seen that an earthquake of magnitude M = 6.2 occurred on 21 July 2013 in China and the enhancements in the TEC data crossing the upper bound (m + σ) occurred on 6, 7, 13 and 19 July. Further, it may be seen from the bottom panels that sporadic magnetic storms (∑Kp ≥ 40) occurred on 6, 10 and 14 July also. Now, we need to explain these enhancements in the light of magnetic storms and earthquakes. The possibility of enhancements on 6 and 7 July may be due to relatively large geomagnetic storm on 6 July (Dst ≈ -60nT and ∑Kp ≥ 40). This needs to be explained as follows; Usually, over the equatorial and low latitudes, the main phase (MP) of the magnetic storm is characterized by negative storm (depletion in TEC) and recovery phase (RP) is characterized by the positive storm i.e. large enhancement in TEC. The TEC enhancements observed on 6 and 7 July correspond to recovery phase of the magnetic storm on 6 July as found from the examination of hourly Dst data, where recovery phase starts in the evening of 6 July itself. The enhancements of 13 July may also be influenced by the magnetic storm of 10 July (Dst ≈ -40nT and ∑Kp ≥ 40) as effect of magnetic storms may take few days to one week to reach the low latitude ionosphere (Jain et al., 1977; Lakshmi et al., 1997). So, we neglect these enhancements from our analysis. The enhancement of 19 July may possibly be due to combined effect of magnetic storm of 14 July (Dst ≈ -40nT and ∑Kp ≥ 37) and precursory effect of the earthquake on 21 July, as it is difficult to attribute the cause of this anomaly to a single source. However, the possibility of this anomaly due to earthquake is larger because of its large magnitude and shallow depth. The effect of magnetic storm may not be as large as that of the earthquake because it is not so severe and also occurred 5 days before the ionospheric anomaly. In contrast to this, the other magnetic storms of 6 July and 10 July considered in this paper are relatively stronger and they occurred less than 3 days before the anomalies. Although, the earthquake is also of relatively smaller

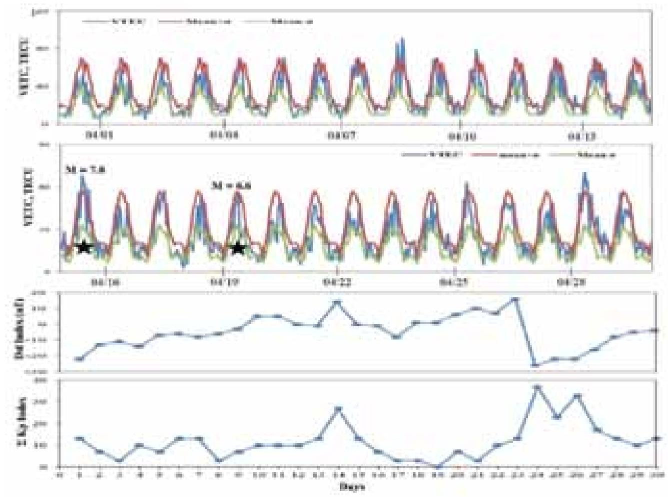


**Figure 2.** Two top panels show the variation of GPS-TEC for the period of April 2013, in blue colour. The corresponding deviations m + σ, and m – σ are shown in red, and green colours, respectively. The black stars show the days of earthquakes. The variation of Dst and Σ Kp Indices are shown in the lower two panels.

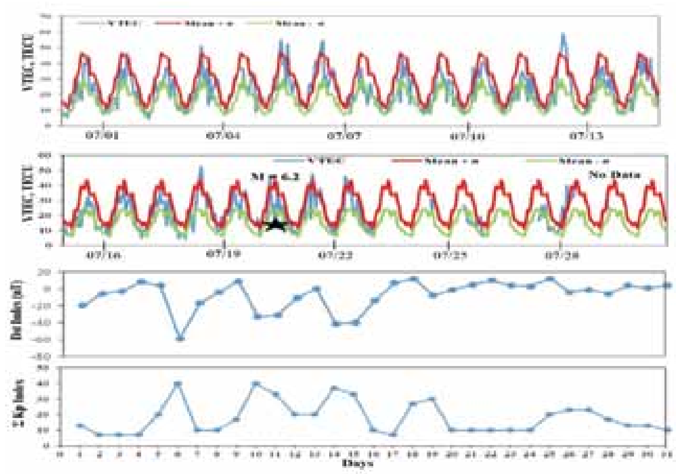


**Figure 3.** Similar as Figure 2 but for the month of July 2013 in which an earthquake of magnitude M = 6.2 occurred.

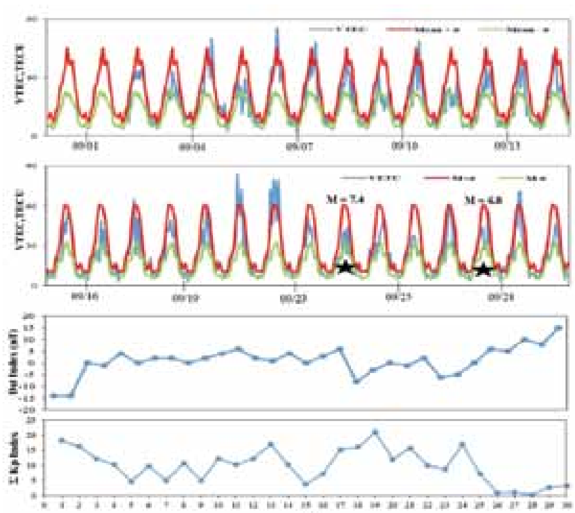


**Figure 4.** Similar to Figure 2 but for the month of September 2013 in which earthquakes of magnitudes M = 7.4 and 6.8 occurred.

magnitude, as it is greater than 6 its effect may extend to large ionospheric perturbations zones as stated earlier. The minor enhancements and depletions have also occurred on other days in this month but they are insignificant as compared to these enhancements.

The top two panels of Figure 4 show the variation of GPS-TEC at observing station Agra. They correspond to the earthquakes that occurred in the month of September 2013. The bottom two panels show the variations of Dst and ∑Kp index as usual to examine the effect of geomagnetic storm. From Table 1 and Figure 4 it may be seen that a large earthquake of magnitude M = 7.4 occurred on 24 September, followed by another large magnitude earthquake (M = 6.8) on 28 September. From Figure 4 it may be seen that unusually large TEC enhancements crossing ($m + \sigma$) limit occurred on 7, 21 and 22 September. We also see some minor enhancements and depletions in the data in this month but they are insignificant. This month was magnetically quiet as ∑Kp remained less than 20 throughout. This case is simpler to interpret in terms of the precursory effect of earthquakes on 24 and 28 September because no magnetic storm occurred in this month. The effects of these earthquakes are pronounced as compared to those occurred in April because these are shallower (depth < 20 km) earthquakes. As shown in table 2 the precursory periods of the larger earthquake (M = 7.4) are 17, 3, and 2 days. The earthquake of magnitude M = 6.8 seems to be an aftershock of the earlier one because of its close location and short period of occurrence from the main shock of M = 7.4. Hence, its effect on the ionosphere over Agra may possibly be a combined effect of both the earthquakes (as considered for the April earthquake). In the light of this, precursory period of 4 days is added to the earlier one for this earthquake.

The three panels of Figure 5 show the days of occurrence and magnitude of earthquakes (by histograms) and days of precursors in TEC enhancements (by arrows) so that we may have clear information about the magnitude of earthquakes and corresponding precursory days for the three months of data under study. These data are presented column-wise in table 2 also. Now, we make pairs between columns of earthquakes and columns containing different enhancements in TEC data and different precursory days as shown in table 2 and calculate correlation coefficients. Here, it may be noted that for those columns in which there is no data, we have taken the data of previous columns one after the other to calculate the correlation coefficients. This has been done simply to fill up the gaps with the observed data corresponding to the same earthquake for the purpose of mathematical convenience. Then from the results of calculated correlation coefficients (C.C.) we select two columns, one for enhancements giving largest positive correlation coefficient and the other for precursory days giving most negative correlation coefficient. The selection of these two columns is based on the assumption that the enhancements in TEC increase and precursory days decrease with the increasing magnitude of the earthquakes. The results of this exercise are shown in table 3 in which the columns of average TEC enhancements giving a correlation coefficient of 0.98 and the same of precursory days giving a correlation coefficient of -0.52 are shown.

The results are also shown graphically in Figure 6 where solid triangles show the increasing TEC enhancements and solid squares show the decreasing relation between precursory days with increasing magnitude of earthquakes. In other words, the enhancements in TEC increase with the increase in the magnitude of the earthquake, whereas the precursory days decrease with increase of the magnitude of the earthquake. Finally, we find the probability (p) for these pairs to test the null hypothesis using 't' test. The results of probability are also shown on the bottom of table 3. The value of probability for the average TEC enhancements is less than 0.05 or 5%. It shows that our results are significant and null hypothesis is satisfied. On the other hand, the probability of 0.37 for precursory days is large but it may be considered as significant especially for geophysical measurements like this.

We have also calculated the correlation coefficient between one case of magnetic storm of Figure 2 and three cases of Figure 3 (total four cases) and corresponding average TEC enhancements and found a positive correlation of 0.86. This result supports our argument that the enhancements in TEC on the days after the earthquakes in April and prior to the earthquake in July are caused by magnetic storms. Such an exercise cannot be done for effective days of the storm because of uncertainty of penetration characteristics of the electric field in the low latitude ionosphere (Jain et al., 1977; Lakshmi et al., 1983).

Now, the question arises how these earthquake-induced anomalous enhancements have occurred in the TEC data at low latitudes. Several mechanisms have been suggested by the researchers but none of them has received proper approval from the global scientific community. However, there is a growing consensus that it is due to $E \times B$ drift mechanism, where the electric field (E) triggered by an earthquake preparatory process penetrates the ionosphere and, in the presence of local magnetic field (B), causes upward or downward movement of the ionization depending upon the direction of the electric field (Depueva and Ruzhin, 1993). Then, the question remains about the mechanism of the electric field generation from the earthquake region. Pulinets (2004) has suggested that radon emissions come out from earthquake epicentral region, and ionize the near earth atmosphere over the seismic zones that lead to formation of quasi-neutral ion clusters, which are destroyed by the air motion caused by acoustic gravity waves generated by accumulation of greenhouse gases over the seismic region. The breaking of ion clusters

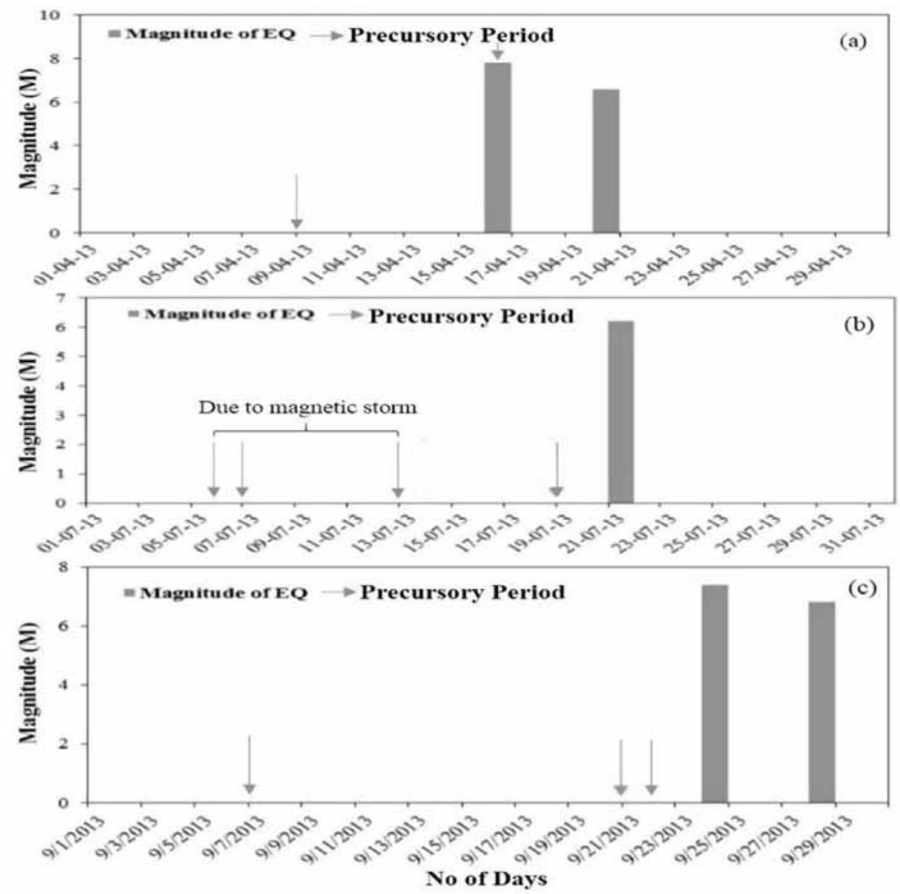


**Figure 5.** The three panels show the histograms of magnitude of earthquakes and corresponding days of anomalies (shown by downward arrows) for the three months of April, July, and September, 2013.

**Table 2.** Details of average TEC enhancements and precursory days corresponding to earthquakes occurred.

| Sl. No. | Magnitude | Average TEC Enhancements (TECU) | | | Precursory days | | |
|---|---|---|---|---|---|---|---|
| 1 | 7.8 | 10.5 | 4.8 | --- | 0 | 7 | --- |
| 2 | 6.6 | 10.5 | 4.8 | --- | 4 | 11 | --- |
| 3 | 6.2 | 3 | --- | --- | 2 | --- | --- |
| 4 | 7.4 | 7.18 | 9.31 | 11.9 | 17 | 3 | 2 |
| 5 | 6.8 | 7.18 | 9.31 | 11.9 | 21 | 7 | 6 |

**Table 3.** Results of correlation coefficients and probability showing most significant data on TEC enhancements and precursory days.

| Sl. No. | Earthquake magnitude | Average TEC enhancements (TECU) giving most positive C. C. | Precursory days giving most negative C. C. |
|---|---|---|---|
| 1 | 7.8 | 10.5 | 0 |
| 2 | 6.6 | 4.8 | 4 |
| 3 | 6.2 | 3 | 2 |
| 4 | 7.4 | 9.31 | 2 |
| 5 | 6.8 | 7.18 | 6 |
| **C.C.** | | 0.98 | -0.52 |
| **Probability (p)** | | 0.003 | 0.37 |

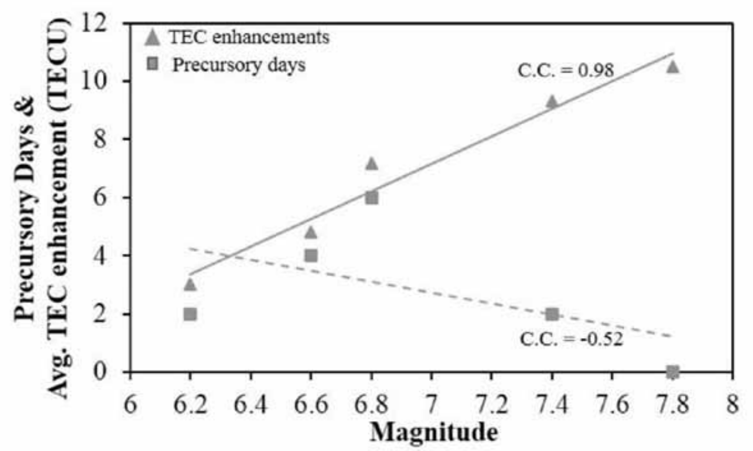


**Figure 6.** Variation of anomalous TEC enhancements (shown by solid triangles) and precursory days (shown by solid stars), with increasing magnitude of earthquakes. The continuous and dashed lines correspond to the positive and negative values of the correlation coefficients.

makes the near ground layer of the atmosphere rich in ion (concentration $\approx 10^5 - 10^6$ $cm^{-3}$). The charge separation process leads to generation of anomalously strong vertical electric field ($\approx$1KV$m^{-1}$) in comparison with the fair weather electric field ($\approx$ 100 V$m^{-1}$). Pulinets (2009) provides the explanation of the existence of a vertical atmospheric electric field and coupling between the ground and ionosphere using the concept of Global Electric Circuit (GEC). In brief, Global Electric Circuit (GEC) is the system of quasi-stationary electric current between ground and ionosphere driven by global thunderstorm activity and works in transmitting the information from ground surface up to the ionosphere through the changing of its electric properties due to natural ionization and ion induced nucleation changing the conductivity of atmosphere.

In addition to the electric field generation mechanism mentioned as above, more convincing mechanism has been proposed by some researchers recently. For example Oyama et al., (2011), while interpreting the anomalous trough (precursor ionization anomaly, PIA) in the variations of atomic oxygen ion ($O^+$) and molecular ion observed by DE-2 satellite over the epicenter of a large magnitude earthquake (M = 7.5) suggested that the PIA trough was caused by lifting the plasma upward by eastward electric field, which was possibly generated as a result of disturbing the dynamo wind by internal gravity waves in the E-region of the ionosphere. This trough was in addition to the usual trough at the magnetic equator due to equatorial ionization anomaly (EIA). Sun et al., (2011) also supported a similar mechanism and, in order to support it, they studied the relationship between the height profile of neutral temperature (Tn) and critical frequency of F-layer ($foF_2$) for two large earthquakes, the Wenchuan (M = 7.9) and Pungtung Doublet (M = 6.9) occurred on 12 May, 2008 and 26 December, 2006 ,respectively. They found a clear relation between the $foF_2$ and the intensity of the amplitude with a vertical wavelength of 22-30 km in Tn height profiles suggesting that the electric field is generated in the E-region of the ionosphere under the influence of internal gravity waves.

Since there were no other factors like nuclear explosions, volcanic activities, and dust storms during this period of observations in the region of the earthquakes, the anomalous variations in TEC cannot be attributed to these factors. The only reason for anomalies has been caused by the occurrence of earthquakes. This fact is supported by statistical analysis also.

In our results presented above, we have found the enhancements in TEC as the precursors of major earthquakes in Indian subcontinent but these results are in contrast with the results of other researchers ,who have found the depletions also (Liu et al., 2004a, b, and 2009). This contrast in results may be due to latitude dependence and the enhancements in TEC data caused by the upward electric field that penetrated the ionosphere eastward, according to the mechanism mentioned above.

## CONCLUSIONS

In this paper, we have analyzed six months of GPS-TEC data observed at Agra station between April-September, 2013 in order to examine the effect of the earthquakes on the diurnal variation of TEC data. We have found that during months of April, July, and September five major earthquakes (M > 6) have occurred around India.Hence, detailed analysis of TEC data corresponding to these months have been undertaken. We have found significant enhancements in TEC 1-21 days prior to the earthquakes. The enhancements are examined in the light of magnetic storm data (Dst and $\sum$Kp) also and those affected by such storms are ignored. Then we have calculated correlation coefficients between magnitude of the earthquake and enhancements in TEC and also between magnitude of the earthquakes and precursory period. Finally, we have tested the null hypothesis. The overall results of the exercise show that there clearly exists a positive correlation between magnitude of the earthquakes and enhancements in TEC.

## ACKNOWLEDGEMENTS

The authors are thankful to Department of Science and Technology and Ministry of Earth Sciences, Government of India, New Delhi for financial support. Authors thank anonymous reviewers for valuable inputs. They also thank the Chief Editor for refining the manuscript at editing stage.

## Compliance with Ethical Standards

The authors declare that they have no conflict of interest and adhere to copyright norms.

## REFERENCES

Calais, E., and Minster, J.B., 1995. GPS detection of ionospheric TEC perturbations following the January 17, 1994, Northridge earthquake, Geophys. Res. Lett., v.22, pp: 1045-1048.

Dabas, R.S., Das, R. M., Sharma, K., and Pillai, K.G.M., 2007. Ionospheric pre-cursors observed over low latitudes during some of the recent major earthquakes, J. Atmos. Solar Terr. Phys., v.69, no.15, pp: 1813–1824.

Dautermann, T., Calais, E., Haase, J., and Garrison, J., 2007. Investigation of ionospheric electron content variations before earthquakes in southern California, 2003–2004. J Geophys. Res. (USA), v.112, no. B02106.

Depueva, A.H., and Ruzhin, Y.Y., 1993. The equatorial earthquake preparatory stage as a reason of fountain effect in the ionosphere, Preprint IZMIRAN, N82 (1029), pp: 10.

Dobrovolsky, I. P., Zubkov, S. I., and Miachkin, V. I., 1979. Estimation of the size of earthquake preparation zones, Pure Appl. Geophys., v.117, pp: 1025–1044.

Galperin, Y. I., Gladyshev, V.A., Jordjio, N.V., and Larkina, V.I., 1992. Precipitation of High- Energy Captured Particles in the Magnetosphere Above the Epicenter of an Incipient Earthquake, Cosmic Res., v.30, pp: 89-106.

Jain, S.K., and Singh, B., 1977. Vertical motions of the low and equatorial-latitude F2 layers during prolonged and isolated magnetic storms, J. Geophys. Res., v.82, pp: 723-726.

Kon, S., Nishihashi M., and Hattori, K., 2011. Ionospheric anomalies possibly associated with M > 6.0 earthquakes in the Japan area during 1998–2010: Case studies and statistical study, J. Asian Earth Sci., v.41, pp: 410–420.

Lakshmi, D.R., Reddy, B.M., and Sastri, S., 1983. A prediction model for equatorial low latitude HF communication parameters during magnetic disturbances, Ind. J. Radio Space Phys. (India), v.12, pp: 1-18,.

Lakshmi, D.R., Veenadhari, B., Dabas, R.S., and Reddy, B.M., 1997. Sudden post-midnight decreases in equatorial in F-region electron densities associated with severe magnetic storms, Ann. Geophysicae, v.15, pp: 306-313.

Liu, J.Y., Chen, Y.I., Pulinets, S.A., Tsai, Y.B., and Chuo, Y.J., 2000. Seismo –ionospheric signatures prior to M ≥ 6.0 Taiwan earthquakes, Geophys. Res. Lett., v.27, pp: 3113–3116.

Liu J. Y., Chen, Y. I., Chuo, Y. J., and Tsai, H. F., 2001. Variations of ionospheric total electron content during the Chi-Chi earthquake, Geophys. Res. Lett., v.28, pp: 1383–1386.

Liu, J. Y., Y. I. Chen, H. K. Jhuang, and Y. H. Lin, 2004a. Ionospheric $foF_2$ and TEC anomalous days associated with M ≥ 5.0 earthquakes in Taiwan during 1997–1999, Terr. Atmos. Oceanic Sci., v.15, pp: 371– 383.

Liu, J. Y., Chuo, Y. J., Shan, S. J., Tsai Y. B., Chen, Y. I., Pulinets S. A., and Yu S. B., 2004b. Pre-earthquake ionospheric anomalies registered by continuous GPS TEC measurements, Ann. Geophysicae, v.22, pp: 1585–1593.

Liu, J.Y., Chen, S.W., Chen, Y.C., Yen, H.Y., Chang, C.P., Chang, W.Y., Tsai, L.C., Chen, C.H., and Yang, W.H., 2008. Seismo - ionospheric precursors of the 26 December 2006 M 7.0 Pingtung earthquake doublet, Terr. Atmos. and Oceanic Sci., v.19, pp: 751–759.

Liu, J. Y., Chen Y. I., Chen C. H., Liu C. Y., Chen C. Y., Nishihashi M., Li J. Z., Xia Y. Q., Oyama, K. I., Hattori, K., and Lin, C. H., 2009. Seismoionospheric GPS total electron content anomalies observed before the 12 May 2008 Mw7.9 Wenchuan earthquake, J Geophys. Res. (USA), v.114, no. A04320, pp: 1-10.

Liu, J.Y., Chen, C.H., Chen, Y.I., Yang, W.H., Oyama, K.I., and Kuo, K.W., 2010. A statistical study of ionospheric earthquake precursors monitored by using equatorial ionization anomaly of GPS TEC in Taiwan during 2001–2007, J. Asian Earth Sci., v.39, pp: 76-80.

Molchanov, O.A., Mazhaeva, O.A., Golyavin, A.N., and Hayakawa, M., 1993. Observation by the Intercosmos-24 satellite of ELF-VLF electromagnetic emissions associated with earthquakes, Ann. Geophysicae, v.11, pp: 431-440.

Oyama, K. I., Kakinami, Y., Liu, J. Y., Abdu, M. A., and Cheng, C. Z., 2011. Latitudinal distribution of anomalous ion density as a precursor of a large earthquake, J. Geophys. Res., v.116, no. A04319.

Pulinets, S., 2004. Ionospheric Precursors of Earthquakes; Recent Advances in Theory and Practical Applications, Terr. Atmos. and Oceanic Sci., v.15, no.3, pp: 413-435.

Pulinets, S., and Boyarchuk, K., 2004. Ionospheric Precursors of Earthquakes, Springer.

Pulinets, S.A., Kotsarenko, A.N., Ciraolo, L., and Pulinets, I.A., 2007. Special case of ionospheirc day- to - day variability associated with earthquake preparation, Adv. in Space Res., v.39, pp: 970–977.

Pulinets, S. A., 2009. Physical mechanism of the vertical electric field generation over active tectonic faults, Adv. in Space Res., v.44, pp: 767-773.

Pulinets, S. A., and Davidenko, D., 2014. Ionospheric precursors of earthquakes and Global Electric Circuit, Adv. in Space Res., v.53, pp: 709-723.

Pundhir, D., Singh, B., and Singh, O.P., 2014. Anomalous TEC variations associated with the strong Pakistan-Iran border region earthquake of 16 April 2013 at a low latitude station Agra, India, Adv. in Space Res., v.53, pp: 226–232.

Singh, A.K., Kumar, S., Singh, R., Singh, A.K., 2012. Pre-Earthquake Ionospheric Anomalies Observed using Ground Based Multi-Instruments", Int. J. Adv. Earth Sci., v.1, no.1, pp: 13-19.

Singh, O.P., Chauhan V., Singh, V., and Singh, B., 2009. Anomalous variation in Total electron content (TEC) associated with earthquake in India during September 2006 – November 2007, J Phys Chem Earth, v.34, pp: 479-484.

Sorokin, V.M., and Chmyrev, V.M., 1999. The Physical Model of Electromagnetic and Plasma Response of the Ionosphere on the Pre-Earthquake Processes, Ed. M. Hayakawa (TERRAPUB), pp: 819-828.

Sun, Y. Y., Oyama, K. I., Liu, J. Y., Jhuang, H. K., and Cheng, C. Z., 2011. The neutral temperature in the ionospheric dynamo region and the ionospheric F region density during Wenchuan and Pingtung Doublet earthquakes, Nat. Hazards Earth Syst. Sci., v.11, pp: 1759–1768.

Zhao, B., Wang, M., Yu, T., Wan, W., Lei, J., Liu, L., and Ning, B., 2008. Is an unusual large enhancement of ionospheric electron density linked with the 2008 great Wenchuan earthquake? J Geophys. Res. A: Space Phys, v.113, no. A11304.

J. Ind. Geophys. Union ( May 2016 )
**v.20, no.3, pp: 334-341**

# Structural Inferences from Radiometric Surveys in and around Ramadugu Lamproite Field, NW margin of the Cuddapah basin, Eastern Dharwar craton

**G.Sri Ramulu, G.Ramadass and B.Veeraiah***

Center of Exploration Geophysics, Osmania University, Hyderabad-500 007, India
*Corresponding Author: veer.cegou@gmail.com

**ABSTRACT**

An attempt has made to map radiometric intensity over a part of the Ramadugu, Vattikod, and Somvarigudem lamproite fields of Nalgonda District, Telangana State, North Western margin of the Cuddapah basin and their relationship with geological structures and tectonics.

Interpretation of radiometric data brought out the structural features, trends, faults and contacts corresponding to the lithological formations observed in the area. The formations are amphibolites, schists, biotite gneisses, granites, granodiorites and dolerites. They are qualitatively inferred from the radiometric map, which may enable more precise geological mapping of these formations. A geological map of the study area with observed radioactivity of each formation is presented. The corresponding radioactivity for amphibolites, schist, biotite gneiss, granites, granodiorite, quartz vein and dolerites are 23.15 $\mu$R/hr (22.87 $\mu$R/hr to 23.4 $\mu$R/hr), 22.77 $\mu$R/hr (20.94 $\mu$R/hr to 24.8 $\mu$R/hr), 27.69 $\mu$R/hr (20 $\mu$R/hr to 37.05 $\mu$R/hr), 25.62 $\mu$R/hr (24.77 $\mu$R/hr to 27.7 $\mu$R/hr), 20.85 $\mu$R/hr (15.69 $\mu$R/hr to 23 $\mu$R/hr) and 26.5 $\mu$R/hr (12.38 $\mu$R/hr to 40.71 $\mu$R/hr), respectively. A low radioactivity has been registered over Ramadugu lamproite field (18.25 $\mu$R/hr to 21.58 $\mu$R/hr) and Yacharam lamproites field (19.91 $\mu$R/hr to 20.41 $\mu$R/hr), Vattikod lamproites field 25.56 $\mu$R/hr to 27.82 $\mu$R/hr ) and Somavarigudem lamproites field ( 17.38 $\mu$R/hr to 18.13 $\mu$R/hr) .

Coefficient of variation values calculated for the radiometric data revealed seven deep-seated faults (F1 to F7), two running NW-SE, three NE-SW, one N-S and one another NNW-SSE. In addition, radiometric data revealed in the region disposition of schist belts, various faults and other lineaments /dykes and contact between granite gneiss and dolerite dykes.

**Key words**: Radiometric surveys, Lamproite field, clusters, enclaves and Geological structures.

## INTRODUCTION

Radiometric methods employed are mainly in the exploration of Uranium and Thorium mineral deposits. In recent times, the application of radiometric methods of exploration is more diversified (Nsikak E Bassey et al., 2013 and Labani Ray et al., 2015) , and are used for the indirect location of deposits of certain rare elements and of certain rare earth metals occurring in genetic or paragenetic association with radioactive minerals. As different rocks contain varying amounts of radioactive minerals, the radiometric methods find application also in geological mapping (Amadi, 2012 and Aswathanarayana, 1971), like delineation of contact between different rock types (Himabindu and Ramadass, 2003), location of faults, shear zones etc, overlain by a thin soil cover.

Recent geological and geochemical studies carried out by Geological survey of India (Alok Kumar et al., 2013, Reddy et al., 2003, Sridhar and Rau, 2005, Chalapathi Rao et al., 2004 and 2014), under systematic diamond exploration program at the Northwestern margin of the Cuddapah basin, Eastern Dharwar craton (EDC) to identify the new zones of diamondiferous lamproites, helped in the delineation of new clusters of lamproites named as Vattikod, Ramadugu and Somavarigudem clusters (Sridhar and Rau, 2005).These lamproites are emplaced within the granitic rocks of Peninsular Gneissic Complex, Eastern Dharwar Craton, Southern India.

The present paper details the result of radiometric surveys carried out over a part of the Ramadugu, Vattikod, and Somvarigudem lamproite fields in the Nalgonda District, Telangana State, along the North Western margin of the Cuddapah Basin, Eastern Dharwar Craton, to understand the radioactive nature of the litho- structural entity of the study area.

### Geology of the Area

The study area is located along the NW margin of the Cuddapah basin bounded by Longitudes 79° 5' to 79° 25' and Latitudes 16° 42' to 16° 58' Figure 1. Geologically the area forms a part of the Eastern Dharwar Craton (EDC), which is recognized for its emplacement of numerous lamproite bodies. The geological formations in the area (GSI, 1999) include unclassified granites and gneisses of Archaean age, Cumbum Shales, Phyllites, Srisailam quartzites of the Cuddapah super group, and Shales of the younger Kurnool group. The hornblende schist and

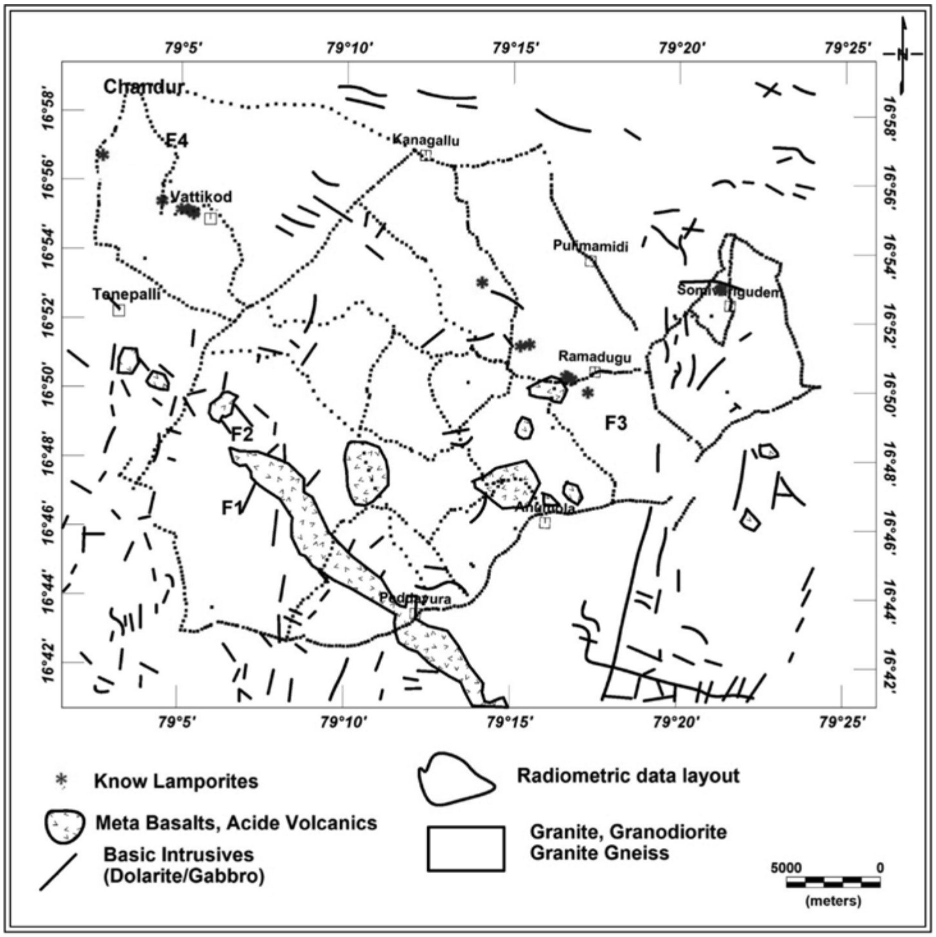


**Figure 1.** Layout map of radiometric data superimposed on Geological map of the study area

amphibolites (Older Metamorphic), which are the oldest rocks, occur as rafts, enclaves and discontinuous linear bands, within the Peninsular Gneissic Complex. West and Southwest of the study area comprises migmatities, granites granodiorite, tonalitic-trondhjemite suite of rocks and hornblende-biotite schist, meta-basalts, meta-rhyolite and banded hematite quartzite. Dharwar super group rocks are exposed as linear belts near Peddavura on the Hyderabad-Nagarjuna sagar road. They are trending in the NNW-SSE direction and run for about 20 Km with a variable width of 500 m to 2 Km, flanked on either side by the peninsular gneissic complex. A number of dolerite dykes and quartz reefs traverse these rocks trending N-S, E-W, NE-SW and NW-SE directions. Sridhar and Rau (2005) recorded a total of 10 NW-SE trending lamproite dykes. They are found over an area of 25 Km$^2$ in three different clusters in the Ramadugu area, namely, first at Ramadugu (R1, R2, R3, R4 and R5), second near Yacharam (Y1 and Y2) and third near Somavarigudem (S1, S2 and S3). These lamproites occur as dykes and trend essentially along NW-SE direction, as discontinuous isolated outcrops associated with intrusive contact with the basement granitoids.

Ten lamproite bodies near west of Vattikod ( VL-1 to VL-10 ) village, one lamproite dyke located 1.5 km west of Marepalli (Ml-1) village and one located in the close vicinity of Gundrapalli (Gl-1) village, have been discovered (Alok Kumar et al., 2013). These lamproites are emplaced along the WNE-ESE to NW-SE trending fractures in the granite-gneiss basement. Apart from these, indications for the presence of more lamproites are noticed in the form of stray boulders at two other locations at Kastala and Samulonobavi in the Paluvayi block.

## Data Acquisition

Semi-detailed radiometric observations have been taken along the available roads, accessible paths and tracks with a station interval of 200 m, to give a fairly even distribution of radioactive values for the entire study region covering the total area of ~700 Sq. km, using the ECIL Scintillometer type SM141 instrument. The Scintillometer is a light weight portable radiation measuring instrument powered by a D-size dry cells featuring solid state design and is ideally suited for radiometric investigations. It has time constant of

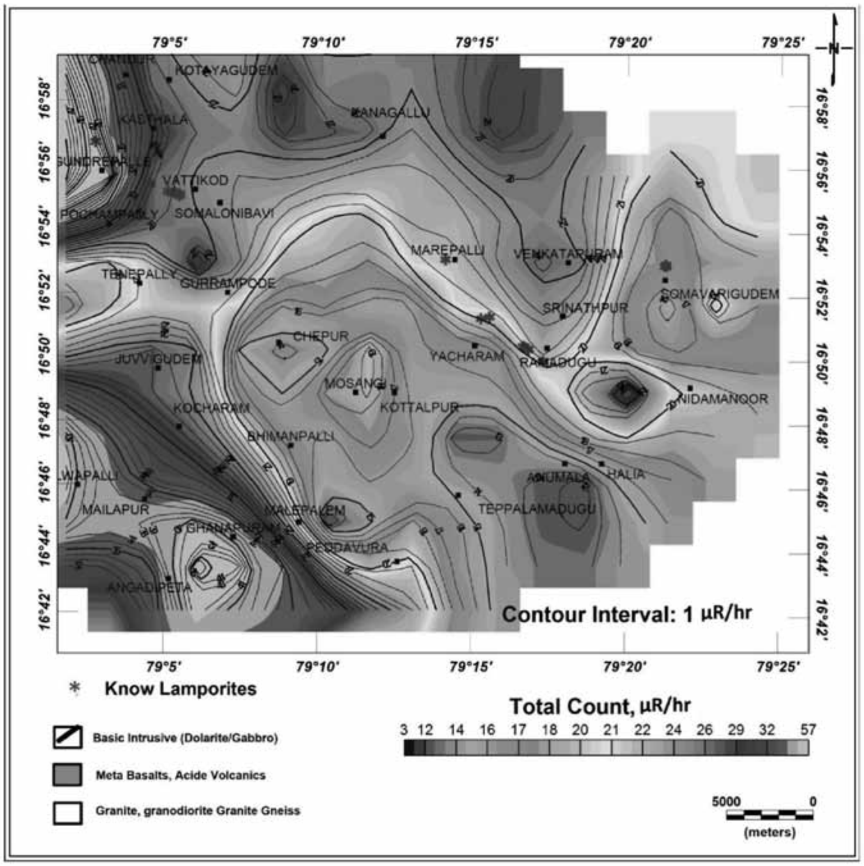


**Figure 2.** Total Radiometric Intensity Map of Study Area

5.5 sec. It is directly calibrated in $\mu$R/hr (micro roentgens per hour). The sensitivity of the measurement varies from 0.1 to 1 $\mu$R/hr. The layout map of radiometric observation is shown in Figure 1. A total of 1200 stations are occupied along Nalgonda- Nagarjuna sagar road, south of Chandur to Kanagallu, Ramadugu in the Anumala mandal, Nalgonda district (Corresponding to scale of 1:50,000). The N-S and E-W extends of this area fall under Survey of India (SOI) Topo sheet No. E44T1, E44T2 and E44T5. The position of the observation points was taken by using Global Position System (GPS) with an accuracy of 1m, to ensure reliability and accuracy of the radiometric and GPS elevation, location of geographic coordinates. Twenty (20%) percent of observations were repeated. The overall effective accuracy obtained for the radiometric data is +/- 2 $\mu$R/hr.

## RESULTS AND DISCUSSIONS

Figure 2 shows the shaded contour map of radiometric data in and around Ramadugu region. The locations of towns/villages are shown on it to get a representative picture of radiometric variation of the region, to understand the lithological and structural fabric of the area. This map has been contoured with an interval of 1$\mu$R/hr. It is evident that the region has radioactivity range from 5 $\mu$R/hr to 47 $\mu$R/hr. High responses are observed at central western part to southern part and these highs are reflected by bulging in essentially linear contours, with distinct individual closures at places within the linear system. Low radioactivity of about 10 $\mu$R/hr anomalies is observed near Anumala, Peddavura and towards Vattikod, trending in NW-SE direction. The area is occupied by metabasalt and Biotite gneiss, exhibiting elliptical contours. Other low radioactivity has been recorded over Banded Iron formation (Gundrapalle, and in between Vattikod to Yacharam) ranging from 12.55 to 22.65 $\mu$R/hr. Intermediate anomalies in the range of 20 to 30 $\mu$R/hr are observed over the metamorphic basement, partly occupied by a migmatite gneiss, homophorous granite, alkali Feldspar granite, hornblende granite and granodiorite near Kanagallu and Ramadugu regions.

From a close examination of Figure 3, the distinct features along the entire traverse representing geological contact, faults, and shear zones can be observed. The broad low of 10 to 20$\mu$R/hr corresponds to the quartz & pegmatite veins and within quartz & pegmatite veins a NW –SE trending schist belt (5-23 $\mu$R/hr). The western and eastern margins of this belt are sheared and faulted and

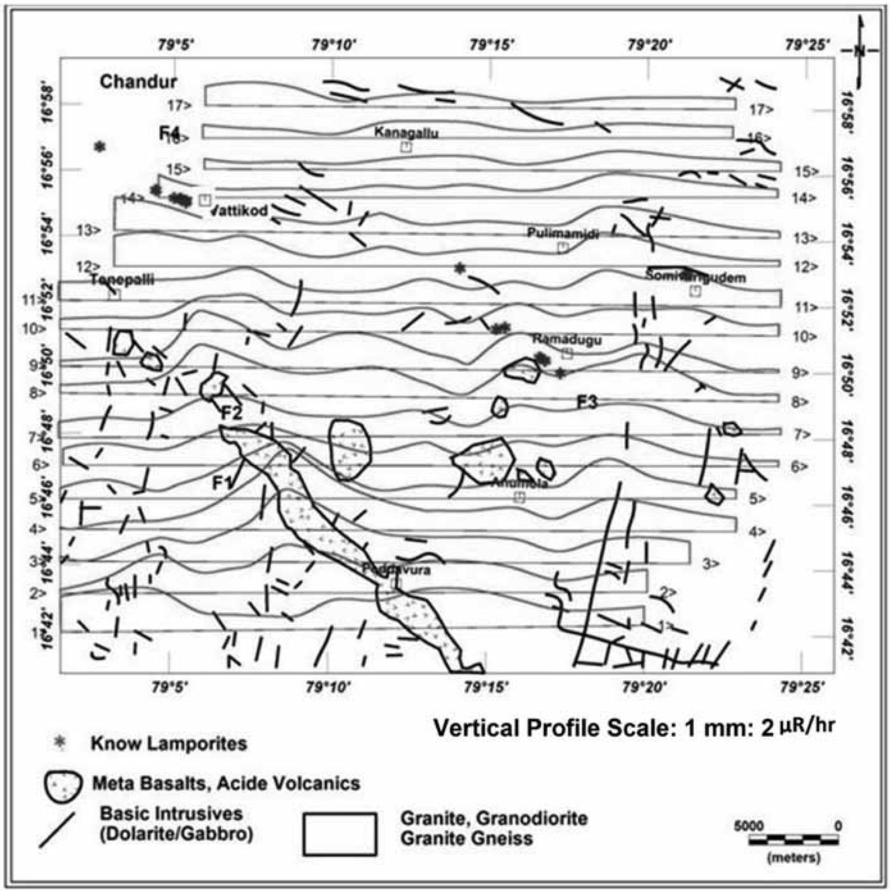


**Figure 3.** Stacked profile map the radiometric data superimposed on geology

are reflected by sharp peaks. The highs flanking the low over the schist belt can be attributed to younger granites and peninsular gneisses, with the former registering higher radio activity (20.73 - 36.67 $\mu$R/hr) as compared to the later (11.32 - 27.08 $\mu$R/hr). Pegmatites found in the region are also reflected by relatively high radioactivity.

The orientation and disposition of shear zones can be identified from a contour map from either a change in gradient or truncation of contours along a linear, curvilinear zones and/or dislocation fractures (Ramachandran et al., 1999 and Ramadass et al., 2013). Thus, features inferred from the profile map can more readily be appreciated from the radiometric intensity contour map Figure 2. From this Figure, it is observed that while shear zones appear on both the western and eastern side of schist, the shear on the western margin is more clearly demarcated than its eastern, with attendant leaching of radioactive minerals. Correspondingly, it shows low radioactivity. The decrease in radiation intensities associated with the tectonically disturbed zones delineated strengthens the analysis.

Coefficient of variation is a statistical technique employed for detection of weak radiometric (any geophysical) signals for analysis of concealed litho-logical contacts, faults and structural trend detection. The coefficient of variation Figure 4 of radiometric data was computed along stacked radiometric profiles Figure 3 using a moving 5-point average window (Bhimasankaram, 1980) to improve the signal to noise ratio, using following equation.

$$C.V = \frac{\sigma}{x} \times 100\%$$

Where, σ is the standard deviation and x is average value of window

Based on lithological observation with coefficient map and radioactivity intensity map of the study region a geological map of in around Ramadugu (Chalapathi Rao et al., 2014 and Alok Kumar et al., 2013) region was prepared Figure 5. Each formation details are shown in Table. 1 and Figure 6. The corresponding radioactivity for amphibolite's schist, Biotite Gneiss, granites, granodiorite, quartz vein and dolerites are 23.15 $\mu$R/hr (22.87 $\mu$R/hr to 23.4 $\mu$R/hr), 22.77 $\mu$R/hr (20.94 $\mu$R/hr to 24.8 $\mu$R/hr), 27.69 $\mu$R/hr (20 $\mu$R/hr to 37.05 $\mu$R/hr), 25.62 $\mu$R/hr (24.77 $\mu$R/hr to 27.7 $\mu$R/hr), 20.85$\mu$R/hr (15.69 $\mu$R/hr to 23 $\mu$R/hr) and 26.5 $\mu$R/hr (12.38 $\mu$R/hr to 40.71 $\mu$R/hr), respectively.

In Figure 5 lineaments are mapped following structural closures or nosings of radiometric anomalies. Some of these lineaments correlate/or are coincident with the mapped structures such as faults, shear zones, dykes and

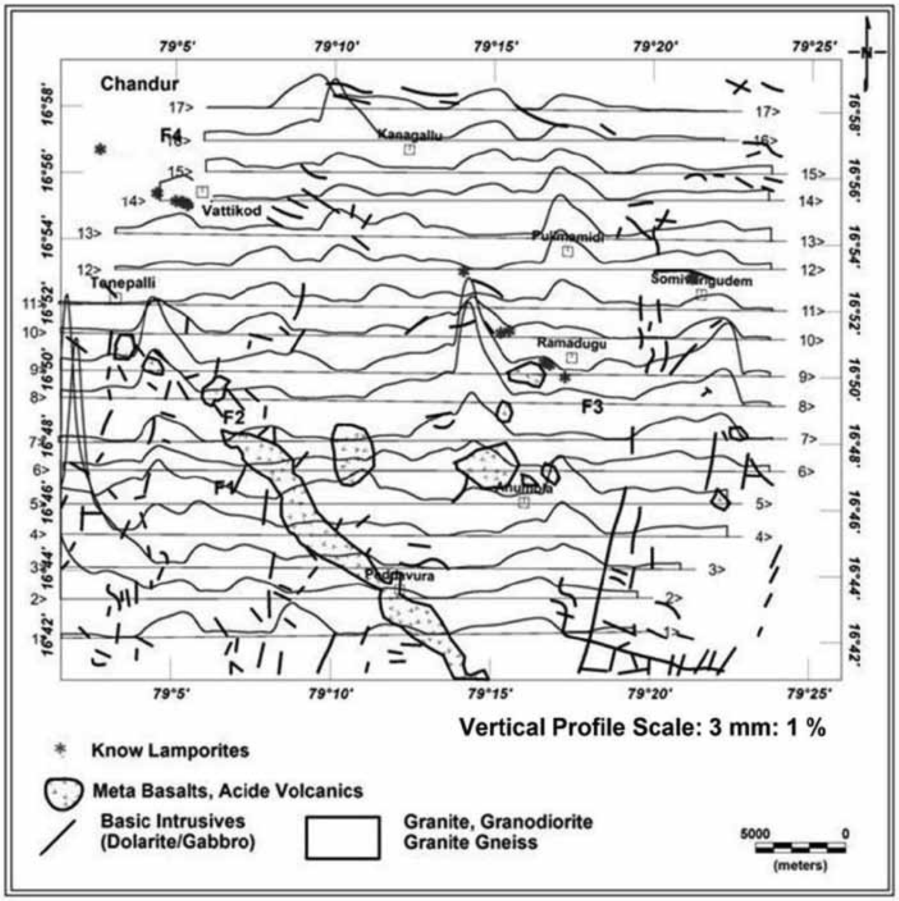


**Figure 4.** Stacked profile map of coefficient of variation of the radiometric data superimposed on geology.

foliation. They are also parallel or sub-parallel to fluvial channels. Seven (F1-F7) faults/lineaments are mapped, using radiometric data Figure 5. The fault/lineament F1 observed in southwestern part of the study area is the contact zone between the younger/ homophorous granites and granite, granoditorite granite gneiss. The fault F2 indicates the contact between the western margin of Peddavura schist and granite, granoditorite granite gneiss. F3 observed near Tenepalli is abutting to the northwestern part of the schist belt. The fault F4 is trending in NE-SW direction. The western part of this fault is associated with high radioactive nature formations like homophonous granite, alkali Feldspar Granite, whereas the eastern part is occupied by a low radioactive nature of the biotite gneiss and banded biotite gneiss. The fault F5 (NW-SE) and F6 (NE-SW) are the important tectonic lineaments/fault zones in the study area, which are of highly disturbed nature. The emplacement of lamporites near Somvarigudem, Marepalli, Yacharam and Ramadugu regions are associated within fault/shear environment of F5 & F6. The F7 fault separates the Lamporites of Vattikod from Gudrapalli Lamporites. The observed radioactivity over the Gudrapalli lamporites is high compared to the Vattikod Lamporites. The high radioactivity observed over the Gundrpalli is due to the association with the homophonous granite, whereas moderate radioactivity over the Vattikod lamproites is due to the association with the granite, granoditorite granite gneiss.

Lamproites in the study area emplaced along NE-SW directions are parallel to oblique to the foliation, joint, dyke and regional fault/fracture trends. Ramaudgu and Yacharam lamproites are emplaced along the contact zone between the dyke environment and granitie gneisses and imply the involvement of distinct deep-seated faults/fractures in controlling their emplacement. Likewise, the Ramadugu lamproites occur as dykes. Lamproites at Somavarigudem occur in close association with dolerite dykes. Fault contact environment is observed in lamproite emplacement in the study area.

At Vattikod most of the lamproites are emplaced at the contact zone between the Alkali Feldsapar granite and biotite gneiss granitic – gneiss basement and in dolerite dykes. They are also observed along NE-SW to NW-SE trending fractures.

A fault contact environment (Alok kumar et al., 2013) is observed in lamproite emplacement in the study area. At

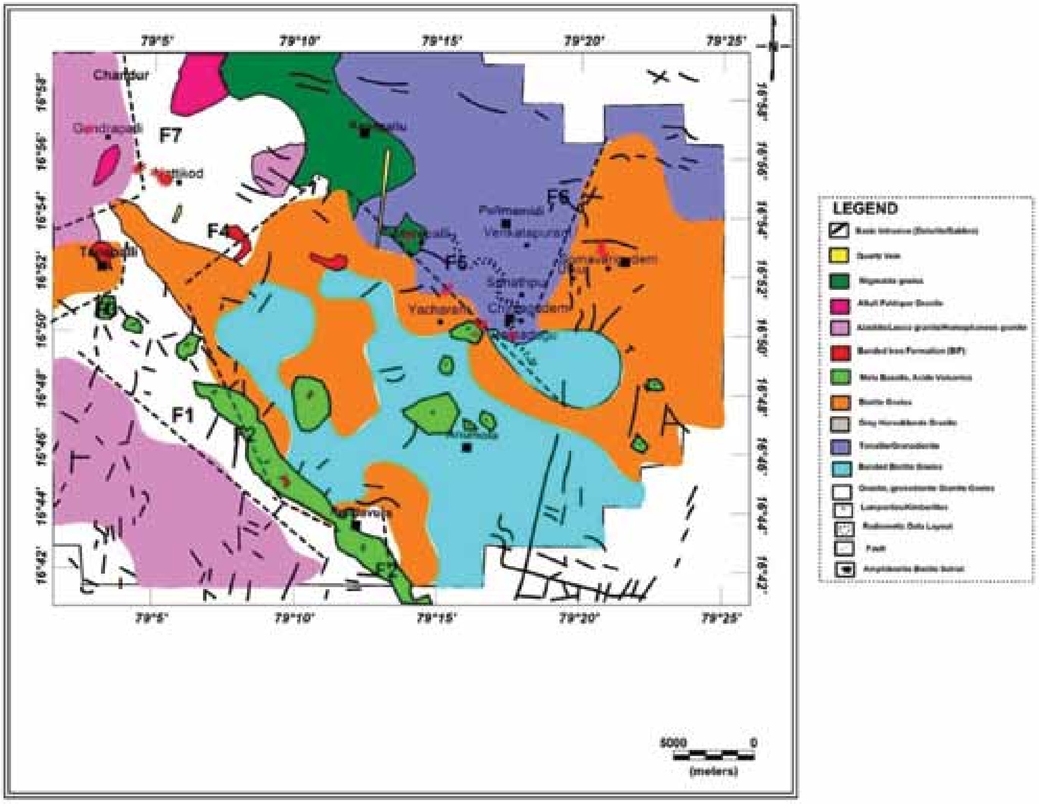


**Figure 5.** Interpreted geological map of the study area by using radiometric data

**Table 1.** Radioactivity of geological formations

| S.No | Foramtion (New) | Minimum Radioactivity (μR/hr) | Maximum Radioactivity (μR/hr) | Average Radioactivity (μR/hr) |
|---|---|---|---|---|
| 1. | Amphibolite Biotite Schist | 22.87 | 23.44 | 23.15 |
| 2. | Banded Iron Formation | 12.55 | 22.65 | - |
| 3. | Biotite Gneiss | 20.94 | 24.89 | 22.77 |
| 4. | Granite, Granodiorite, Granite Gneiss | 24.77 | 27.78 | 25.62 |
| 5. | Alkali Feldspar Granite | 20.00 | 37.05 | 27.69 |
| 6. | Homophorous Granite | 19.01 | 41.31 | 28.84 |
| 7. | Quartz Vein | 15.69 | 23.03 | 20.85 |
| 8. | Basic Intrusive (Gabbro/Dolerite) | 12.38 | 40.71 | - |
| 9. | Vattikod Lamporites | 25.56 | 27.82 | - |
| 10. | Gundrapalli Lamporites | | 40.77 | |
| 11. | Marepalli Lamporites | | 21.44 | |
| 12. | Yachram Lamporites | 19.91 | 20.41 | - |
| 13. | Ramadugu Lamporites | 18.25 | 21.58 | - |
| 14. | Somvarigudem Lamporites | 17.38 | 18.13 | - |
| 15. | Migmatite Gneiss | 21.91 | 28.25 | 25.40 |
| 16. | Tonalite Granite | 16.90 | 23.08 | 19.65 |
| 17. | Metabasalt, Acid Volcanics | 12.43 | 13.18 | 12.80 |

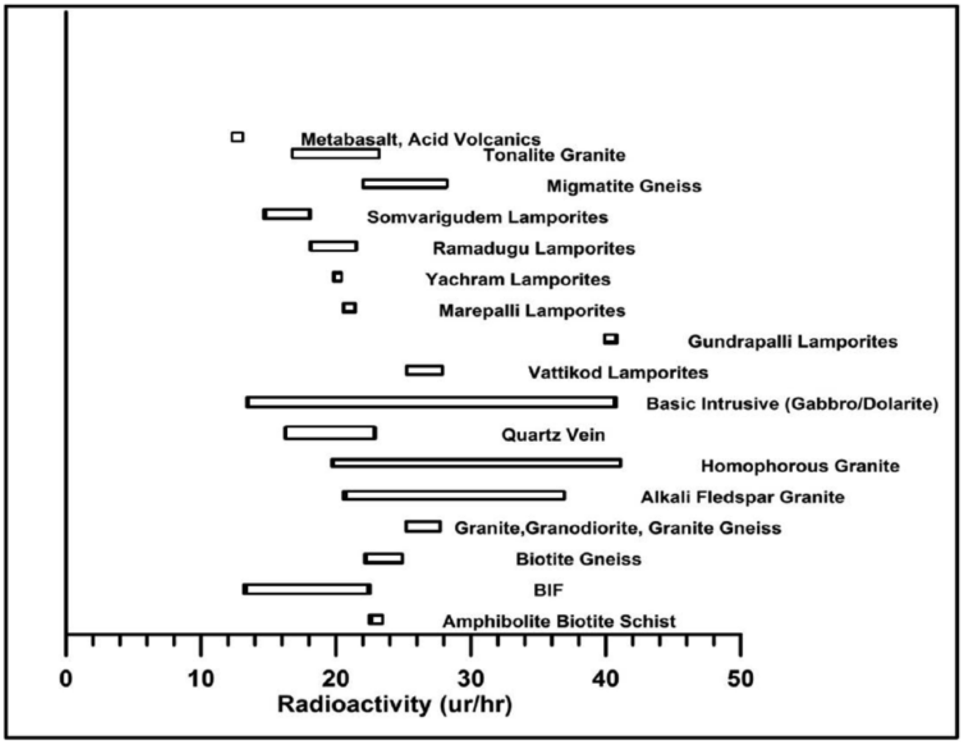


**Figure 6.** Distribution of radioactivity in different formations in the study area

Vattikod (25.56 $\mu$R/hr to 27.82 $\mu$R/hr) most of the lamproite zones are emplaced at the contact zone between the alkali feldspar granite and biotite gneiss. They exhibit 27.69 $\mu$R/hr and 22.77 $\mu$R/hr radioactivity, respectively. Ramadugu and Yacharam lamproites emplaced along the contact zone of schist and granite gneisses exhibit radioactivity in the range of 23.44 $\mu$R/hr and 22.78 $\mu$R/hr.The Somavarigudem lamproites (17.38 $\mu$R/hr to 18.13 $\mu$R/hr) lie on the contact of dolorite dyke and granite gneisses (24.77 $\mu$R/hr to 27.78 $\mu$R/hr).

## CONCLUSIONS

Radiometric investigations are successfully employed to map various geological formations and structural elements, orientation and disposition of lineaments, dykes, minor / major shear zones and structural features.

The corresponding radioactivity for amphibolites biotite schist, banded Iron formation, biotitie gneisses, alkali feldspar granite, quartz vein and basic intrusive (gabbro/dolerite), migmatite gneiss, tonalite granite and metabasalt, acid volcanic are 23.15 (22.87-23.44) $\mu$R/hr, (12.55-22.65) $\mu$R/hr, 22.77 (20.94-24.89) $\mu$R/hr, 25.65 (24.77-27.78) $\mu$R/hr, 27.69 (20-37.05) $\mu$R/hr, 28.84 ((19.01-41.31) $\mu$R/hr, 20.85 (15.69-23.03) $\mu$R/hr, (12.39-40.71) $\mu$R/hr (25.56-27.82) $\mu$R/hr, 24.40 (21.91-28.25) $\mu$R/hr, 19.65 (16.9-23.08) $\mu$R/hr and 12.80(12.43-13.18) $\mu$R/hr, respectively. A low radioactivity has been observed over Ramadugu lamproites field (18.25 $\mu$R/hr to 21.58 $\mu$R/hr) and Yacharam lamproites field ( 19.91 $\mu$R/hr to 20.41 $\mu$R/hr), Vattikod lamproites field ( 25.56 $\mu$R/hr to 27.82 $\mu$R/hr). Somavarigudem lamproites field (17.38 $\mu$R/hr to 18.13 $\mu$R/hr) lies on the contact of dolerite and granidiorite granites.

Broadly, younger granites register high radioactivity and the irregular variation is attributed to the exposure of granite at places and due to the variation of radioactive mineral content in the weathered portion of granites. The schist is found to be associated with low to moderate high radioactivity. Coefficient of variation map brought seven deep-seated faults F1 to F7, lineaments, fractures and dykes extending along NW-SE, NE-SW, N-S and E-W trends. They are responsible for the emplacement of the lamproites at contact between granite gneiss and dolerite dykes. Based on lithological observation and radiometric anomalies, a new lithological structural map of the study area has been prepared.

## ACKNOWLEDGEMENTS

The authors are extremely grateful to the UGC New Delhi for the financial support extended by granting Emeritus professor to Prof. G. Ramadass, Department of Geophysics, Osmania University, Hyderabad. Authors are thankful to anonymous reviewers for their constructive suggestions to improve the manuscript. Apt editing by Chief Editor enhanced quality of the manuscript.

## Compliance with Ethical Standards

The authors declare that they have no conflict of interest and adhere to copyright norms.

## REFERENCE

Amadi, A.N., 2012. Radiometric surveys as a useful tool in geological mapping of western Nigeria, Journal of Georaphy and Geology., v.4, no.1, pp: 242-249.

Aswathnarayana, U., 1971. Th. U Ratio as an Aid in prospecting for diamonds in the Kimberlitic rocks of India. Current Science., v.40, no.24, pp: 663.

Alok Kumar, A., Ahmed, S., Priya, R., and Sridhar, M.2013. Discovery of lamproites near Vattikod area, NW margin of the Cuddapah basin, Eastern Dharwar craton, southern India. Journal of the Geological Society of India, v.82, pp: 307–312.

Bhimasankaram, V.L.S., 1980. The philosophy of integrated geophysical exploration technology and interpretation, Jour. Assoc. Exploration Geophysicists., v.1, no.2, pp: 1.

Chalapathi Rao, N.V., Gibson, S.A., Pyle, D.M., and Dickin, A.P., 2004 Petrogenesis of Proterozoic Lamproites and Kimberlites from the Cuddapah basin and Dharwar Craton, southern India, Journal of Petrology, v.45, pp: 907-948.

Chalapathi Rao, N.V., Alok Kumar, Samarendra Sahoo, Dongre, A.N., and Debojit Talukdar., 2014. Petrology and petrogenesis of Mesoproterozoic lamproites from the Ramadugu field, NW margin of the Cuddapah basin, Eastern Dharwar craton, southern India. Lithos., v.196-197, pp: 150-168.

Geological Survey of India., 1999. District resource map of Nalgonda district, Andhra Pradesh,1:250,000 scale.

Himabindu, D., and Ramadass, G., 2003. A note on qualitative appraisal of radiometric investigations along the Goa-Kushtagi profile. J.Ind.Geophys.Union., v.7, no.1, pp: 37-41.

Labani Roy, P., Nagaraju, S.P., Singh, G., Ravi and Sukanth Roy., 2015. Radioelmental, petrological and geochemical characterization of the Bundelkhand craton, Central India: Implication in the Archaean geodynamic evolution. Int. J. Earth, Sci. (Geol Rundsch), 20 August.

Nsikak E Bassey, Usman Kaigama, and Ajibola Oluwasegu., 2013. Radiometric Mapping of Song Area Environs. Hawal Basement Complex, Northeast Nigeria, IJST., v.2, no.9, pp: 692-699.

Ramachandran, C., Kesavamani, M., and Prasad, R.M.C., 1999. A geophysical prognostication of primary diamond deposits in peninsular India. Jour. Geophysics., v.20, no.4, pp: 155-178.

Ramadass, G., Subhash Babu, A., and Udaya Laxmi, G., 2013. Structural Analysis of Airborne Radiometric data for Identification of Kimberlites in Parts of Eastern Dharwar Craton International Journal of Science and Research., v.4, no.4, pp: 2375-2380.

Reddy, T.A.K., Sridhar, M., Ravi, S., and Chakrawarthy, V., 2003. Petrology and geochemistry of the Krishna lamproites field, Andhra Pradesh, Journal of the Geological Society of India., v.61, pp: 131-140.

Sridhar, M., and Rau, T.K., 2005. Discovery of a new lamproite field- Ramadugu Lamproite field (RLF), Nalgonda district, Andhra Pradesh. Proceedings of Group Discussion on Kimberlites and related rocks. Geol. Soc. India, Bangalore, pp: 55-57.

J. Ind. Geophys. Union ( May 2016 )
**v.20, no.3, pp: 342-350**

# Red beds in the Cuddapah Basin, eastern Dharwar craton, India: Implications for the initiation of sedimentation during the Proterozoic Oxygenation event

**V. V. Sesha Sai*[1], Tarun C. Khanna[2] and N. Rama Krishna Reddy[3]**
[1]Petrology Division, Geological Survey of India Training Institute, Hyderabad - India
[2]CSIR-National Geophysical Research Institute, Hyderabad – 500 007, India
[3]Loyola Degree College (YSRR), Pulivendula, Andhra Pradesh – 516390, India
*Corresponding Author : seshubb@yahoo.co.in

**ABSTRACT**
Based on the field, petrological and geochemical studies we make a detailed report on the occurrence of Proterozoic red beds from the intra-cratonic Cuddapah basin of South India. Studies in old Kadiri Ghat – K. K. Kottala section in SW part of the Cuddapah Basin indicate the presence of extensive red bed sequence with varied mineralogical, textural and lithological composition forming part of the Gulcheru Formation in the Paleoproterozoic Cuddapah Super group. Studies further reveal that a greater part of the clastic sedimentary rocks from the lowermost Gulcheru Quartzite of Papaghni Group to Bairenkonda Quartzite of Nallamalai Group are ferruginous. The present studies also highlight the existence of a thick sequence (~ 400 m) of ferruginous lithic arenite interbedded with a non-clastic reddish jasper and dolomite sequence in the middle part of Tadpatri Formation of Chitravathi Group in Mallela section and an iron oxide rich ferruginous siltstone (with 37 % $Fe_2O_3$) in lower part of Bairenkonda Quartzite in Nandyal-Nandikanuma pass section of Nallamalai Group. An age of 1.9 Ga for the mafic-ultramafic sill emplacement in Tadpatri Formation within the Chitravathi Group of Cuddapah Supergroup indicates the age of deposition of the host sediments to be older than this date. Considering the 1900-2000 Ma age of Vempalle dolomites, it is inferred that the Gulcheru red beds were deposited around 2.1 Ga; a period that corresponds to the global oxygenation event and a period that witnessed deposition of red beds in the platform type of Proterozoic basins in the world.

**Key words:** Red beds, Proterozoic Cuddapah basin, Eastern Dharwar Craton, Sedimentation, Oxygenation event

## INTRODUCTION

The Proterozoic Cuddapah basin of the Eastern Dharwar Craton (EDC) is bounded by Archaean greenstone belts and Peninsular Gneissic Complex to the west and south respectively, while 2.7 Ga Nellore schist belt (NSB) is present towards east (Ravikant, 2010). The basin covers an area of 44,500 sq km and extends over a length of 440 km in N-S direction with a maximum width of 145 km in the central part of the basin Figure 1.

The basin hosts the Paleoproterozoic Cuddapah Supergroup of rocks with clastic and non-clastic sequences and associated igneous rocks and the Neoproterozoic Kurnool Group of rocks with essentially a clastic and non-clastic sequence (Nagaraja Rao et al., 1987). In the Cuddapah Supergroup, the lithounits constituting the lower Papaghni and Chitravathi Groups are unmetamorphosed (Nagaraja Rao et al., 1987, Tripathy and Saha, 2013), while the rocks belonging to the upper Nallamalai Group are subjected to multiple phases of deformation (Saha, 2002; Chetty, 2011). "Red beds" are essentially clastic sedimentary rocks that may consist of rudaceous, arenaceous and argillaceous sequences, which are predominantly red in color due to the presence of Fe oxides; mainly hematite. Study of red beds offers important information concerning past climates and depositional environments (Mc Laren, 1978). The two major periods of red beds, dolostones and marine sulphate deposition in the Fennoscandian greenstone belt are Paleoproterozoic in age; 2.3 and 2.0 Ga (Melezhik et al., 2005). Strahler (1981) also reported formation of thick red beds during the Proterozoic. The appearance of red beds in the stratigraphic record is often cited as evidence for the Great Oxygenated Event (Holland, 2006). Extensive deposition of arenaceous and argillaceous red beds are recorded in the Early Proterozoic Aphebian sequences in Superior Craton of Canada (Chandler, 1980). The present paper brings to light the occurrence of Proterozoic red beds in the Gulcheru Formation of the Cuddapah Supergroup and infers that the initiation of sedimentation in the Cuddapah basin corresponds to the 2.1 Ga Proterozoic oxygenation event.

### Geological Setting

Thick sequences of clastic and non-clastic sedimentary rocks along with a wide range of igneous rocks forming

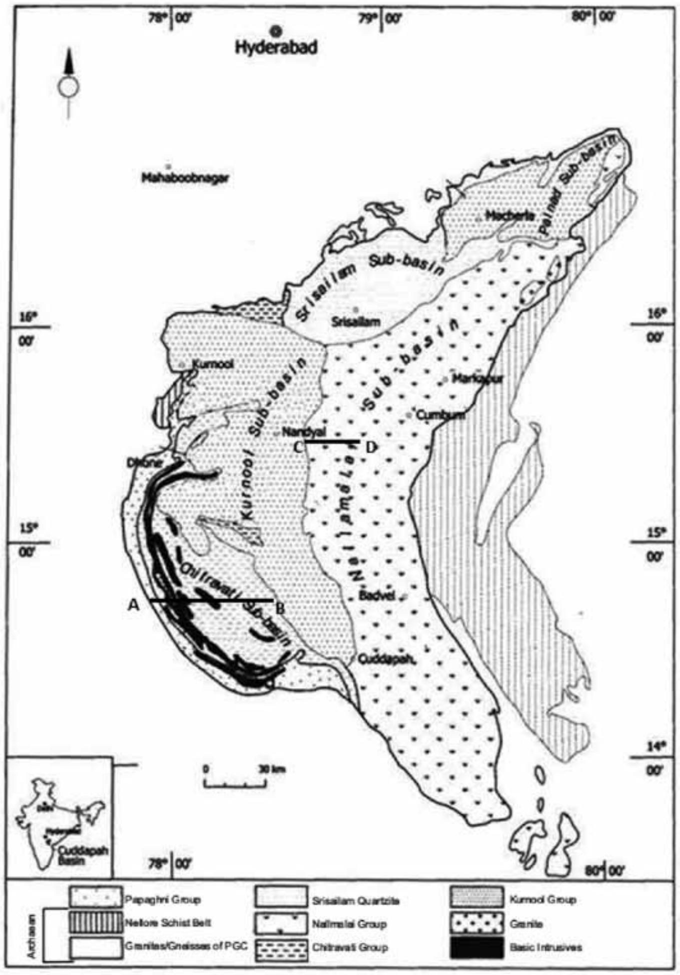


**Figure 1.** Geological map of the Cuddapah basin showing sub-basins (after Nagaraja Rao et al., GSI 1987), A-B Old Kadiri Ghat section-Pulivendla-Mallela section, C-D Pacherla-Nandikanuma pass-Diguvametta section.

part of the Paleoproterozoic Cuddapah Supergroup are well exposed in the Old Kadiri Ghat – K.K. Kottala - Pulivendula section, Lingala section, Tonduru- Mallela section in the SW part of Cuddapah basin and Nandyal-Giddaluru section of Nallamalai Fold Belt (NFB) in EDC. Reddish clastic sedimentary beds occur in form of deep reddish brown conglomerate, coarse grained ferruginous pebbly arenite and coarse to medium grained cross bedded ferruginous arenite in the Gulcheru Formation in Old Kadiri Ghat – K.K. Kottala - Pulivendla section Figure 2. Similarly, red beds are also found in the basal Gulcheru Formation near Veldurti along Veldurti-Ramallakota section (Bhattacharjee, 2015 pers.com.). Quartzites with variable iron contents have been reported at various stratigraphic horizons in the Cuddapah basin (Pulla Reddy et al., 1990). In Lingala section a reddish brown conglomerate horizon is overlain by reddish cross bedded arenite. A thick sequence (~ 400 m) of ferruginous lithic arenite interbedded with a non-clastic reddish jasper and dolomite is recorded in the middle part of Tadpatri Formation of Chitravathi Group in Mallela section, while an iron oxide rich ferruginous siltstone (with 35.61 to 37 % $Fe_2O_3^T$) overlain by a thick sequence of cross bedded ferruginous arenite is well exposed in the lower part of Bairenkonda Quartzite in Pacherla-Nandikanuma pass-Diguvametta section along the western margin of the section of Nallamalai Fold Belt (NFB).

## DISCUSSION

### Gulcheru Red beds in old Kadiri ghat – K.K. Kottala section

Resting over the Archaean granite basement, the lowermost sedimentary rock deposited in the Proterozoic Cuddapah basin at the base of Gulcheru Quartzite in the Old Kadiri Ghat – K.K. Kottala section is a deep reddish brown pebbly horizon Figure 3a varying in thickness from 15 cm to 70 cm. The pebbles are mainly represented by rounded to sub rounded clasts of quartz that float in relatively finely grained hematite rich ferruginous cement. Red beds

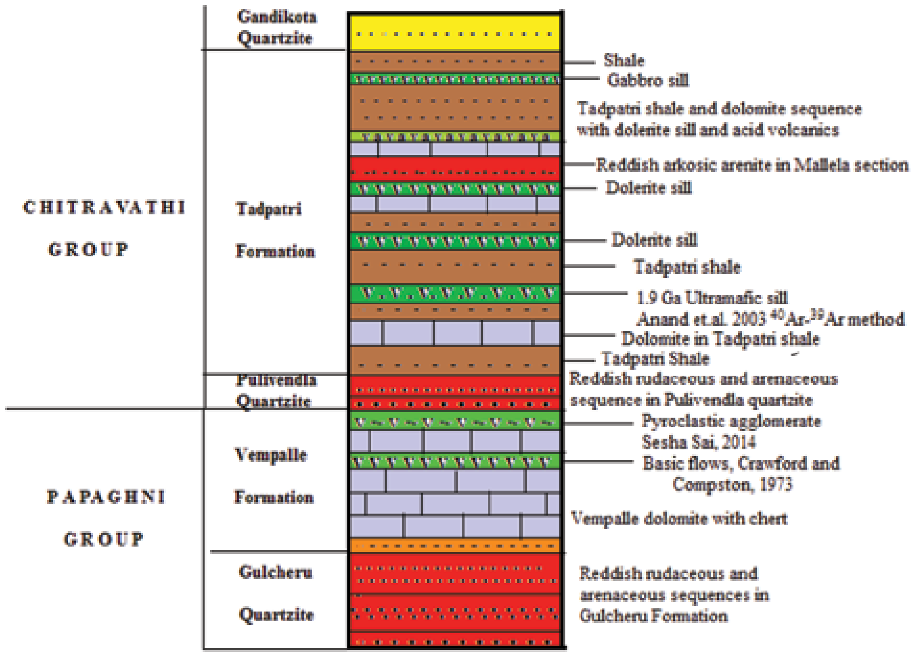


**Figure 2.** Litholog showing the red clastic sequences in Papaghni and Chitravathi Groups in the old Kadiri ghat – Pulivendla – Lingala – Mallela section in the Proterozoic Cuddapah basin (log not to scale).

are clastic sedimentary rocks stained red by hematite (Chandler, 1980). Larger quartz ranges from 4 mm to 1cm i.e. particle size ranging from granule to pebble, while the finer detrital quartz in the matrix range in size from 0.8 mm to 1 mm i.e. medium to coarse size sand particles. The pebbly horizon grades into a cross bedded reddish arenite Figure 3b. Rounded to sub rounded clasts of K-feldspar and microcrystalline chert are noticed in sub ordinate along with the quartz within the reddish arenite studies from the middle and upper part of Gulcheru Formation. Microscopic studies indicate that fine reddish iron oxide cement is conspiciously noticed in Gulcheru red beds Figure 3c. In conformity with the petrological observations the Gulcheru beds analysed high $SiO_2$ ranging from 83.03 to 86.95 %, $K_2O$ ranging from 2.22 to 3.47 % and $Al_2O_3$ ranging from 5.19 to 9.6 %, while the $Fe_2O_3^T$ contents in these red beds vary from 2.68 to 3.12 % Table-1. In K.K. Kottala – Pulivendla section an extremely fine grained ferruginous siltstone interbedded with dolomite is recorded in the lower part of Vempalle Formation.

## Ferruginous arenite in Pulivendla Formation – Lingala section

Pulivendla Quartzite, the oldest lithounit of the Chitravathi Group is well exposed in Lingala section in SW part of Cuddapah basin. A NNW-SSE striking reddish brown conglomerate (~ 6 m thick) essentially composed of 85 to 90 % of well-rounded to sub rounded chert clasts bound by iron oxide (0.89 % $Fe_2O_3^T$) occurs at the base of Pulivendla Quartzite. The chert clasts vary in size from 0.6 cm to 2.5 cm. The conglomerate horizon is overlain by (~ 80 m thick) medium to fine grained ferruginous arenite (1.03 % $Fe_2O_3^T$) with a sharp contact Petrographically the arenite is composed of chert, chalcedony and quartz clasts in decreasing order of abundance. The lithounits show shallow dips of 8 to 10$^o$ due east. Tadpatri shale with intercalated dolomite overlies the Pulivendla quartzite.

## Ferruginous lithic arenite of Tadpatri Formation – Mallela section

Mallela section is located between Pulivendla and Muddanuru transect in SW part of the Cuddapah basin. In Mallela section a thick horizon (~ 400 m) of ferruginous lithic arenite (6 to 11 % $Fe_2O_3^T$) interbedded with non-clastic reddish jasper Figure 3d and dolomite sequence is well exposed in middle part of the Tadpatri Formation of Chitravathi Group Table-2. Petrographic studies reveal that the ferruginous lithic arenite is glauconite bearing Figure 3e and composed of sub rounded quartz clasts, glauconite, carbonate and chert fragments. Mineral chemical analyses through Electron Probe Micro Analyser (EPMA) indicate that the $K_2O$ content in glauconite range from 7.94 to 9.64 %, indicating their evolved nature (Odin and Matter, 1981). Chert fragments are oval and well rounded Figure 3f. Both clasts and lithic fragments are bound by deep brownish ferruginous material. Chert and carbonate clasts make about 40 to 45 % of the rock. Bulk chemical analysis

**Table 1.** Major oxide and trace element analyses (XRF) of the ferruginous clastic beds from the Proterozoic Cuddapah Supergroup of Rocks, Eastern Dharwar Craton, South India.

| | Gulcheru Formation | | | Pulivendla Formation | | Tadpatri Formation | | | | Bairenkonda Formation | |
|---|---|---|---|---|---|---|---|---|---|---|---|
| Oxide% | CGR-1 | CGR-2 | CGR-3 | CPR5 | CPR6 | CTR7 | CTS8 | CTS8A | CTS9 | CBR10 | CBR11 |
| $SiO_2$ | 83.03 | 88.64 | 86.95 | 98.22 | 97.92 | 73.799 | 58.91 | 57.82 | 65.52 | 60.2 | 58.2 |
| $TiO_2$ | 0.4 | 0.27 | 0.45 | 0.04 | 0.04 | 0.28 | 0.89 | 0.89 | 0.57 | 0.15 | 0.15 |
| $Al_2O_3$ | 9.6 | 5.19 | 6.62 | 0.38 | 0.55 | 7.2 | 13.54 | 12.94 | 16.09 | 1.26 | 1.22 |
| $Fe_2O_3$ | 2.68 | 3.12 | 2.79 | 0.89 | 1.08 | 11.07 | 9.59 | 10.42 | 1.57 | 35.61 | 37.61 |
| MnO | 0.02 | 0.02 | 0.01 | 0.01 | 0.01 | 0.04 | 0.05 | 0.05 | 0.02 | 0.01 | 0.01 |
| MgO | 0.65 | 0.42 | 0.4 | 0.18 | 0.21 | 4.13 | 6.85 | 6.85 | 1.45 | 1.29 | 1.29 |
| CaO | 0.05 | 0.04 | 0.05 | 0.12 | 0.11 | 0.31 | 1.25 | 1.25 | 1.11 | 0.18 | 0.18 |
| $Na_2O$ | 0.06 | 0.05 | 0.05 | 0.03 | 0.03 | 1.41 | 5.44 | 5.44 | 7.45 | 0.05 | 0.05 |
| $K_2O$ | 3.47 | 2.22 | 2.62 | 0.08 | 0.07 | 1.72 | 3.35 | 3.35 | 6.13 | 1.2 | 1.2 |
| $P_2O_5$ | 0.03 | 0.04 | 0.08 | 0.03 | 0.03 | 0.05 | 0.1 | 0.1 | 0.08 | 0.05 | 0.05 |
| Total | 99.99 | 100.01 | 100.01 | 99.97 | 100.05 | 100.009 | 99.97 | 99.11 | 99.99 | 100 | 99.96 |
| Element | Trace element analyses (in ppm) | | | | | | | | | | |
| Cr | 60.77 | 39.98 | 34.37 | 20.96 | 41.63 | 99.98 | 125.45 | 124.24 | 19.72 | 44.88 | 46.54 |
| Ni | 35.28 | 36.31 | 34.64 | 35.90 | 42.58 | 41.41 | 52.94 | 51.32 | 30.94 | 16.90 | 15.80 |
| Rb | 61.18 | 49.71 | 56.04 | 9.53 | 11.81 | 40.06 | 68.68 | 67.52 | 111.69 | 18.26 | 18.62 |
| Y | 18.86 | 21.34 | 20.57 | 5.51 | 6.33 | 21.01 | 34.95 | 35.04 | 92.62 | 2.22 | 2.23 |
| Zr | 57.98 | 66.14 | 248.92 | 7.95 | 3.16 | 204.81 | 89.99 | 89.24 | 998.32 | 6.50 | 6.48 |

**Table 2**. Sedimentary succession in southwestern part of the Proterozoic Cuddapah basin.

| | | GROUP | FORMATION | SUCCESSION |
|---|---|---|---|---|
| PALEOPROTEROZOIC | CUDDAPAH SUPERGROUP | NALLAMALAI GROUP | CUMBUM PHYLLITE | Greyish phyllite / slate with intercalated dolomite / tuffaceous sequence / arenite |
| | | | BAIRENKONDA (NAGARI) QUARTZITE | Ferruginous arenite with intercalated phyllite<br>Ferruginous arenite with intercalated reddish haematite rich siltstone |
| | | CHITRAVATHI GROUP | GANDIKOTA QUARTZITE | Quartz arenite<br>Glauconite bearing sub arkosic arenite<br>Greyish shale |
| | | | TADPATRI SHALE | Shale / Ferruginous arkosic arenite<br>Reddish brown ferruginous litharenite and dolomite with banded jasper and felsic volcanics<br>Finely laminated pale greenish shale with intercalated stromatolitic dolomite (with mafic-ultramafic sills) |
| | | | PULIVENDLA QUARTZITE | Reddish quartz arenite<br>Reddish sub lithic arenite<br>Reddish matrix supported conglomerate |
| | | PAPAGHNI GROUP | VEMPALLE FORMATION | Mafic Pyroclastic zone<br>Stromatolitic Dolomite / chert (mafic sills/flows)<br>Reddish ferruginous siltstone<br>Ferruginous chert breccia |
| | | | GULCHERU QUARTZITE | Reddish sub lithic arenite<br>Reddish arkosic arenite<br>Ferruginous matrix supported polymict conglomerate |
| | | ARCHAEAN BASEMENT (GRANITE-GNEISS-GREENSTONE) | | |

**Table 3.** Mineral chemistry of glauconite from Tadpatri Red beds of the Proterozoic Cuddapah Basin determined by Electron Probe Micro Analyser (EPMA)

| | | | | | | | | | | | | |
|---|---|---|---|---|---|---|---|---|---|---|---|---|
| $SiO_2$ | 50.45 | 50.25 | 51.40 | 51.59 | 50.06 | 51.98 | 50.38 | 50.51 | 51.26 | 45.82 | 47.02 | 46.12 |
| $TiO_2$ | 0.15 | 0.04 | 0.06 | 0.03 | 0.06 | 0.03 | 0.08 | 0.07 | 0.04 | 0.06 | 0.02 | 0.02 |
| $Al_2O_3$ | 16.32 | 16.39 | 16.43 | 23.56 | 24.12 | 21.45 | 23.64 | 22.26 | 22.47 | 24.11 | 24.18 | 24.12 |
| FeO | 10.87 | 11.59 | 10.73 | 5.21 | 5.05 | 4.96 | 6.26 | 6.63 | 6.93 | 6.97 | 6.89 | 6.68 |
| MnO | 0.03 | 0.01 | 0.01 | 0.01 | 0.01 | 0.03 | 0.01 | 0.01 | 0.04 | 0.05 | 0.03 | 0.01 |
| MgO | 3.32 | 3.40 | 3.31 | 2.43 | 2.45 | 2.36 | 2.53 | 2.76 | 2.64 | 4.74 | 4.73 | 4.37 |
| CaO | 0.17 | 0.12 | 0.10 | 0.16 | 0.12 | 0.18 | 0.21 | 0.31 | 0.22 | 0.31 | 0.36 | 0.32 |
| $Na_2O$ | 0.12 | 0.10 | 0.10 | 0.11 | 0.15 | 0.10 | 0.14 | 0.17 | 0.20 | 0.11 | 0.14 | 0.14 |
| $K_2O$ | 9.12 | 8.93 | 9.12 | 9.45 | 9.64 | 9.12 | 9.54 | 9.22 | 9.34 | 7.94 | 8.05 | 8.38 |
| $P_2O_5$ | 0.01 | 0.01 | 0.03 | 0.01 | 0.03 | 0.00 | 0.00 | 0.03 | 0.02 | 0.00 | 0.04 | 0.01 |
| Total | 90.56 | 90.84 | 91.29 | 92.56 | 91.69 | 90.21 | 92.79 | 91.97 | 93.16 | 90.11 | 91.46 | 90.17 |


**Figure 3a.** Photograph showing pebbly red bed at the base of Gulcheru Formation in K.K.Kottala section. **Figure 3b.** Photograph showing cross bedded reddish arenite in Gulcheru Formation, Motnutalapalli. **Figure 3c.** Photomicrograph in plane polarised light (PPL)showing fine reddish iron oxide cement in Gulcheru red bed, Old Kadiri Ghat- K.K.Kottala section **Figure 3d.** Photograph showing reddish jasper intercalated with dolomite in Tadpatri Formation, Mallela section. **Figure 3e.** Glauconite (in PPL) within the ferruginous lithic arenite of Tadpatri Formation. Note the opaque ferruginous binding material. **Figure 3f.** Microphotograph in Xed showing well rounded oval shaped chert clast within the ferruginous lithic arenite in Tadpatri Formation. Note the opaque ferruginous binding material.

through XRF spectrometry reveal that the total $Fe_2O_3$ content range between 9.59 to 11.07 %. The relatively high MgO contents between 4.13 and 6.85 % (Table-3) is attributed to the dolomite lithic fragments in the reddish brown ferruginous lithic arenite. Abundance of carbonate and cryptocrystalline chert lithic fragments in ferruginous lithic arenite indicate relatively short lived action of mechanical energy involved during post depositional process. Both chert and carbonate clasts are derived from the older Vempalle Formation from within the basin. Presence of glauconite indicates role of marine diagenesis during the lithification of the Tadpatri ferruginous lithic arenite, which must have occurred prior to 1.9 Ga i.e.; the age of emplacement of ultramafic sill in Tadpatri Formation (Anand et al., 2003).

### Bairenkonda quartzite – Pacherla-Nandikanuma pass section

Intercalated sequence of NNW-SSE striking ferruginous siltstone and cross bedded ferruginous sandstone with gentle easterly dips occur in Bairenkonda Formation in Pacherla-Nandikanuma pass section along the western margin of the section of NFB. Well rounded grains of quartz with iron oxide coating are noticed in ferruginous quartz arenite. This unit is interbedded by a thinly laminated ferruginous siltstone horizon, which is the most conspicuous ferruginous bed recorded with significant iron content in the Proterozoic Cuddapah basin. It is made of 10 - 15 % of very fine grained detrital quartz that floats in essentially dominantly ferruginous (hematite) material. The rock gives a cherry red to deep brown streak and contains total $Fe_2O_3$ between 35.61 to 37.61 % (Table-1). Ferruginous siltstone horizon varies in thickness from 2m to 3.5 m. It is thinly laminated and the individual laminae vary from 0.7 to 0.8 cm.

### Interbedded dolomite and red bed sequences

Stratigraphic sequences constituting the Papaghni, Chitravathi and Nallamalai Groups of the Cuddapah Supergroup are charecterized by rudaceous, arenaceous and argillaceous rocks of clastic origin interbedded with dolomite and chert of non-clastic origin with variable thickness. Stromatolitic dolomites have been recorded in Vempalle and Tadpatri Formations in the basin (Gururaja and Chandra, 1987). The Vempalle Formation of the Proterozoic Cuddapah basin has a well developed sequence of carbonate rocks, which are interbedded with shales, siltstones and chert. The stromatolitic carbonates show banding of alternate carbonate and cherty layers. The latter are rich in organic matter indicating prevalence of profuse biogenic activity (Mathur et al., 2014). Stromatolites of Vempalle Formation, characteristic of the Paleoproterozoic period have been proposed to be formed by cyanobacterial filaments (Sharma and Shukla, 1998). Geological, isotopic, and chemical evidence suggest that the Paleoproterozoic Great Oxygenation Event (GOE) happened at 2.3 Ga (Zimmer Carl, 2013). Cyanobacteria that appeared about 200 million years before the GOE began producing oxygen by photosynthesis. Before the GOE, any free oxygen they produced was chemically captured by dissolved iron or organic matter. The GOE was the point when these oxygen sinks became saturated and could not capture all of the oxygen that was produced by cyanobacterial photosynthesis (Flannery and Walter 2012). The interval 2.2-1.8 Ga has both carbon isotopic evidence for a stepwise increase in the organic reservoir and also paleosol evidence for an $O_2$ increase (DesMarais, 1997). The pattern of Fe retention in paleosols and the record of mass independent fractionation in sulphur isotopes confirm that the transition to more oxidising conditions took place during Paleoproterozoic (Sreenivas and Murakami, 2005). Early Proterozoic red beds occur at the western, north western and near the northern margin of the Kapavaal Craton (Truswell, 1990). In the Fennoscandian greenstone belt, the two major periods of red beds, dolostones and marine sulphate deposition are Proterozoic in age between 2.3 and 2.0 Ga (Melezhik et al., 2005). The Paleoproterozoic Great Slave Supergroup of Canada contains numerous red beds, glauconitic horizons and sedimentary uranium deposits (Stanworth and Badham, 1984). The increase in the global oxygen levels in atmosphere had a direct impact on the prolific growth of stromatolites both in Vempalle and in Tadpatri carbonates. Occurrence of Red beds, abundant carbonates and stromatolites is widely recorded during Paleoproterozoic (Figure 4). The Paleoproterozoic red beds are deposited in the more stabilised platform type of sedimentary basins worldwide.

### Implications

The timing of initiation of sedimentation in the Proterozoic Cuddapah basin of EDC is an extremely important ongoing subject, since a clear understanding on this aspect will throw light on the onset of deposition in the platform type of sedimentary basin in Dharwar Craton and on the Indian sub-continent. Since it is difficult to date the sedimentary rocks, associated magmatic rocks provide limiting ages. A 12 km long forsterite olivine-phlogopite-enstatite rich ultramafic sill is emplaced in the lower part of the Tadpatri Formation (Sesha Sai, 2010). Several attempts to date this sill have been made (eg. Bhasker Rao et al., 1995; Chatterjee and Bhattacharji, 2001 and French et al., 2008). An age of 1.9 Ga by $^{40}Ar$–$^{39}Ar$ laser fusion was constrained for the phlogopite mica from mafic-ultramafic sill complex of Tadpatri Formation (Anand et al., 2003), which can be considered as the limiting lower most age for

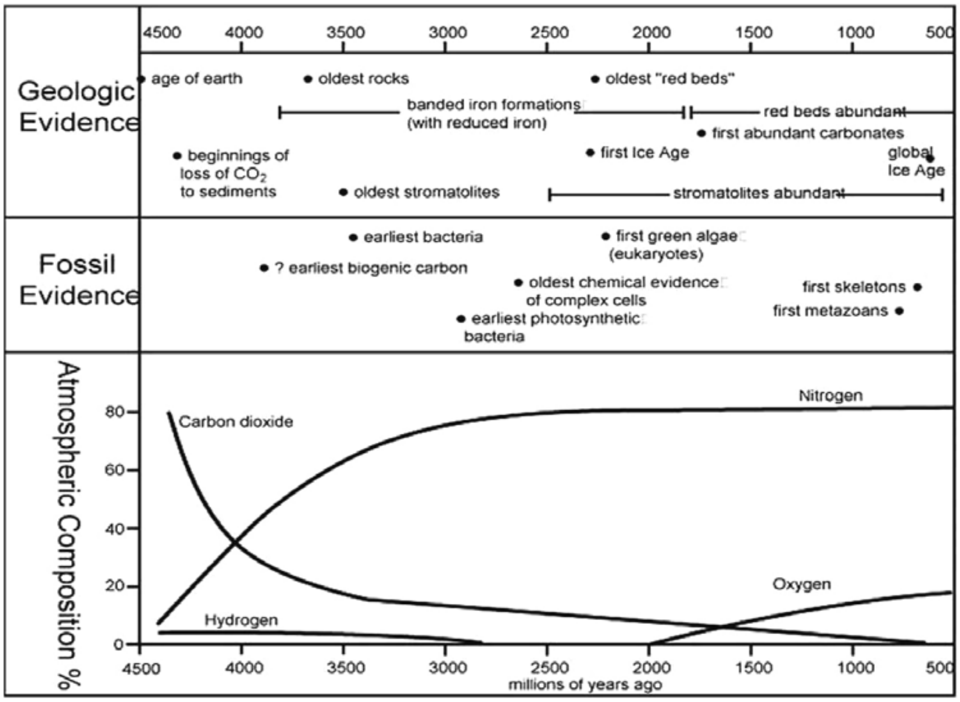


**Figure 4.** Diagram showing the occurrence of Red beds and stromatolitic carbonates during Paleoproterozoic. After Brimblecombe and Davies (1981); modified by David. G. Smith (1981).

deposition of the Tadpatri Formation. No upper age limit estimates of deposition of these sediments are currently available. Globally the oldest red beds recorded are the early Proterozoic Red beds, which appeared only after free oxygen was released into the atmosphere, beginning about 2.1 to 1.8 billion years ago. During the period 2.45–1.85 Ga atmospheric oxygen levels rose to values estimated to have been between 0.02 and 0.04 atm. The shallow oceans became mildly oxygenated (Holland, 2006). Paleomagnetic studies aid significantly in the reconstruction of past plate motions. Palaeomagnetic studies of red beds contributed to unravel the palaeogeography of the 1.8 Ga King Leopold glaciation in the Kimberley Group of Western Australia (Phillip and Williams, 2008). Interbedded ferruginous sandstones, siltstones and jasper are recorded in the Koolpin Formation of Pine Creek Supergroup in the Early Proterozoic (2.0 – 1.8 Ga) El Sherana and Edith basins in Northern Australia (Friedmann, 1990). PbSL studies revealed an age of deposition, diagenesis, dolomitisation and syn-diagenetic uranium mineralization, in the Vempalle dolomites at 1900-2000 Ma (Rai et al., 2015); thus indicating an older age for the Gulcheru red bed sequence referred in the present study in Old Kadiri - K. K. Kottala section of Cuddapah basin. Detailed field and petrological studies as part of the present work have proven that the red beds constitute a significant volume of the clastic sediments in the Gulcheru Formation of the Cuddapah Super group of rocks. The limited geochronological constraints indicate the possibility of deposition of these rocks during Paleoproterozoic.

## CONCLUSIONS

The present studies reveal that the deposition of the red bed sequences in the Cuddapah Supergroup of rocks in the Proterozoic Cuddapah basin in EDC correlate with a major Paleoproterozoic Oxygenation Event. Considering the 1.9 Ga age of emplacement of mafic-ultramafic sills in Tadpatri Formation (Anand et al., 2003), it can be inferred that a greater part of sedimentation in the Paleoproterozoic Cuddapah Supergroup was already deposited prior to 1.9 Ga. Based on the 1900-2000 Ma age of Vempalle dolomites (Rai et al., 2015) it is inferred that the Gulcheru red beds were deposited around 2.1 Ga; a period that corresponds to the global oxygenation event and a period that witnessed deposition of red beds in the platform type of Proterozoic basins in the world.

## ACKNOWLEDGEMENTS

Shri. S.Balakrishnan, ADG (Retd.), GSI is thanked for according permission to publish this work. Shri. S.T.Narahari, GSI and Dr. A. Keshav Krishna, CSIR-NGRI, Hyderabad are thanked for EPMA and XRF facilities, respectively. We express our profuse thanks to Prof. N.C. Pant, Delhi University, Dr. Shantanu Bhattacharjee, GSI, Kolkata and Prof. M. Srinivas, Osmania University, Hyderabad, for their scrutiny and invaluable suggestions. VVSS is grateful to Dr. P.R. Reddy and Dr. T. R. K. Chetty, CSIR-NGRI for their support and encouragement.

## Compliance with Ethical Standards

The authors declare that they have no conflict of interest and adhere to copyright norms.

## REFERENCES

Anand, M.A., Gibson, S.A., Subba Rao, K.V., Kelley, S.P., and Dicken, A.P., 2003. Early Proterozoic melt generation process beneath the intracratonic Cuddapah basin, Southern India. Jour. Petrology., v.44, pp: 2139-2171.

Bhasker Rao, Y.J., Pantulu, G.V.C., Damodar Reddy, V., and Gopalan, K., 1995. Time of early sedimentation and volcanism in the Proterozoic Cuddapah basin, South India: Evidence from Rb-Sr age of Pulivendla mafic sill. Geol. Soc. India Mem., v.33, pp: 329–338.

Bhattacharjee, S., 2015. Personnel communication on the Field observations on red bed occurrence in Gulcheru Formation in the Veldurti-Ramarlakota section of Proterozoic Cuddapah basin, Andhra Pradesh.

Brimblecombe, P., and Davies, T.D., 1981. Atmosphere, water and weather (Figure 17-1; Chapter 17). In: David G. Smith, 1981. Cambridge Encyclopedia of Earth Sciences. Cambridge University Press.

Chandler, F.W., 1980. Proterozoic Red bed Sequences of Canada, Energy, mines and resources of Canada, Geological Survey of Canada Bulletin, v.311, pp: 1-62.

Chatterjee, N., and Bhattacharji, S., 2001. Petrology, geochemistry and tectonic setting of the mafic dykes and sills associated the evolution of the Proterozoic Cuddapah basin, South India. Proceedings of the Indian Academy of Sciences, v.110, pp: 433-453.

Chetty, T.R.K., 2011. Tectonics of Proterozoic Cuddapah Basin, southern India: A conceptual model. Jour. Geol. Soc. Ind., v.78, pp: 446-456.

Crawford, A.R., and Compston, W., 1973. The age of Cuddapah and Kurnool systems, Southern India. Jour. Geol. Soc. Australia, v.19, pp: 453-464.

David G. Smith, 1981. Cambridge Encyclopedia of Earth Sciences. Cambridge University Press, pp: 496.

Des Marais, D. J., 1997. Isotopic Signature of the Ancient Biosphere. Gordon Research Conference; 27 Jul. - 1 Aug. 1997; Henniker, NH; United States.

Flannery, D. T., and Walter, R.M., 2012. Archaean tufted microbial mats and the Great Oxidation Event: new insights into an ancient problem. Australian Jour. Earth Sci., v.59, pp: 1–11.

French, J.E., Heamen, L.M., Chacko, T., and Srivastava, R.K., 2008. 1891–1883 Ma Southern Bastar–Cuddapah mafic igneous events, India: a newly recognised large igneous province. Precam.Res., v.160, pp: 308–322.

Friedmann, J.S., 1990. Stratigraphy, sedimentology and tectonic evolution of the 1.86 Ga El Sherana and Edith River Groups, Northern Territory, Australia. Unpub. Work submitted to Dept. of Earth, Atmospheric and Planetary Sciences, Massachusetts Institute of Technology.

Gururaja, M.N., and Chandra, A., 1987. Stromatolites from Vempalle and Tadpatri Formations of Cuddapah Supergroup (Proterozoic), Andhra Pradesh and their significance. Geol. Soc. Ind. Mem., v.6, pp: 399-427.

Holland, H.D., 2006. The oxygenation of the atmosphere and oceans. Phil. Trans. R. Soc., v.361, pp: 903-915.

Mathur, R., Udai Raj, B., and Balaram, V., 2014. Petrographic characteristics of the Proterozoic Vempalle carbonates, Cuddapah Basin, India and their implications. Jour. Geol. Soc. Ind., v.84, pp: 267-280.

McLaren, D.J., 1978. Preface of the Bulletin Proterozoic Red bed Sequences of Canada, v.311, pp: 1-62.

Melezhik, V.A., Lepland, A., Romashkin, A. E., Rychanchik, D. V., Mesli, M., Tor Erik Finne, Ronald Conze, and Far-Deep Scientists., 2005. The Great Oxidation Event Recorded in Paleoproterozoic Rocks from Fennoscandia. International Continental Scientific Drilling Program (ICDP) - The Fennoscandia Arctic Russia – Drilling Early Earth Project (FAR-DEEP).

Nagaraja Rao, B.K., Rajurkar, S.T., Ramalingaswamy, G., and Ravindra Babu, B., 1987. Stratigraphy, structure and evolution of the Cuddapah basin. In: Radhakrishna, B.P. (Ed.), Purana Basins of Peninsular India (Middle to Late Proterozoic), Geo-logical Society of India Memoirs, 6, pp: 33-86.

Odin, G.S., and Matter, A., 1981. De glauconiarum origine. Sedimentology, v.28, pp: 611–641.

Phillip W. Schmidt, and George E. Williams., 2008. Palaeomagnetism of red beds from the Kimberley Group, Western Australia: Implications for the palaeogeography of the 1.8 Ga King Leopold glaciation. Precambrian Res., v.167, pp: 267-280.

Pulla Reddy, V., Subba Reddy, N., and Prasad, C.V.R.K., 1990. Quartzites of the Cuddapah Group and Their Environment of Deposition Jour. Geol. Soc. Ind., v.35, pp: 408 to 420.

Rai, A.K., Pandey, U.K., Syed Zakaulla, and P.S., Parihar., 2015. New 1.9-2.0 Ga, Pb-Pb (PbSL), Age of Dolomites from Vempalle Formation, Lower Cuddapah Super group, Eastern Dharwar Craton, India. Jour. Geol. Soc. Ind., v.86, pp: 131-126.

Ravikant, V., 2010. Paleoproterozoic (1.9 Ga) extension and breakup along the eastern margin of the Eastern Dharwar Craton, SE India: New Sm–Nd isochorn age constraints from anorogenic mafic magmatism in the Neoarchean Nellore greenstone belt. Jour. Asian Earth Sci., v.12, pp: 67-81.

Saha, D., 2002. Multi-Stage Deformation in the Nallamalai Fold Belt, Cuddapah Basin, South India - Implications for

Mesoproterozoic Tectonisrn Along Southeastern Margin of India. Gondwana Res., v.5, pp: 701-719.

Sesha Sai, V.V., 2010. Petrology and Mineral Chemistry of Picrite Sill from Peddakudala-Velpula Area in Southwestern Part of the Proterozoic Cuddapah Basin, Andhra Pradesh, India. In: R.K. Srivastava (Ed.), Dyke Swarms: Keys for Geodynamic Interpretation, Springer-Verlag, Berlin Heidelberg, pp: 115-124.

Sesha Sai, V.V., 2014. Pyroclastic Volcanism in Papaghni Sub-basin, Andhra Pradesh: Significant Paleoproterozoic Tectonomagmatic Event in SW Part of the Cuddapah Basin, Eastern Dharwar Craton. Jour. Geol. Soc. India. v.83, pp: 355-362.

Sharma, M., and Shukla, M., 1998. Microstructure and microfabric studies of Paleoproterozoic small digitate stromatolites (Ministromatolites), from the Vempalle Formation, Cuddapah Supergroup, India. Jour. Pal. Soc. Ind., v.43, pp: 89-100.

Sreenivas, B., and Murakami, T., 2005. Emerging views on the evolution of atmospheric oxygen during Precambrian. Jour. Min. Pet. Sci., v.100, pp: 184-201.

Stanworth C. W., and Badham, J. P. N., 1984. Lower Proterozoic red beds, evaporites and secondary sedimentary uranium deposits from the East Arm, Great Slave Lake, Canada. Jour. Geol. Soc., v.141, pp: 235-242.

Strahler, A.N., 1981. Physical Geology. Harper and Row publications., pp: 612.

Tripathy, V., and Saha, D., 2013. Plate margin paleostress variations and intracontinental deformations in the evolution of the Cuddapah basin through Proterozoic. Precambrian Res., v.235, pp: 107-130.

Truswell, J.F., 1990. Early Proterozoic red beds in Kaapvaal Craton. University of Witwatersrand, Science, pp: 96.

Zimmer, C., 2013. Earth's Oxygen: A Mystery Easy to Take for Granted. New York Times. 3rd October 2013.

J. Ind. Geophys. Union ( May 2016 )
**v.20, no.3, pp: 351-361**

# Grain Size Distribution of Coastal Sands between Gosthani and Champavathi Rivers Confluence, East Coast of India, Andhra Pradesh

**Bangaku Naidu, K.,* Reddy, K.S.N., Ravi Sekhar, Ch., Ganapati Rao, P., and Murali Krishna, K.N.**
Department of Geology, Andhra University, Visakhapatnam-530003
*Corresponding Author: naidu0756@gmail.com

**ABSTRACT**
The studies on grain size characteristics are valuable to understand the source for the evolution of coastal sand environments. Seventy one sediment samples from twenty traverses of costal sediments in between Gosthani River mouth in south and Champavathi River in the north (Lat.17°52'-18°.02' N; Long.83°26'-83°36' E) have been collected and studied. The coastal sediments are medium to fine grained (1.68 Ø – 2.80Ø), very well sorted to moderately well sorted (0.26Ø – 0.67Ø), strongly coarse to fine skewed (-0.63 Ø to 0.31Ø) and pltykurtic to leptokurtic (0.74Ø – 1.27Ø) in nature and deposited in moderate to high energy environment conditions with dominant rolling, bottom and graded suspension mechanisms. The observations are supported by the frequency distribution curves, CM plots and scatter plots between parameters, conforming to the bimodal nature to dominant fine sand in different microenvironments (dune, backshore, berm, and foreshore). These textural parameters have been further examined to understand the hydrodynamic conditions of the depositional environments.

**Key words:** Textural parameters, coastal sands, coastal sediments, Dune, Backshore, Berm, Foreshore, Gosthani and Champavathi rivers

## INTRODUCTION

The 20 km stretch of study area (83°26'- 83°36'E longitudes and 17°52'-18°.02' N latitudes) extends from the Gosthani River in the south to the Champavathi River in the north. The area has different geological and geomorphic features generated by the rivers, small creeks, altered coastal trends, and dynamic seasonal winds. The ephemeral Gosthani and Champavathi rivers originate in Ananthagiri hill (1275m) ranges of Eastern Ghats constitute the drainage system. These rivers carry huge amount of sediments and debouch in to the Bay of Bengal at Bhimunipatnam and Konada in the study area. The present study deals with the grain size distribution of coastal sands between Gosthani and Champavathi rivers confluence in order to understand sediment depositional environments and the depositional patterns of the sediments in the study area.

The grain size characteristics of the sediments in the coastal areas are influenced of by various transporting and depositional agents such as rivers, rivulets, streams, waves and currents, sea level oscillations, shoreline configuration, winds, etc. and the distance from the shoreline, distance from the source material, nature of the source material and topography of the area. Earlier, many attempts have been made by several sedimentologists (Udden, 1914; Mason and Folk, 1958; Friedman, 1961, 1967; Sahu, 1964; Veerayya and Varadachari, 1975; Ramamohan Rao et al., 1982; Jagannadha Rao and Krishna Rao, 1984; Dhanunjaya Rao et al., 1989; Frihy et al., 2005; Hanamgoda and Chavidi, 1997; Mohan and Rajamanickam, 1998; Prabhakara Rao et al., 2000; Nageswara Rao et al., 2005; Rajesh et al., 2007; Ergine et al., 2007; Ramanathan et al., 2009; Rajasekhara Reddy et al., 2011; Ganesh et al., 2013; Karuna Karudu et al., 2013) to differentiate the sediments of various environments, such as fluvial, fluviatile, estuarine and other coastal environments. The present study is based on such interpretations to improvise the understanding of the depositional environments and depositional process of the sediments in the study area.

## MATERIALS AND METHODS

### Sampling and Grain size Analysis

A total of seventy one surficial sediment samples were collected in microenvironments viz. foreshore, berm, backshore and dune along twenty traverses, with an interval of 1 km (A, B, C…... T. from south to north). These traverses are laid perpendicular to the coast. The sample stations are shown in Figure 1. The grain size parameters data are given in the Tables 1 and 2. About one kg of sample is collected from each site/station, using a PVC pipe of 3 inches diameter and 40cm in length. The pipe is carefully inserted into the sediment layers to a depth of 40cm, taking all possible care against contamination. The sediment samples are repeatedly washed with distilled water for removal of salts and then dried. After drying, a sub sample weighing about 100grams is obtained by coning and quartering; to remove carbonate and organic matter. Samples were then treated with 10% dilute HCl and 6% $H_2O_2$ respectively and then

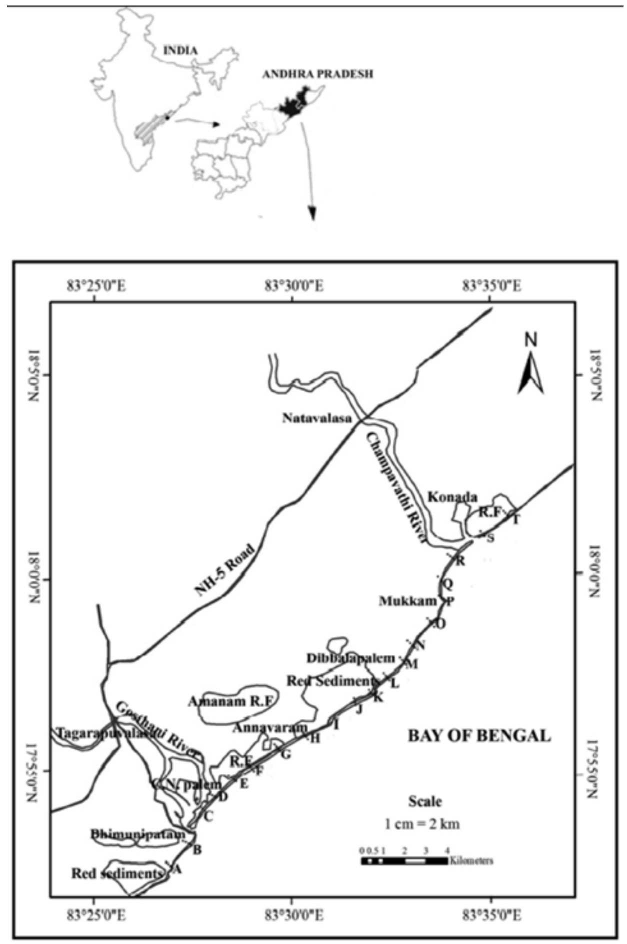


**Figure 1.** Sample Location Map of the Study Area.

dried. These samples were subjected to sieving with ASTM test sieves of 8″diameter, with successive sieves stoked at ½ Ø intervals for 10-20min. The grain size data obtained was used to determine the Mean size (Mz), Standard deviation ($\sigma_I$), Skewness ($SK_I$) and Kurtosis ($K_G$) based on method given by Folk and Ward (1957) and G-Stat software (Dinesh, 2009). Frequency curves, scatter plots and CM diagrams were drawn and data was analyzed.

## RESULTS AND DISCUSSION

The detailed representation of the grain size parameters in terms of grain size analysis, frequency distribution curves, scatter plots and CM diagrams have been presented and data analyzed.

### Grain size analysis

### Mean size (Mz)

The graphic mean size is the average size of the sediment represented by Ø mean size and it is an index of energy conditions. The average values show the dominance of fine sediments in all micro environments; the sediments of dune (1.78Ø -2.76Ø), backshore (1.69Ø -2.69Ø), berm (1.69Ø -2.61Ø) and foreshore (1.69Ø -2.69Ø) environments are in medium to fine size. It indicates the high energetic conditions of transportation in the coastal sediments (Folk and Ward (1957). The variations in Ø mean size is a reflection of the differential energy conditions of the depositing media and indicates average kinetic energy of depositing agent (Sahu, 1964).

### Standard Deviation ($\sigma_I$):

The graphic standard deviation ($\sigma_I$) measures sorting of sediments and indicates the fluctuations in the energy conditions of depositional environment. It, however, does not necessarily measure the degree to which the sediments have been mixed (Spencer, 1963). Standard deviation of the present samples range in between 0.26Ø-0.62Ø, with an average of 0.53Ø.It is within the range of well sorted. The sediments of dune, back shore, berm environments are moderately well sorted. Fore shore sediments are well

**Table1**. Grain size parameters of the coastal sediments between Gosthani River and Champavathi River confluence

| Travers No's | Samples No. | Mean(Ø) | Standard Deviation(Ø) | Skewness (Ø) | Kurtosis (Ø) |
|---|---|---|---|---|---|
| A | A1 | 2.78 | 0.26 | -0.04 | 1.17 |
| | A2 | 2.44 | 0.50 | -0.28 | 0.83 |
| | A3 | 2.34 | 0.58 | -0.26 | 0.81 |
| | A4 | 2.54 | 0.44 | -0.12 | 1.01 |
| B | B1 | 2.29 | 0.48 | -0.34 | 0.88 |
| | B2 | 2.18 | 0.59 | -0.28 | 0.79 |
| | B3 | 1.91 | 0.58 | 0.16 | 0.75 |
| | B4 | 1.98 | 0.58 | 0.20 | 0.74 |
| C | C1 | 2.41 | 0.59 | -0.12 | 0.91 |
| | C2 | 2.33 | 0.52 | -0.13 | 1.02 |
| | C3 | 1.94 | 0.54 | 0.22 | 0.89 |
| D | D1 | 1.73 | 0.58 | 0.31 | 0.88 |
| | D2 | 1.89 | 0.64 | 0.18 | 0.74 |
| | D3 | 2.29 | 0.53 | -0.26 | 1.01 |
| | D4 | 2.39 | 0.48 | -0.37 | 0.89 |
| E | E1 | 2.05 | 0.62 | 0.01 | 0.75 |
| | E2 | 2.50 | 0.61 | -0.33 | 0.92 |
| | E3 | 2.28 | 0.62 | -0.27 | 0.86 |
| | E4 | 2.19 | 0.58 | -0.15 | 0.88 |
| F | F1 | 2.5 | 0.49 | -0.21 | 1.1 |
| | F2 | 2.19 | 0.58 | -0.15 | 0.88 |
| | F3 | 2.56 | 0.45 | -0.12 | 1.07 |
| | F4 | 2.11 | 0.56 | 0.28 | 0.78 |
| G | G1 | 2.5 | 0.49 | -0.21 | 1.1 |
| | G2 | 2.19 | 0.58 | -0.15 | 0.88 |
| | G3 | 2.56 | 0.45 | -0.12 | 1.07 |
| | G4 | 2.11 | 0.56 | 0.28 | 0.78 |
| H | H1 | 2.8 | 0.49 | -0.63 | 0.92 |
| | H2 | 2.40 | 0.59 | -0.18 | 0.89 |
| | H3 | 2.17 | 0.62 | 0.05 | 0.78 |
| | H4 | 2.18 | 0.67 | -0.15 | 0.76 |
| I | I1 | 2.38 | 0.48 | -0.29 | 0.86 |
| | I4 | 2.76 | 0.48 | -0.47 | 0.83 |
| J | J1 | 2.14 | 0.56 | -0.05 | 0.86 |
| | J2 | 2.33 | 0.52 | -0.13 | 1.02 |
| | J4 | 2.62 | 0.45 | -0.09 | 0.94 |
| K | K1 | 2.38 | 0.59 | -0.25 | 0.84 |
| | K3 | 2.18 | 0.68 | -0.02 | 0.80 |
| | K4 | 2.46 | 0.45 | -0.13 | 0.96 |
| L | L1 | 2.6 | 0.46 | -0.13 | 0.98 |
| | L2 | 2.61 | 0.41 | -0.09 | 0.99 |
| | L3 | 1.91 | 0.58 | 0.16 | 0.75 |
| | L4 | 2.38 | 0.57 | -0.16 | 0.84 |
| M | M1 | 2.15 | 0.55 | 0.24 | 0.85 |
| | M2 | 2.61 | 0.39 | 0.01 | 0.96 |
| | M3 | 2.15 | 0.46 | -0.06 | 1.05 |
| | M4 | 2.61 | 0.41 | -0.09 | 0.99 |
| N | N1 | 2.14 | 0.58 | -0.09 | 0.9 |
| | N2 | 2.04 | 0.66 | 0.20 | 0.79 |
| | N3 | 2.29 | 0.53 | -0.26 | 1.01 |
| | N4 | 2.09 | 0.52 | 0.25 | 0.89 |
| O | O1 | 2.11 | 0.46 | -0.03 | 1.01 |
| | O2 | 1.72 | 0.59 | 0.24 | 1.22 |
| | O3 | 1.69 | 0.65 | 0.13 | 0.99 |
| | O4 | 1.78 | 0.59 | 0.30 | 1.15 |
| P | P1 | 1.88 | 0.47 | 0.11 | 0.8 |
| | P2 | 1.72 | 0.48 | 0.22 | 1.15 |
| | P3 | 2.12 | 0.42 | -0.03 | 1.04 |
| | P4 | 2.33 | 0.52 | -0.13 | 1.02 |
| Q | Q1 | 2.48 | 0.46 | -0.15 | 1.1 |
| | Q4 | 2.42 | 0.49 | -0.11 | 0.89 |
| R | R1 | 1.84 | 0.49 | 0.18 | 0.85 |
| | R2 | 1.69 | 0.53 | 0.21 | 1.25 |
| | R3 | 1.82 | 0.52 | 0.22 | 0.86 |
| | R4 | 2.50 | 0.63 | -0.20 | 0.88 |
| S | S1 | 1.68 | 0.51 | 0.24 | 1.23 |
| | S4 | 2.69 | 0.49 | -0.11 | 1.23 |
| T | T1 | 2.58 | 0.38 | -0.24 | 1.27 |
| | T2 | 2.39 | 0.48 | -0.37 | 0.89 |
| | T3 | 2.38 | 0.59 | -0.25 | 0.84 |
| | T4 | 2.19 | 0.58 | -0.15 | 0.88 |
| | **1=Foreshore 2=Berm 3=Back Shore 4=Dune** | | | | |

**Table2**. Range and average values of grain size parameters of the coastal sediments between Gosthani River and Champavathi river confluence.

| Micro Environments | Range | Mean Size (Mz) | Standard Deviation ($\sigma 1$) | Skewness (Sk) | Kurtosis (kG) |
|---|---|---|---|---|---|
| **Fore Shore** | Min. | 1.69 | 0.26 | -0.27 | 0.75 |
| | Max. | 2.69 | 0.62 | 0.22 | 1.23 |
| | Avg. | 2.28 | 0.49 | -0.09 | 0.97 |
| **Berm** | Min. | 1.69 | 0.39 | -0.37 | 0.74 |
| | Max. | 2.61 | 0.66 | 0.24 | 1.25 |
| | Avg. | 2.21 | 0.54 | -0.06 | 0.96 |
| **Back Shore** | Min. | 1.69 | 0.42 | -0.27 | 0.75 |
| | Max. | 2.69 | 0.68 | 0.22 | 1.23 |
| | Avg. | 2.12 | 0.55 | -0.04 | 0.92 |
| **Dune.** | Min. | 1.78 | 0.41 | -0.47 | 0.74 |
| | Max. | 2.76 | 0.67 | 0.30 | 1.23 |
| | Avg. | 2.33 | 0.53 | -0.08 | 0.92 |
| **Total** | **Min.** | **1.68** | **0.26** | **-0.63** | **0.74** |
| | **Max.** | **2.80** | **0.67** | **0.31** | **1.27** |
| | **Avg.** | **2.25** | **0.53** | **-0.07** | **0.94** |

sorted in nature. The Moderately well sorted nature can be attributed to partial winnowing action and addition of sediments in beach environment by aeolian process (Ramamohan Rao et al., 1982; Narayana Rao et al., 1991; Angusamy et al., 2006; Rajesh et al., 2007).

## Skewness ($SK_I$)

The graphic skewness measures the symmetry of the distribution, i.e. predominance of coarser or fine-sediments. The negative value denotes coarser material in coarser-tail i.e., coarse skewed, whereas, the positive value represents more fine material in the fine-tail i.e., fine skewed. Skewness value ranges in between -0.63 Ø and 0.31 Ø, with an average of -0.07 Ø. Positive skewness of sediments indicates the deposition of the sediments in sheltered low energy, whereas negative skewness of sediments indicates deposition at high energy environments (Rajasekhara Reddy et al., 2011). The negative skewness shown by majority of the samples of the study area indicates high energy nature of the beach deposits in general (Friedman, 1961) and multidirectional sediment transport (Martins 1965).

## Kurtosis ($K_G$)

The graphic kurtosis represents the peak distribution and measures the ratio between the sorting in the tails and central portion of the curve. The values of graphic kurtosis range from 0.74 Ø to 1.27 Ø, with an average of 0.94 Ø. Most of the samples fall under meso-kurtic category. Friedman (1962) suggests that extreme high or low values of kurtosis imply that part of the sediments achieved its sorting elsewhere in a high energy environment. The variation of kurtosis values is reflection of the flow characteristics of the depositional medium (Ramamohan Rao et al., 1982; Seralathan and Padmalal, 1994; Hanamgond et al., 1998).

## Frequency Distribution Curves

Frequency distribution curves (FDC) are the pictorial representation of weight percentage of different fractions of sediment. FDC are used to describe the nature of sediments. The assemblages of FDC from five sectors in four microenvironments of Bhimunipatnam to Konada are shown in Figures 2 (a - d). Bhimunipatnam, Nagamayyapalem and Annavaram sectors show bimodal nature and the other two sectors exhibit unimodal nature and fine sand. The majority of samples prominent peaks show the size range between 1.50Ø and 3.00Ø. The sediments seem to have been supplied from two sources, probably from river and beach environments.

## Scatter Plots

Scatter plots are used to understand the geological significance of the size parameters by studying the interrelationship between two variables. The grain size parameters of the sediments that are often environmentally sensitive are used to interpret various aspects of depositional environment (Folk and Ward, 1957; Inman, 1949; Friedman 1961, 1967; Moiola and Weiser 1968; Visher 1969). Combinations of various grain size parameters, in the form

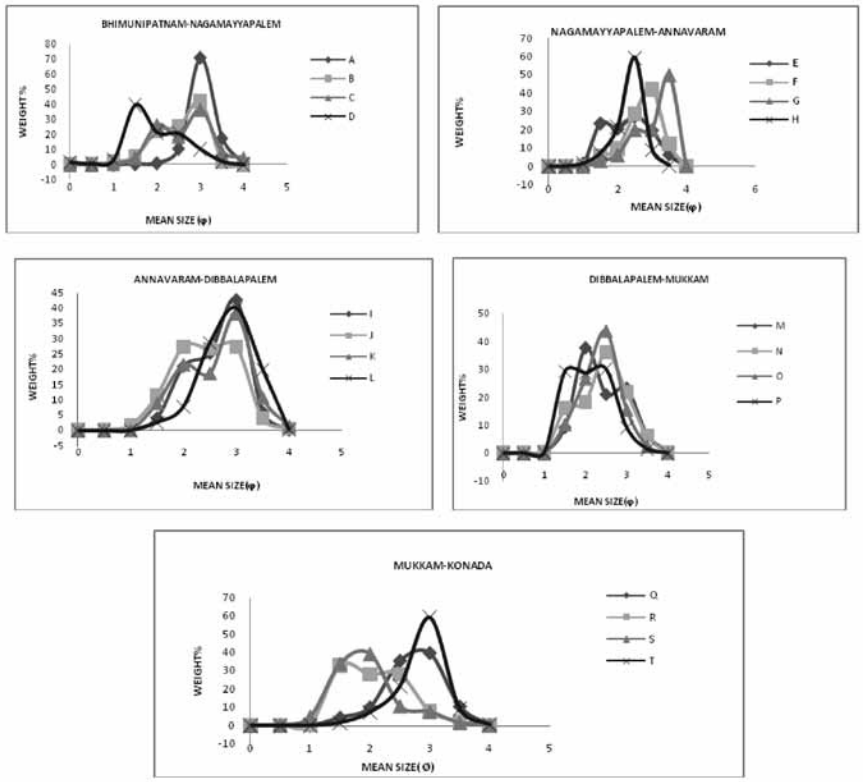


**Figure 2a.** Frequency Distribution Curves of Fore Shore Sediments, Bhimunipatnam-Konada Coast.

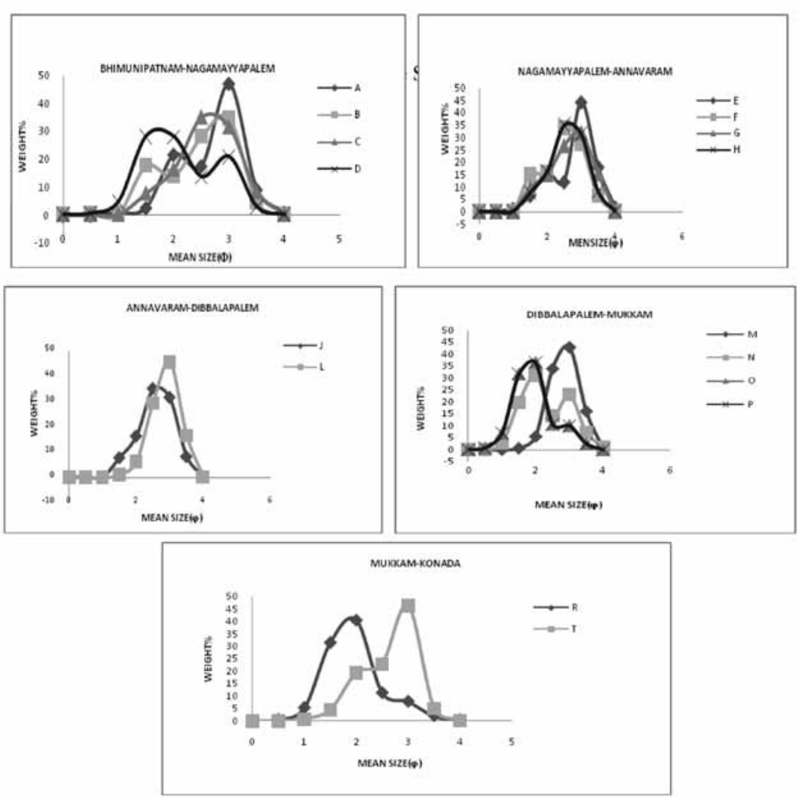


**Figure 2b.** Frequency Distribution Curves of Berm Sediments, Bhimunipatnam- Konada Coast.

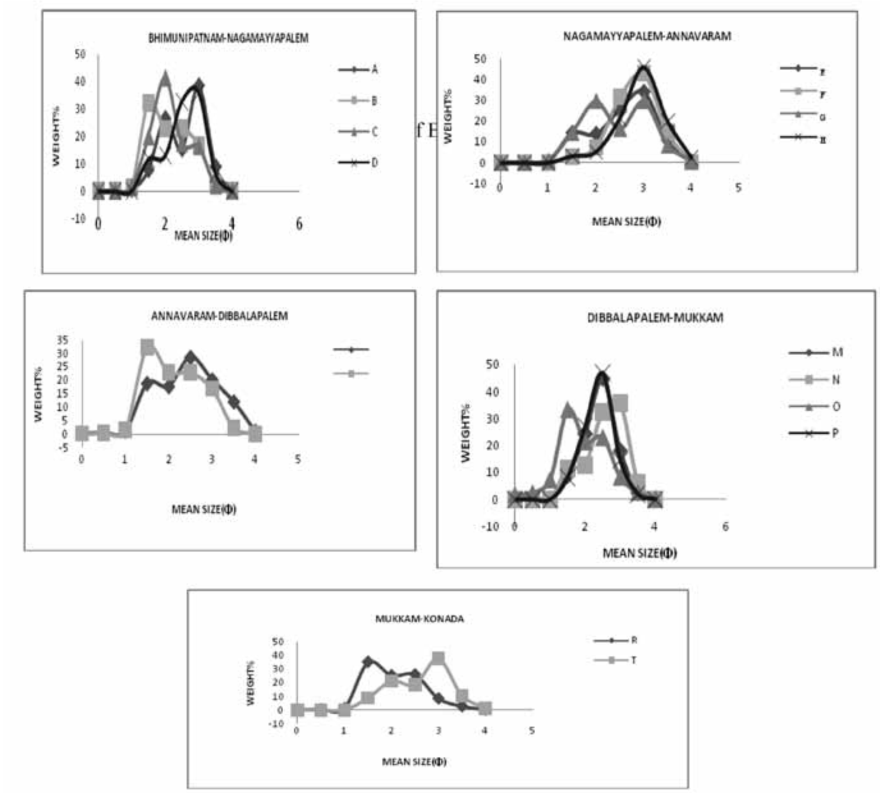


**Figure 2c.** Frequency Distribution Curves of Back Shore Sediments, Bhimunipatnam – Konada Coast.

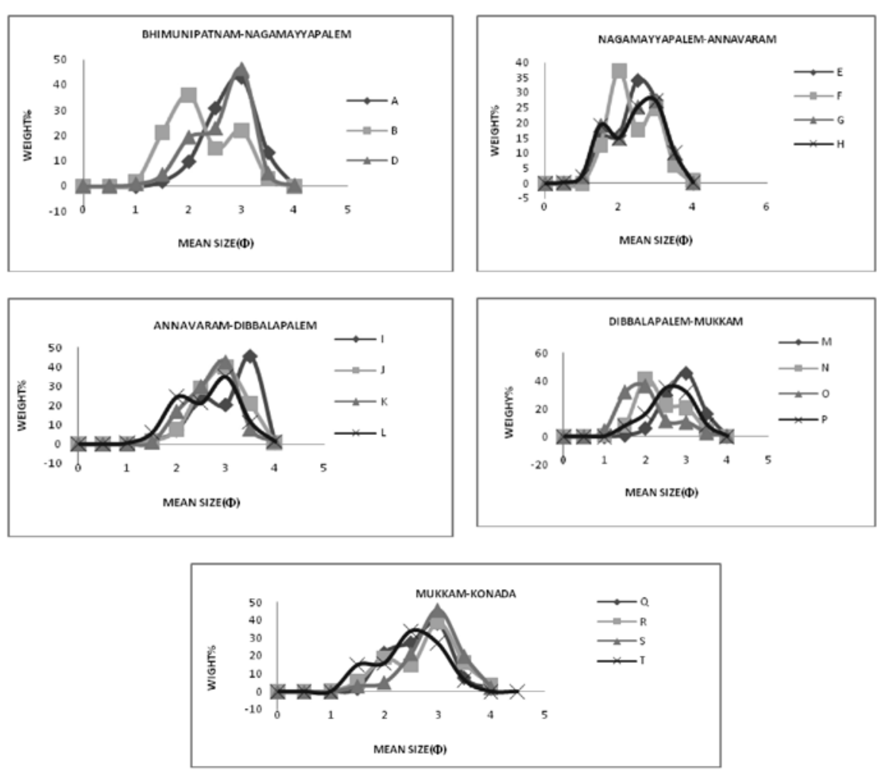


**Figure 2d.** Frequency Distribution Curves of Dune Sediments, Bhimunipatnam-Konada Coast

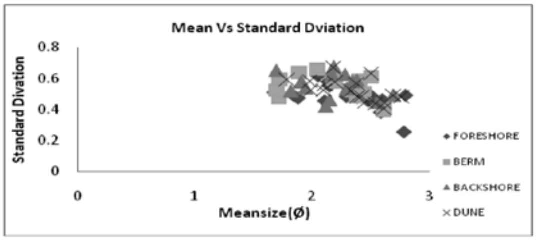


(a) Mean Size vs Standard Deviation

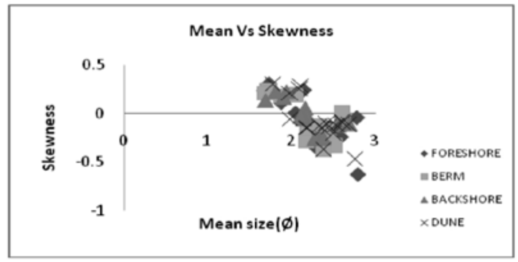


(b) Mean Size vs Skeweness

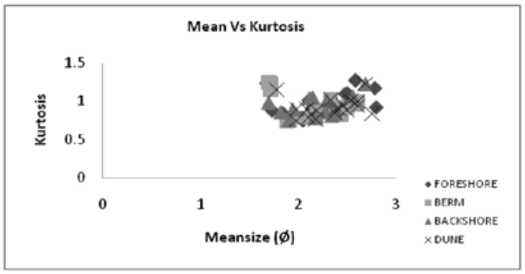


(c) Mean Size vs Kurtosis

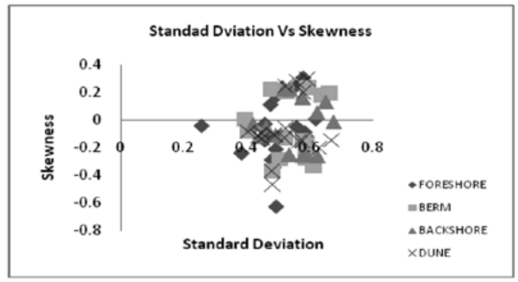


(d) Standad Deviation vs Skewness

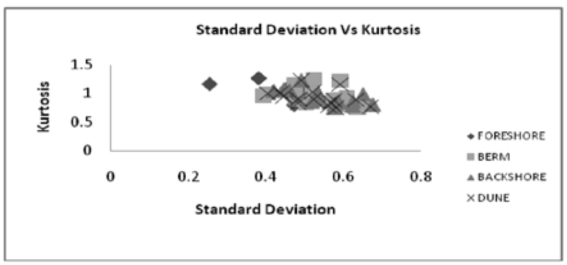


(e) Standard Deviation vs Skewness

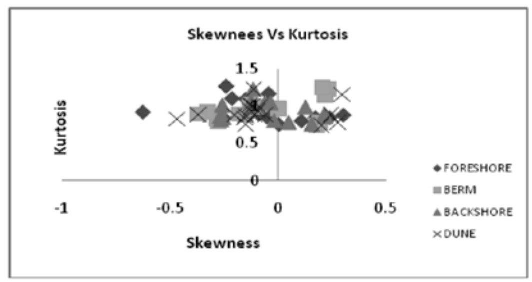


(f) Skewness vs Kurtosis.

**Figure 3.** Scatter plots of grain size parametars (a) Mean Size vs Standard Deviation ,(b) Mean Size vs Skeweness(c) Mean Size vs Kurtosis ,(d) Standad Deviation vs Skewness, (e) Standard Deviation vs Skewness and (f) Skewness vs Kurtosis.

of scatter plots, have been used to identify the depositional environment (Friedman, 1967). Scatter plots reasonably describe the role of addition and removal of fine and/or coarse fraction during the transit of sediment along beaches as well as in river beds, in controlling the variation in grain size/statistical parameters among the sediments. The relationship between different size parameters were studied by drawing various scatter plots viz. mean size vs. standard deviation, mean size vs. skewness, mean size vs. kurtosis, standard deviation vs. skewness, standard deviation vs. kurtosis and skewness vs. kurtosis Figure 3.

## Mean size vs. Standard Deviation

The scatter plot between mean size and standard deviation Figure 3a clearly indicates that sorting decreases with increase of mean size of the dune, backshore, berm and foreshore sediments from bimodal and the dominant constituent is fine sand. Similar types of observations have been reported in the sands of East Coast of India (Nagamalleswara Rao, 1998; Prabhakara Rao et al., 2000; Nageswara Rao et al., 2005).

## Mean Size vs. Skewness

The scatter plots between mean size and skewness Figure 3b indicate that in general, the sediments having mean size range from 1.68Ø – 2.80Ø in dune, berm, backshore and foreshore fine sediments exhibit negative skewness. The sediments of negative skewness occur in high energy environments, while sediments with positive skewness occur in low energy environments.

## Mean Size vs. Kurtosis

The scatter plot between mean size and kurtosis in dune, berm, backshore and foreshore sediments are shown in Figure 3c. The scatter plot values indicate a dominance of mesokurtic nature (0.74Ø -1.27Ø) in the mean size ranges of 1.68Ø – 2.80Ø i.e. medium to fine sediments.

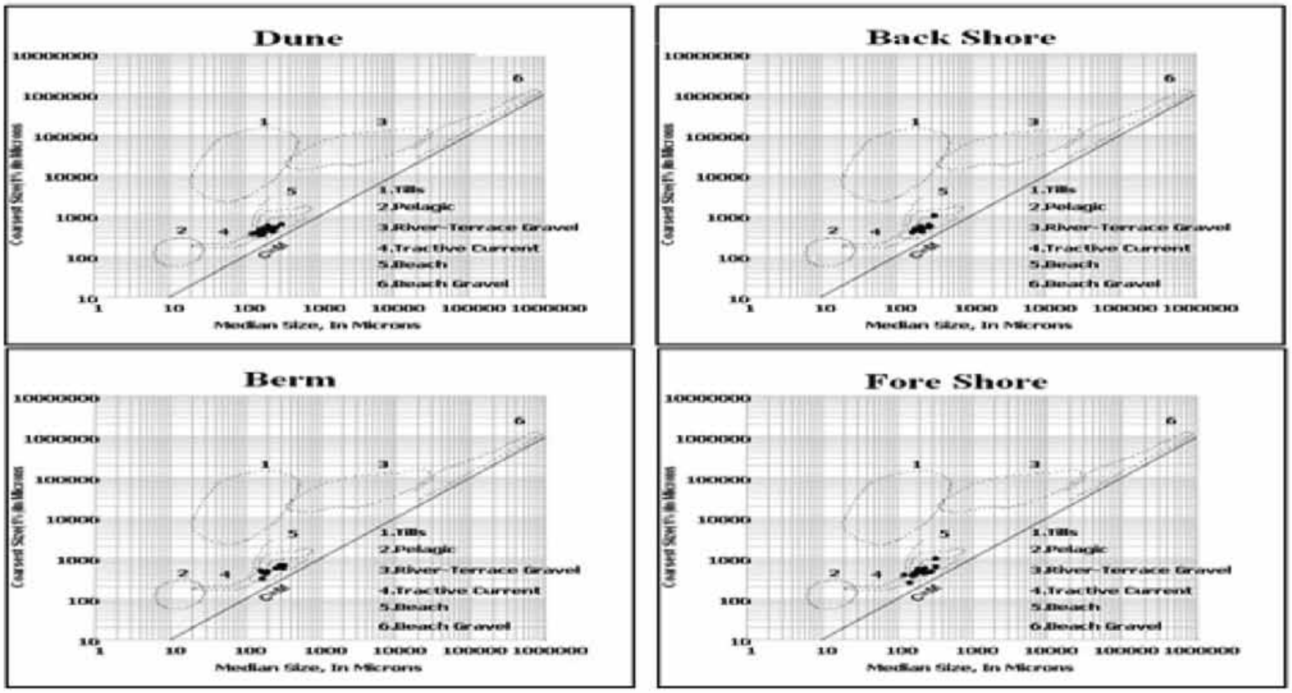


**Figure 4a.** The basic CM pattern of coastal sediments between Gosthani and Champavathi river mouth.

## Standard Deviation vs. Skewness

The scatter plot between standard deviation and skewness Figure 3d shows that sediments are moderately well sorted and negative skewed in backshore, berm, foreshore and dune sediments. If skewness decreases standard deviation improves. This may be due to two conditions i.e. either unimodal samples with good sorting or equal mixture of two models (Ashok et al., 2009; Harsha Sundar et al., 2010).

## Standard Deviation vs. Kurtosis

The scatter plots between standard deviation and kurtosis Figure 3e indicate that majority of the sediment samples are of platykurtic to mesokurtic in nature and moderately well sorted.

## Skewness vs. Kurtosis

The scatter plot between skewness and kurtosis Figure 3f shows that dune, backshore, berm and foreshore sediment values indicate dominance of platykurtic category followed by mesokurtic (0.74Ø-1.27Ø). The majority of samples are negative skewed (Chakraborthy, 1977)

## C M diagrams

The CM patterns of the sediments are useful for analyzing transportation mechanism, depositional environment with respect to size, range and energy level of transportation. They also are useful in determining process and characteristic agents that are responsible for the formation of clastic sediments. The present study is an attempt to identify the modes of transportation and deposition of sediments between Bhimunipatnam to Konada coast, in different microenvironments viz. dune, backshore, berm, foreshore sediments by CM patterns.

The present interpretation is based on procedure adopted by Passega (1957, 1964). He interpreted the distinct pattern of CM plots in terms of different modes of transportation by plotting coarsest first percentile value of the sediments (C). Percentile value is plotted against the median diameter (M) on a double logarithmic paper. Visher (1969) explained a log normal sub populations within the total grain size distribution curves, as representing suspension, saltation and surface creep or rolling modes of transportation mechanisms. The relation between C and M is the effect of sorting by graded turbulence. The C-M plots Figure 4A and 4B show that most of the samples have been formed by two different depositional conditions. The sediment samples of C-M plots Figure 4A from dune, backshore, berm and foreshore fall in region of 4 and 5, which indicates high tractive and beach currents of deposition. Most of the samples fall in the OP, PQ regions Figure 4B. This indicates that part of the load has rolled sediments followed by bottom and graded suspension, representing their deposition through tractive currents. In general, this indicates presence of comparatively more

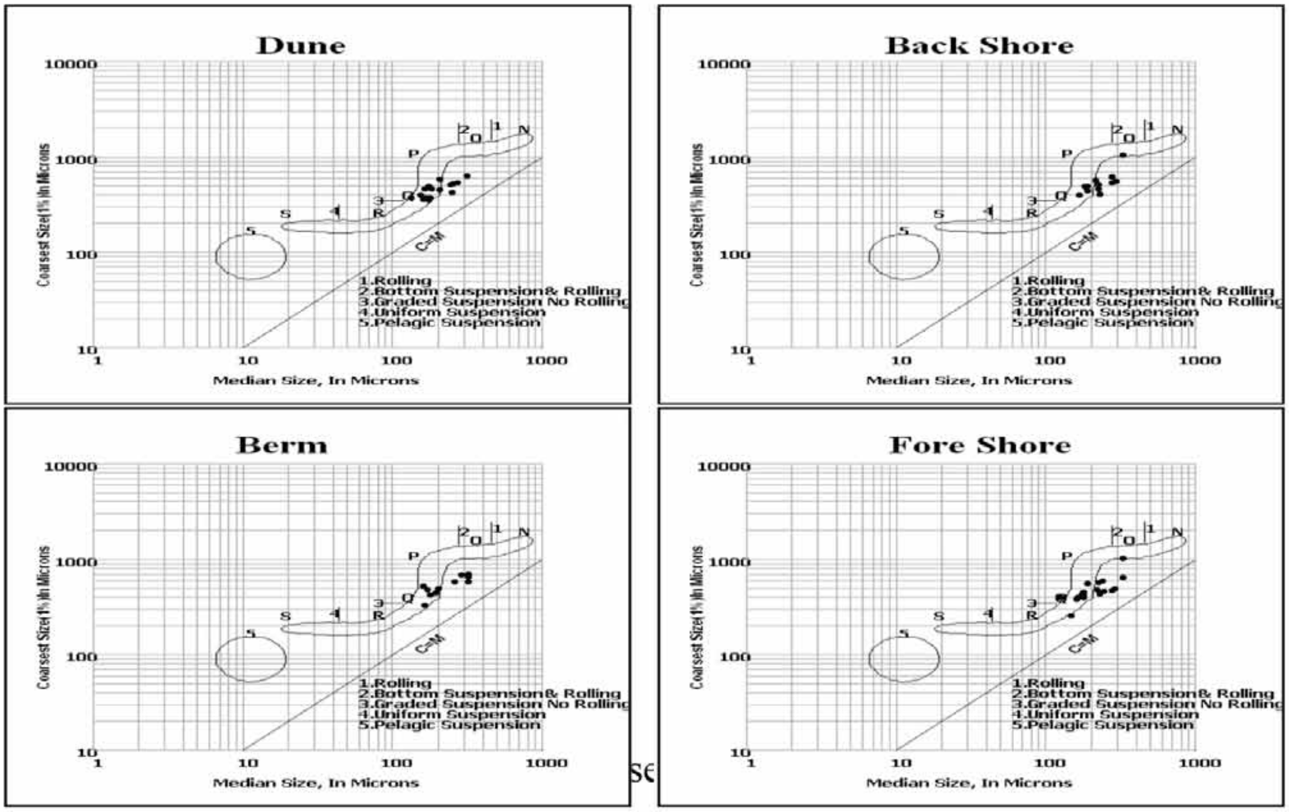


**Figure 4b.** The tracative currents of CM pattern of Coastal sediments between Gosthani and Champavathi river mouth.

percentage of medium to fine sand grained material (Rajasekhara Reddy et al., 2011; Bull, 1962; Passega and Byramjee, 1969)

## SUMMARY AND CONCLUSIONS

The grain size parameters of coastal sediments, between Gosthani and Champavathi rivers confluence, indicate medium to fine sand (1.68Ø – 2.80Ø), well sorted to moderately sorted (0.26Ø -0.67Ø), coarse skewed to fine skewed (-0.63Ø to 0.31 Ø), pltykurtic to leptokurtic (0.74 Ø -1.27 Ø) in nature.

The wide variation of mean size indicates differential energy conditions at different locations. However, the variation in sorting values indicates continuous addition of finer to coarser material in varying proportion at different locations.

Frequency distribution curves and scatter plots drawn between different grain size parameters clearly establish that the sediments are bimodal and composed of mainly fine sand.

The C-M plots indicate that the transportation is mainly in two different depositional conditions, viz. bottom and graded suspension for coastal sediments. This study establishes the usefulness of selecting several stations for better understanding beach environment of deposition.

## ACKNOWLEDGEMENTS

We are thankful to the authorities of Department of Geology and Delta Studies Institute, Andhra University for extending the lab facilities to carry out this work. Financial assistance from CSIR-UGC (NET) to K.Bangaku Naidu, in the form of SRF is acknowledged. Valuable comments/suggestions made by anonymous reviewer and apt editing by Chief Editor enhanced quality of the manuscript.

## Compliance with Ethical Standards

The authors declare that they have no conflict of interest and adhere to copyright norms.

## REFERENCES

Angusamy, N., and Rajamanickam, G.V., 2006. Depositional environment of sediments along the Southern coast of Tamil Nadu, India. Oceanologia., v.48, no.1, pp: 87-102.

Ashok, K., Srivastav and Rupesh, S., Mankar., 2009. Grain size analysis and depositional pattern of upper Gondwana Sediments (Early Cretaceous) of Salabardi area, districts Amravati, Maharashtra and Betul, Madhya Pradesh, Jour. Geo. Soc. of. India, v.73, pp: 393-406.

Bull, W.B., 1962. Relation of textural patterns of depositional environment of Alluvial fan deposits. Jour. Sed. Pet., v.32, pp: 211-216.

Carver, R.W., 1971. Procedures in sedimentary petrology. John wiles, Newyork, pp: 458.

Chakraborthy, A., 1977. Polymodel composition of beach sediments from the East Coast of India. Jour. Sed. Pet., v.47, no.2, pp: 634-641.

Dinesh, A.C., 2009. G-Stat-A Software in VB6 for grain size statistical analysis, CM diagrams, trend diagrams, etc. designed and developed by A.C. Dinesh, Geologist, Marine wing, GSI, Mangalore.

Dhanunjaya Rao, G., Krishnaiah Settey, B., and Rami Naidu, Ch., 1989. Heavy mineral content and textural characteristics of coastal sands in the Krishna-Godavari, Gosthani – Champavathi, and Penna river deltas of Andhra Pradesh, India: a comparative study. Journal of Atomic Mineral Science (Joams), Earfam. v.2.

Ergine, M., Seref Keskin, Umaran Dogan, A., Yusuf, K. K., and Zehra Karakas., 2007. Grain Size and heavy mineral distribution as related to hinterland and environmental condition for modern beach sediments from the Gulf of Antalya and Finke, Eastern Mediterranean. Mar. Geol., v.240, pp: 185-196.

Folk, R.L., and Ward, W.C., 1957. Brazos River Bar: A study in the significance of grain-size parameters. Jour. Sed. Pet., v.27, pp: 3-26.

Friedman, G.M., 1961. Distinction between dune, beach and river sands from their textural characteristics. Jour. Sed. Pet., v.27, pp: 3-26.

Friedman, G.M., 1967. Dynamic processes and statistical parameters compared for size frequency distribution of beach and river sands. Jour. Sed. Pet., v.37, pp: 327-354.

Frihy, O.E., Lofty, M.F and Komar, P.D., 1995. Spatial variation in heavy minerals and patterns of sediment sorting along the Nile Delta, Egypt. Sed. Geol., v.97, pp: 33-41.

Ganesh, B., Naidu, A.G.S.S., Jagannadha Rao, M., Karuna Karudu, T., and Avataram, P., 2013. Studies on textural characteristics of sediments from Gosthani river estuary- Bhimunipatnam, A.P., East Coast of India. Jour. Ind. Geophys. Union., v.17, no.2, pp: 139-151.

Harsha Sundar, E., Reddy, K.S.N., Vani Sailaja, V., and Murthy, K.N.V.V., 2010. Textural characteristics of coastal sands between Kakinada Bay and Tandava River Confluence, Andhra Pradesh, East Coast of India. Jour. Ind. Assoc. of Sed., v.29, pp: 61-69.

Hanamgond, P.T., and Chavadi, V.C., 1998. Sediment Movement and depositional environment of Kawada Bay beaches, Uttara Kannada district, West coast of India., Jour. Geol. Soc. of India., v.56, pp: 193-200.

Inman, D.L., 1949. Sorting sediments in the light of fluid mechanics. Jour. Sed. Petrol., v.19, pp: 10-30.

Jagannadha Rao, M., and Krishna Rao, J.S.R., 1984. Textural and mineralogical studies on red sediments of Visakhapatnam-Bhimunipatnam coast. Geo views, v.12, no.2, pp: 57-64.

Karuna Karudu, T., Jagannadha Rao, M., Ganesh, B., Avataram, P., Naidu, A.G.S.S., 2013. Studies on textural characteristics of Erra Kalva River, west Godavari District, Andhra Pradesh, East Coast of India. International Journal of Geomatics and Geosciences. v.4, no.2, pp: 280-295.

Martins, L. R. 1965. Significance of skewness and kurtosis in environmental interpretation. Jour. Sed. Petrol., v.35, pp: 768-770.

Mason, C.C., and Folk, R.L., 1958. Differentiation of beach, dune and aeolian flat environments by size analysis. Mustang Island, Texas. Jour. Sed. Petrol., v.28, pp: 211-226.

Mohan, P.M., and Rajamanickam, G.V., 1998. Depositional environment: Inferred from grain size along the coast of Tamil Nadu. Jour. Geo. Soc. of. India. v.52, pp: 95-102.

Moiola, R.J., and Weiser, D., 1968. Textural Parameters: An evolution. Jour. Sed. Petrol., v.38, pp: 45-53.

Nagamalleswara Rao, B., 1998. Textural studies of beach and dune placer deposits of Andhra Pradesh coast. Jour. Sed. Petrol., v.41, no.1, pp. 27-32.

Nageswara Rao, N., Suryam, R.K., and Ranga Rao, V., 2005. Depositional environment inferred from grain size parameters of the beach sediments between False Devi Point to Kottapatnam, Andhra Pradesh Coast. Jour. Geo. Soc. of. India., v.65, pp: 317-324.

Narayana, A.C., Pandarinath, K., Karbasi, A.R., and Raghavan, B.P., 1991. Note on silica sands of South Kanara Coast, Karnataka, India. Jour. Geo. Soc. of. India., v.37, pp: 164-171.

Passega, R., 1957. Textural characteristics of clastic deposition. Bull. Amer. Assoc. Petrol. Geol., v.41, no.9, pp: 1952-1984.

Passega, R., 1964. Grain size representation by CM patterns as a Geological tool. Jour. Sed. Petr., v.34, no.4, pp: 830-847.

Passega, R., and Byramjee, R., 1969. Grain size image of clastic deposit. Sedimentology, v.13, pp: 233-252.

Prabhakara Rao, A., Panda, N.K., Subrahmanyam, A.V., Ravi, G.S., and Deshmukh, R.D., 2000. Textural characteristics of sands in the interpretation of depositional environments between River Varaha and Mulapeta Creek, East Coast of India. Jour. Ind. Acad. Geosci., v.43, pp: 1-8.

Rajasekhara Reddy, D., and Karuna Karudu, T., 2009. Textural characteristics of the sediments of Mahanadi Delta, East Coast of India. Jour. Ind. Assoc. of. Sed., v.30, no.1, pp: 73-85.

Rajesh, E., Anbarsu, K., and Rajamanickam, G.V., 2007. Grain size distribution of silica sands in and around Marakkanam Coast of Tamil Nadu. Jour. Geo. Soc. of. India., v.69, pp: 1361-1368.

Ramanathan, A.L., Rajkumar, K., Jayjit Majumdar., Gurmeet Singh., Behera, P.N., Santhara, S.C., and Chidambaram, S., 2009. Textural characteristics of the surface sediments of a tropical mangrove Sundarban ecosystem India. Indian journal of marine sciences., v.38, no.4. pp: 397-403.

Ramamohan Rao, T., Shanmukha Rao, Ch., and Sanyasi Rao, K., 1982. Textural Analysis and Mineralogy of the Black Sand Deposits of Visakhapatnam-Bhimunipatnam Coast, Andhra Pradesh, India. Jour. Geo. Soc. of. India. v.23, pp: 284-289.

Sahu, B.K., 1964. Depositional mechanism from the size analysis of clastic sediments. Jour. Sed. Pet., v.34, pp: 73-83.

Seralathan, P., and Padmalal, D., 1994. Textural studies of surficial sediments of Muvattupvzha river and central vembanad estuary, Kerala. Jour. Geo. Soc. of. India., v.43, no.2, pp: 179-190.

Udden, J.A., 1914. Mechanical Composition of Clastic Sediments. Geol. Soc. Amer. Bull., v.25, pp: 655-744.

Veerayya, M., and Varadachari, V.V.R., 1975. Depositional environments costal sediments of Calangute, Goa. Sedimentary Geology, v.14, pp: 63-74.

Visher, G.S., 1969. Grain Size distribution and depositional processes. Jour. Sed. Pet., v.39, pp: 1074-1106.

J. Ind. Geophys. Union ( May 2016 )
**v.20, no.3, pp: 362-364**

**- A TECHNICAL REPORT**

# Unusual lightning activity over Andhra Pradesh and Telangana on 6 September, 2015: A Report

**Kamaljit Ray[1], S.C. Bhan*[1] and S. Stella[2]**
India Meteorological Department, [1]New Delhi, [2]Chennai
*Corresponding Author: scbhan@gmail.com

## INTRODUCTION

Lightning is an electrical discharge caused when static electricity builds up between thunderclouds, or thunderclouds and the ground. Lightning strokes carry up to 100 million volts of electricity and leap from cloud to cloud, or cloud to ground and vice versa. In India, lack of central database as a record of past disasters is a major constraint for compilation of disaster history in the country. Different sources of data have different figures of casualties and impacts, thereby hindering an objective assessment. However, data compiled by the ministry of Home Affairs suggests lightning, a natural calamity, can injure/ kill fauna and humanbeingswww.undp.org/content/dam/india/.../disaster_management_in_india.pdf). Lightning is always associated with thunder cloud. Thunder is a direct result of lightning. Thunder is the noise caused by the explosive expansion of air due to the heat generated by a lightning discharge. However, it is possible not to hear the thunder on some occasions if it is too far away. Lightning strokes can produce severe injuries and death. The injuries may be caused by thermal burns. However, usually the nerves and muscles may be directly damaged by the high voltage current.

Severe convective activity with lightning occurred over many parts of Andhra Pradesh and Telangana on 6 September, 2015 leading to a number of deaths. As per news paper reports by The Hindustan Times dated 07 September, 2015 (http://www.hindustantimes.com/india-news/20-killed-by-lightning-as-heavy-rains-lashed-andhra-pradesh/article1-1388237.aspx) lightning caused twenty deaths in the two states. The number was 23 as per The Deccan Chronicle and BBC News (http://www.deccanchronicle.com/150907/nation-current-affairs/article/lightning-rain-kill-23-andhra-pradesh, http://www.bbc.com/news/world-asia-india-34171362). Deaths were reported in Nellore, Prakasam, Krishna, East Godavari, Cuddapah & Guntur districts of Andhra Pradesh and Mahbubnagar district of Telangana. A brief analysis of the meteorological conditions leading to the event is given below.

**Key words:** Lightning, thunder cloud, high voltage current, meteorological conditions, Andhra Pradesh, Telangana.

### Meteorological Conditions:

Streamline analysis 0000 UTC of 06 September (Figure 1) shows a trough extended upto 1.5 km above mean sea level from Marathawada to Lakshadweep across interior Karnataka. Streamline convergence over Andhra Pradesh and Telangana is clearly seen in the figure. Relative humidity (RH) analysis over the region (Figure 2a&b) shows that very high RH (>75%) in the lower levels (925 hPa) with a relatively drier atmosphere in the middle (500 hPa). This kind of distribution of moisture coupled with convergence provided a potentially convective atmosphere. Convective available potential energy (CAPE) values were 1500 - 2000 J/kg at 0000 UTC on 6 September (Figure 1a). These conditions led to widespread thunderstorm activity over the region (Table 1) associated with lightning. Convective clouds with cloud top temperature (CTT) < -40°C were seen in satellite imagery from 0800 UTC (1330 IST) to 1600 UTC (2130 IST) of 6 September over Telangana and Andhra Pradesh (Figure 3a-d). Sequence of clouds in Figure 3 shows eastward movement of convection under influence of easterly winds in the upper troposphere (not shown here). Time of occurrence of thunderstorms in Table 1 also shows that the thunderstorms started earlier in eastern parts of the region. This thunderstorm activity was associated with an eastward moving strong lightning activity over the regions from 0800 to 1600 UTC (Figure 4-d).

Most of the persons who died due to lightening on 6 September were working outdoors. Statistics, worldwide, suggest that persons working outdoors are the worst hit. The U.S. National Lightning Safety Institute advises to have a plan for their safety when a thunderstorm occurs and to commence it as soon as the first lightning or thunder is observed. This is important as lightning can strike without rain actually falling. If a thunder is heard or lightning is seen, then there is a risk of lightning. The F-B (flash to boom) method is used to gauge distance to a lightning strike. The flash of a lightning strike and resulting thunder occur at roughly the same time. But light travels 300,000 kilometres in a second, almost a million times the speed of sound (344 m/s). So the flash of lightning is seen before thunder is heard. To use the method, count the seconds between the lightning flash and thunder. Divide by three to determine

**Table 1.** Thunderstorms reported over Andhra Pradesh and Telangana

| Station Name | Thunderstorm duration on 6th September, 2015 (Time in IST) | Rainfall reported in mm |
|---|---|---|
| Nizamabad | 1705-1800, 2030-2230 | 0.9 |
| Ramagundam | 2100-2400 | 0.0 |
| Kalingapatnam | 1100-1300, 1400-1820 | 59.2 |
| Hyderabad | 1545-1930 | 0.4 |
| Tuni | 1315-1445, 1800-2115. | 19.6 |
| Visakhapatnam | 1440-1700 | 22.5 |
| Vijayawada, AP | 1250-1540,1755-2230 | 20.2 |
| Masulipatnam | 1310-1550, 1905-2205 | 30.0 |
| Narsapur | 1400-1450, 1715-2100 | 0.3 |
| Kakinada | 1450-1650 | 15.8 |
| Kurnool | 1715-1745, 1845-2100 | 12 |
| Bapatla | 1350-1915 | 3.7 |
| Ongole | 1245-1820 | 0.0 |
| Anantapur | 2100-2215, 2335-0045 | 18 |
| Kavali | 1100-1330 | 12.2 |
| Nellore | 1315 -1430 ,1430 -1445 | 36.8 |
| Tirupathi AP | 1200-1445 | 11.2 |

the distance in kilometres. Immediate precautions against lightning should be taken if the F-B time is 25 seconds or less, that is, if the lightning is closer than 8 km. The safest place is inside a building or a vehicle. Risk remains for up to 30 minutes after the last observed lightning or thunder. The US National Weather Service (http://www.lightningsafety.noaa.gov/tips.shtml) and the US Centres for Disease Control and Prevention (http://www.cdc.gov/features/lightning-safety/) provides the following tips about lightning safety.

## SAFETY NORMS

### Indoor Lightning Safety

- Stay off corded phones, computers and other electrical equipment that put you in direct contact with electricity.
- Avoid plumbing, including sinks and baths.
- Stay away from windows and doors, and stay off porches.
- Do not lie on concrete floors, and do not lean against concrete walls.
- Stay in safe shelter at least 30 minutes after you hear the last sound of thunder.

### Outdoor Risk Reduction Tips

If caught outside with no safe shelter anywhere nearby, the following actions may reduce risk:

If you hear thunder, lightning is close enough to strike you. Suspend or postpone the outdoor activity and go indoors. Find a safe, enclosed shelter.

- Immediately get off elevated areas such as hills, mountain ridges or peaks
- Never lie flat on the ground
- Never shelter under an isolated tree or a cliff or rocky overhang for shelter
- Immediately get out and away from ponds, lakes and other bodies of water
- Stay away from objects that conduct electricity (barbed wire fences, power lines, windmills, etc.)
- As of now no regulated safety guidelines are available specifically for India. However, if above precautions are followed, deaths and injuries due to lightning can be avoided.

## ACKNOWLEDGEMENTS

We thank various organisations for usage of web links. We place on record our thanks to IMD officials for their support. We thank Chief Editor of JIGU for inviting us to present this report.

### Compliance with Ethical Standards

The authors declare that they have no conflict of interest and adhere to copyright norms.

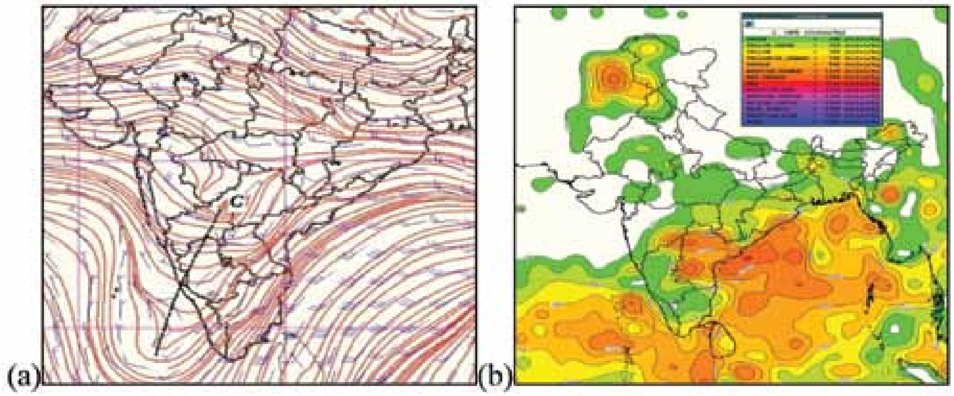

**Figure 1.** Streamline analysis at 925 hPa (a) and CAPE (b) at 0000 UTC of 6 September, 2015.

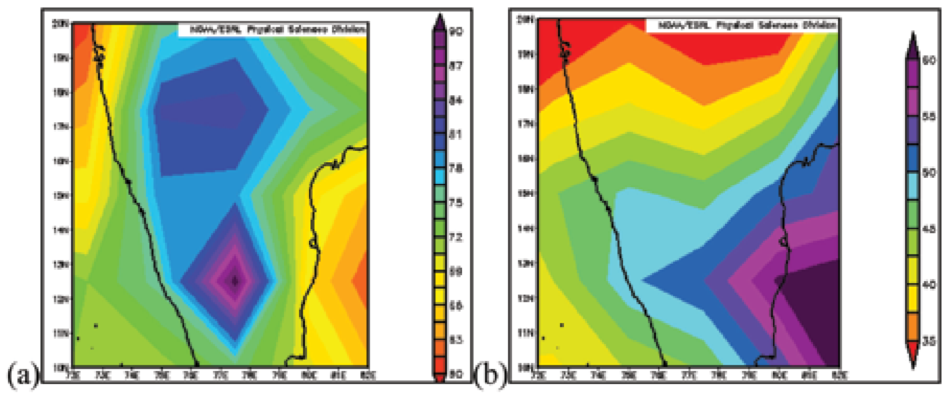

**Figure 2.** Relative Humidity (%) at 925 hPa (a) and 500 hPa (b) on 6 September, 2015.

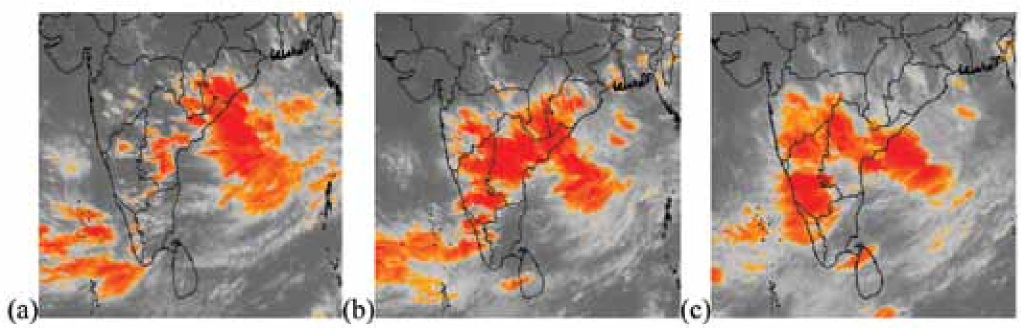

**Figure 3.** Satellite Imagery at 1330 (a), 1730 (b) and 2130 IST (c). Red colour shows area with CTT <-40° C.

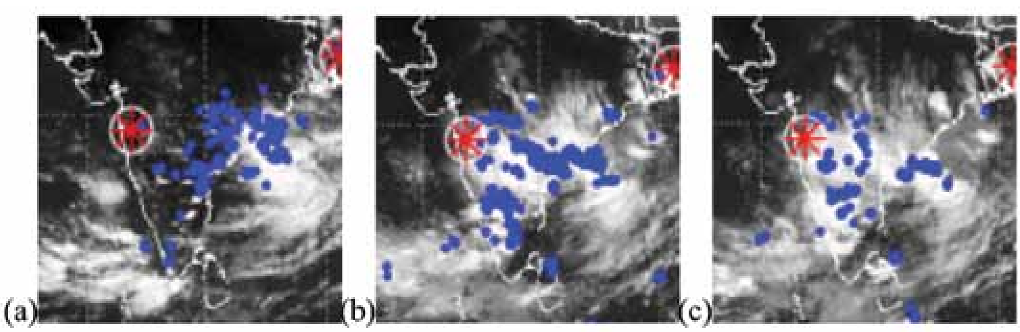

**Figure 4.** Lightning (blue dots) on 6 September, 2015 during 1230-1330 IST (a), 1830-1930 IST (b) and 2030-2130 IST (c). (http://wwlln.net/WWLLN_movies/Movie_of_Lightning_over_Indian_Ocean_BIG.gif).

J. Ind. Geophys. Union ( May 2016 )
**v.20, no.3, pp: 365-367**

**RESEARCH NOTE**

# Lithological Characteristics Analysis of Ridderkerk Area in the Western Netherlands using Wavelet Transform

**Soumya Chandan Panda*[1], Sankar Kumar Nath[1] and Niva Brahma[2]**
[1]Department of Geology & Geophysics, Indian Institute of Technology, Kharagpur
[2]Department of Applied Geophysics, Indian School Of Mines, Dhanbad
*Corresponding Author: scpagp@gmail.com

## ABSTRACT

Various wavelet transform techniques have been used for delineating lithological boundaries and to provide subjective leads for reservoir characterization. A multi-scale analysis of the well log data was performed using both the Continuous Wavelet Transform (CWT) and Discrete Wavelet Transform (DWT) analyses. The gamma ray log was first DWT analyzed using the Haar Wavelet and decomposed 7 times. The discrete coefficients pertaining to the $7^{th}$ level of decomposition were CWT analyzed using the Haar Wavelet at various scales ranging from 2-10 m, 10-20 m, and 20-100 m and the results of the analysis have been presented. This study demonstrates that Wavelet Transforms can effectively be used for bed boundary detection as a first approximation, as demonstrated through the comparison with the facies log presented. This technique can, therefore, be used cost-effectively in a short time span for valuable resource delineations in Geoexploration.

**Key words**: Lithological characteristics, wavelet transform, gamma ray log, Ridderkerk, western Netherlands

## INTRODUCTION

The accurate identification of lithofacies is of prime importance especially in complex geological environment pertaining to hydrocarbon reservoirs. Conventional core has been used extensively for obtaining detailed information of the well, but recovery of cores is an expensive and exhaustive process. An alternate to this is well log analysis, which is incongruous and interpreter dependent, and can lead to multiple interpretations and inferences. Various wavelet transform techniques have been used for delineating lithological boundaries and to provide subjective leads for reservoir characterization. We have tested disparate wavelet-types on radioactivity logs of wells belonging to the Stratton Field and come up with an innovative approach using Continuous Wavelet Transform (CWT) and Discrete Wavelet Transform (DWT) towards lithological characterization , which are very crucial especially in the exploration of hydrocarbons.

## METHODOLOGY

A multiscale analysis of the well log data was performed using CWT and DWT analysis (Perez-Muñoz et al., 2013), which is defined given by Equation 1 and Equation 2.

$$CWT_f(u,s) = \int_{-\alpha}^{\alpha} f(x)\psi_{u,s}(x)dx = \frac{1}{\sqrt{|s|}}\int_{-\alpha}^{\alpha} f(x)\psi\left(\frac{x-u}{s}\right) dx \quad \text{..... (1)}$$

$$DWT_f(m,n) = \int_{-\alpha}^{\alpha} f(x)\psi_{m,n}(x)dx \quad \text{............ (2)}$$

Here f(x) represents the well log data, $\psi_{m,n}(x)$represents the mother wavelet, while u and s represent the translation and scale parameters. The scale parameter varies inversely with frequency while the translation parameter shifts the mother wavelet and analyses various components of the signal. The well log data was analysed under various scales to study the variation of high and low frequency components of the dataset. The CWT and DWT coefficients are together called the scalogram variation, which denote the frequency localization at various scales and depths. It is commonly represented as a colour scale, signifying the variation in magnitudes of the wavelet coefficients. Low pass and high pass filters are generally necessary when evaluating the DWT and are represented by Equations 3, 4, 5 and 6 (Mallet, 1989).

$$\Phi_{j,k}(n) = 2^{j/2}\,\Phi(2^j n-k) \quad \text{..............(3)}$$

$$\psi_{j,k}(n) = 2^{j/2}\,\psi(2^j n-k) \quad \text{..............(4)}$$

$$W_\Phi[j,k] = \frac{1}{\sqrt{N}}\,\Sigma_n\, f[n]\,\Phi_{j,k}[n] \quad \text{..............(5)}$$

$$W_\psi[j,k] = \frac{1}{\sqrt{N}}\,\Sigma_n\, f[n]\,\psi_{j,k}[n] \quad \text{..............(6)}$$

Here $W_\Phi$ represents the detail coefficients given by the high pass filter, and $W_\psi$ approximation coefficients given by the low pass filter, which is the average signal. They are passed onto the next level and again resolved into detail and approximation coefficients, respectively. At each level the frequency is halved while the number of input samples remains the same.

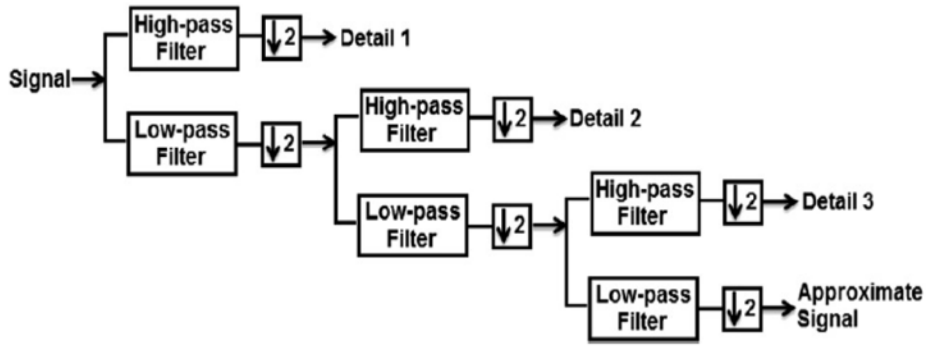


**Figure 1.** Block diagram for decomposition into three levels of a signal

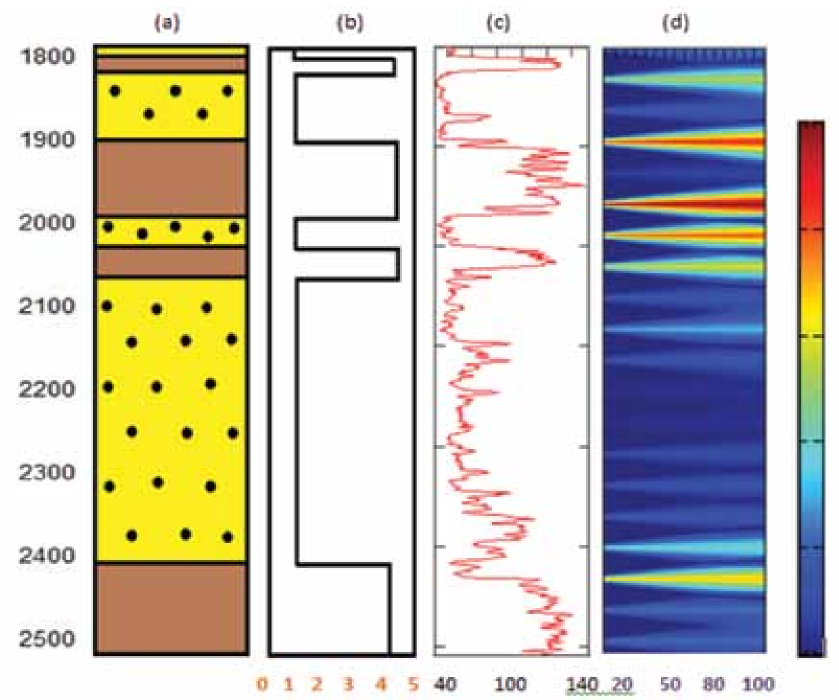


**Figure 2 . (a)**Facies log representation of the given well (1800-2500) m depth.**(b)** Mathematical representation of eFA,**(c)** Given gamma ray response and **(d)**eFA (20-100) m scales**.**

## Analysis of Well logs

The Ridderkerk Field is situated in the western Netherlands, in the province of South Holland.Structures in the upper Jurassic Delfland subgroup are generally rather strongly faulted and IntraDelfland shale seals are typically thin. While these shales are considered to be effective as top seals, most traps at this level also rely on favourable cross fault juxtaposition. The gamma ray log was first DWT analysed using the Haar Wavelet and decomposed 7 times. The discrete coefficients pertaining to the 7$^{th}$ level of decomposition were CWT analysed using the Haar Wavelet at various scales ranging from 20-100 m and the results of the analysis are presented in Figure 2. Other wavelets like Symlet, Morlet, Gaussian, and Coiflets, were also tried but the best results for obtaining stratigraphic formation interfaces was obtained using the Haar Wavelet (Alvaraz et al., 2003).

## RESULTS

The lithological characterization of the well is given by Figure 2(a). The lithological units maintain clear distinct electrofacies association with each other for the sand and the shale series. The mathematical representation of eFA is shown in Figure 2(b). The gamma ray log is represented in Figure 2(c). The low energy red pattern represented in Figure 2(d) represents shale layers, while the high energy blue patterns give sand units.

## DISCUSSION AND CONCLUSION

The Haar wavelet is capable of detecting the abrupt changes in the well log signal, with high energy depositional sequences represented by lower scales and at the same time low frequency components represented by high scales of the signal associated with facies changes. The variations in the depositionary sequences suggest the variations in depositionary energy. The smaller scales (<30) detect the presence of high energy sedimentary deposits, while the high scales (60-100) detect low energy deposits, like shale. The CWT analysis was performed with the d7 detail coefficients, as it corresponded with the largest number of facies association that was found in the region as was inferred from the facies log. Each decomposition corresponds to dyadic decimation, in terms of increase of powers of 2. The study demonstrates that wavelet transforms can effectively be used for bed boundary detection as a first approximation, as demonstrated through the comparison with the facies log presented.

This method can prove to be very effective as it can help us save valuable time and also resources during exploration by not having to take core samples from every well. It is sufficient to have core samples from one well and use them to verify the results.

### Compliance with Ethical Standards

The authors declare that they have no conflict of interest and adhere to copyright norms.

## REFERENCES

Alvarez, G., Sanso, B., Michelena, R.J., and Jimenez, J.R., 2003. Lithologic characterization of a reservoir using continuous wavelet transforms. IEEE Trans. Geosci. Remote Sens. v.49, pp: 59–65.

Mallat, S.G., 1989. A theory for multiresolution signal decomposition: the wavelet representation. IEEE Trans. Pattern Anal. Mach. Intell. v.11, no.7, pp: 674–693.

Perez-Muñoz, Teresa, Jorge Velasco-Hernandez, and Eliseo Hernandez-Martinez, 2013. "Wavelet transform analysis for lithological characteristics identification of siliciclastic oil fields." Journal of Applied Geophysics, v.98, pp: 298-308.

# NEWS AND VIEWS

## SCIENCE NEWS

***The Bermuda Triangle — a region in North Atlantic Ocean —** is notorious for ships and aircraft disappearing under mysterious circumstances without a trace, baffling researchers and general public alike. It is a subject of various conspiracy theories that attribute the phenomenon to paranormal activity and extraterrestrial beings.

A possible explanation has arisen since the discovery of giant underwater craters at the bottom of Barents Sea, off the coast of Norway. Researchers from the Arctic University of Norway have found craters up to half a mile wide and 150ft deep, believed to have been caused by build-ups of methane off the coast of natural gas-rich Norway, probably a cause of enormous blowouts of gas. The scientists explained that explosions causing the craters to open up could pose dangers to vessels travelling through the area, explaining the disappearance of ships and aircraft. Russian scientist Igor Yeltsov of the Trofimuk Institute, explained, "There is a version that the Bermuda Triangle is a consequence of gas hydrates reactions. They start to actively decompose with methane ice turning into gas. It happens in an avalanche-like way — like a nuclear reaction — producing huge amounts of gas. That makes the ocean heat up and ships sink in its waters mixed with a huge proportion of gas."

***Volcanic Ash Disperses After an Eruption**

Volcanic ash affects not only air transit but also public health and agriculture in nearby communities. How particles scatter after an eruption is incredibly complex and chaotic because of the different behaviour of particles of different size and the uncertain distribution of particles at the source. Some particles can linger in the air for just a few minutes, whereas others can remain airborne for years, travelling thousands of miles around the world. Researchers investigate how particles from a volcanic plume disperse and what factors govern the uncertainties associated with dispersal. Using a Lagrangian particle dispersal model, which computes the trajectories of a large numbers of volcanic particles on the basis of their physical properties, the researchers investigated how uncertainty in the initial size distribution of particles and their sphericity—a measure of how round an object is—affected how each particle scattered following a volcanic eruption. This model also accounted for realistic conditions such as wind. The scientists found that the uncertainty in the distribution of particles greatly reduces with distance from the source because of the effective segregation imposed by the atmospheric dispersal process. Moreover, rounder pieces of volcanic ash experienced less drag in the air, so they slipped out of the atmosphere sooner and didn't travel as far. Conversely, particles that weren't as spherical experienced more drag and remained in the atmosphere longer. As a consequence, sphericity mostly controls the grain size distribution at a given distance from the source. The authors also found much more variation in the size of particles that stayed aloft compared with those on the ground.

(*Journal of Geophysical Research: Solid Earth,* doi:10.1002/2015JB012536, 2016)

***Predicting Changing Human Preferences in Water Basin Management**

Humans are now more than ever active participants, rather than passive bystanders, in the natural hydrologic system. To assist with making long-term strategic decisions about water management within this new context, socio-hydrologists are developing models that incorporate social processes into their study of water use. Coupling these very different systems and their feedbacks, however, is challenging; despite recent studies that highlight the importance of the trends in our changing societal values, these variables have yet to be fully incorporated into human-water system models.

To address this gap, researchers developed a simple conceptual model that simulates the socio-hydrologic interactions in Florida's Kissimmee River Basin from 1948 to 2012. In response to extensive flooding there, the community decided in the 1960s to channelize downstream portions of the river. By the 1990s, however, a shift in priorities led to the ongoing restoration of both the river and the affected wetlands. The researchers hypothesized that these expensive modifications resulted from changing societal values as well as a disparity in power between the more numerous and wealthier upstream urban residents—who prioritized the restoration of wetlands—and the more rural downstream residents, who prioritized protection from floods. To simulate this complexity, the team included a "community sensitivity variable" in this system that quantifies the differences between the two portions of the basin, as well as the two-way environmental and societal feedbacks.

After calibrating the model to reflect the basin's historic trends, the researchers incorporated projected population data to predict changes in this basin from 2013 to 2032. Under a constant-precipitation scenario, the results show that over the next couple of decades the wetlands will continue to recover and the community sensitivity will return to neutral. This study demonstrates the potential of socio-hydrologic models to describe complex interactions using straightforward concepts and simple mathematical equations. These models have the potential to become important planning tools to minimize the unintended and expensive consequences of changing societal preferences.

(*Water ResourcesResearch*,doi:10.1002/2015WR018194, 2016)

## LIVING LEGENDS

**Shri T.S.Balakrishnan**

Shri Balakrishnan born on 5.10.1927 was educated in Bombay and Allahabad. He took his Master's Degree in Physics in 1947. Thereafter he worked as a Research Scholar in the Indian Institute of Science, Bangalore in Dr. C.V. Raman's laboratory. In 1953 he joined the Geological Survey of India and two years later he switched over to the then newly formed Oil and Natural Gas Commission, as one of its first scientific officers. For the next three years he carried out geophysical exploration in Cauvery, Jaisalmer and Punjab basins. In 1958 he went to the USA under the Technical Cooperation Mission plan to study multifarious methods used in oil exploration. After returning from USA in 1959 he continued exploration programmes in Punjab, U.P. and Bihar. Being a member of the first team of exploration geophysicists in ONGC, he initiated and supervised such programmes in several other sedimentary basins. The first successes were visible in Gujarat and Assam.

Shri Balakrishnan was a pioneer in ONGC's hydrocarbon exploration. The discoveries of oil and gas in Gujarat and Assam led ONGC to consider the prospects in the offshore areas. Here again, despite total inexperience in this field, Shri Balakrishnan was called upon to plan, organize and conduct ONGC's first offshore venture in the Gulf of Cambay. It took some time to study the material requirements and imported them from abroad. Simultaneously, there was a search for a suitable vessel to operate in that area. The high tidal range, swift currents, sand bars etc. posed an unusual challenge. Ultimately a shallow draft vessel was located in Bombay. This was rigged up with accommodation and equipment so as to make it suitable for seismic surveys, and christened M.V. Mahendra. Actual surveys commenced late in 1963, and within the next few months the first offshore structures of Alia Bet and North Tapti were mapped. Shri Balakrishnan also initiated ONGC's first offshore drilling project in the Gulf of Cambay in 1970-71. In the intervening period he worked as Superintending Geophysicist in charge of 10 seismic and 6 well logging crews. He was Project Manager of Cauvery Project from 1972 to 1973.

In the latter half of 1973 he was called upon to organize and carry out ONGC's first foreign seismic operations in Iraq. It was here that the technique of distributed surface charges was introduced to overcome the shot hole drilling problems. This was subsequently replaced by the vibroseis method. After an eventful stint in data acquisition, he took over as Head of Exploration in ONGC's Institute of Petroleum Exploration in Dehra Dun, where he worked for 8 long years from 1974 to 1982. During this period he initiated the task of consolidation and interpretation of geoscientific data on a regional scale over the Indian subcontinent. He realized the potential of non-seismic methods such as gravity and magnetic data for understanding regional tectonics and deep seated features. He worked towards the integration of offshore and onshore gravity, magnetic and seismic data. In 1982 he joined Bombay Offshore Project as Director of Geophysics and worked there until his retirement in 1986. He was responsible for the acquisition of ONGC's second seismic survey vessel. Even during his Bombay posting he continued working on data interpretation. Even after superannuation he continued to be active on consolidation and interpretation of data, particularly in upstream areas to produce a rational model for exploration. This was his personal hobby, and not at the instance of any organization. His initial Tectonic Map was published by the Geological Society of India in 1997. From 1977 to 1979 he continued his studies in collaboration with Dr.Mita Rajaram of the Indian Institute of Geomagnetism, Bombay. The result was the publication of the composite magnetic intensity map of the Indian subcontinent including the shelf areas.

Even today he is active and recently, the concept of isostasy has been brought into play and integrated into the analysis. This brings out the correlation between topography and other geophysical parameters. It is strikingly successful in delineating the deep structure of the Nepal Himalayas and S.Tibet. Overall the effort has been stupendous. Shri Balakrishnan is known for his uncompromising yardsticks for quality of scientific investigations, and is an upright geoscientist with a comprehensive insight into the tectonic framewonk of India. As an administrator and scientist his contributions are par excellence. The Association of Exploration Geophysicists presented the "Actively Engaged Geoscientist Award" during the Twenty Third Annual Convention, 1997, in Shillong. The Society of Petroleum Geophysicists at its Delhi Meeting in February 2000 awarded him the Gold Medal for Lifetime Achievement in Petroleum Geophysics.

**Prof. R. Vaidyanadhan**

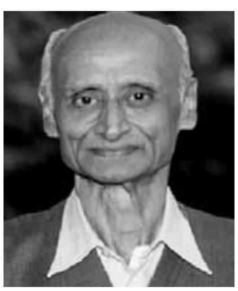

Rajagopala Vaidyanadhan, born on the 21st September, 1931 had his schooling in Vijayawada (A.P.) and obtained his M.Sc. and Ph.D. degrees in Geology from the Andhra University, Visakhapatnam. He taught Geology of India, Geomorphology and Remote Sensing for 20 years from 1953 to 1973 at the Geology Department and Photogrammetry, Geomorphology and Remote Sensing for 18 years at the Geography Department from 1973 to 1991, when he superannuated as Professor in the Department.

He had his training in Photogrammetry and Photo-interpretation at the Institute of Cartography, Geodesy and Photogrammetry, and Geomorphology at the Geology Department of the Ohio State University, Columbus, Ohio, USA on a Smith-Mundt- Fulbright Scholarship during 1959-1960, followed by training in Photogeology at the United States Geological Survey, Washington D.C.

He served as Professor in Geology at the Geology Department, University of Dar-es-Salam, Tanzania for a period of two academic years during 1981-1983. He conducted training Work Shops in Geomorphic Mapping for students selected from different parts of India and professional geologists, sponsored by the Department of Science and Technology and Geological Survey of India, respectively.

He has about 70 papers published in national and international journals, with his scholars being the lead authors in most of them. He had supervised 12 students for their Ph.D. degrees both from the Geology and Geography Departments of Andhra University and professional geologists from the Geological Survey of India and the Oil and Natural Gas Commission. Some of his notable publications are: edited volume on the "Quaternary Deltas of India" (Mem. Geological Society of India, 1991), a Monograph titled "Geomorphology of the Indian Subcontinent" published by the Indian Society of Remote Sensing, Dehra Dun(2002), a 2-volume book on the "Geology of India" with Dr. M. Ramakrishnan (of the Geological Survey of India) published by the Geological Society of India (2008) and revised in 2010, an ATLAS on "Landforms of India from Topomaps and Images" published by the Geological Society of India (2014) with Prof. K.V. Subbarao (formerly of IIT, Bombay and UOH, Hyderabad). Dr. B.P. Radhakrishna was his mentor during the latter part of his life and mainly responsible for the encouragement provided for all the publications that emanated from the Society. He was Editor of the Journal of the Geological Society of India during 1992-1995 and Vice president of the Society during 1998-2004 and again now for the period 2013-2016.

He has carried out projects sponsored by UGC, CSIR, ONGC, DST, ISRO, Ministry of Defence, Planning Commission etc. He was in the Evaluation Committees of UGC, CSIR, WIHG and ISRO.

He is the recipient of the Best Teacher Award (1983) from the Government of Andhra Pradesh, and the Golden Jubilee Honour for contribution to Earth Sciences from the Geological Society of India (2008).

**P.R.Reddy**

# GUIDE LINES TO AUTHORS

The Journal of Indian Geophysical Union (J-IGU), published bimonthly by the Indian Geophysical Union (IGU), is an interdisciplinary journal from India that publishes high-quality research in earth sciences with special emphasis on the topics pertaining to the Indian subcontinent and the surrounding Indian Ocean region. The journal covers several disciplines of earth sciences such as the Geosphere, its watery and gaseous envelopes (the Hydrosphere, the Cryosphere and the Atmosphere), and life (the Biosphere). It also publishes articles on Space and Planetary sciences. J-IGU welcomes contributions under the following categories:

- Research papers reporting new findings, results, etc.
- Review articles providing comprehensive overview of a significant research field related to earth sciences

In addition, J-IGU also welcomes short communications on opinion and report on scientific activity, personal information, book reviews, news and views, etc.

The manuscript should be submitted electronically as a single pdf file including the main text, figures, tables, and any other supplementary information along with the signed "Declaration Letter". The manuscript should be submitted by email ((jigu1963@gmail.com) to the Editor.

After acceptance of the manuscript the corresponding author would be required to submit all source files (text and Tables in word format) and figures in high resolution standard (*.jpg, *.tiff, *.bmp) format. These files may be submitted to the Editor as a single *.zip file along with the "Copyright Transfer Statement".

IMPORTANT INFORMATION

***Ethics in publishing***

J-IGU is committed to ensuring ethics in publication and takes a serious view of plagiarism including self-plagiarism in manuscripts submitted to the journal. Authors are advised to ensure ethical values by submitting only their original work and due acknowledgement to the work of others in case used the manuscript. Authors must also refrain from submitting the same manuscript to more than one journal concurrently or publish the same piece of research work in more than one journal which is unethical and unacceptable. Editor of J-IGU is committed to make every reasonable effort to investigate any allegations of plagiarism brought to his attention, as well as instances that come up during the peer review process and has full authority to retract any plagiarized publication from the journal and take appropriate action against such authors if it is proven that such a misconduct was intentional.

Similarly, Editor and Reviewers are also expected to follow ethical norms of publishing by ensuring that they don't use any unpublished information, communicated to them for editorial or review purpose, in their own research without the explicit written consent of the author. They are also expected to keep manuscript/ data/ observations/ any other information related to the peer review confidential to protect the interest of the authors. Reviewers should refrain from reviewing the manuscripts in which they have conflicts of interest resulting from competitive, collaborative, or other relationships or connections with any of the authors, companies, or institutions connected to the manuscript.

***Conflict of interest***

All authors are requested to disclose any actual or potential conflict of interest including any financial, personal or other relationships with other people or organizations within three years of beginning the submitted work that could inappropriately influence, or be perceived to influence, their work.

***Submission declaration***

Submission of a manuscript implies that the work has not been published previously and it is not under consideration for publication elsewhere, and that if accepted it will not be published elsewhere in the same or any other form, in English or in any other language, without the written consent of the publisher. It also implies that the authors have taken necessary approval from the competent authority of the institute/organization where the work was carried out.

***Copyright***

After acceptance of the manuscript the corresponding author would be required to sign and submit the "Copyright Transfer Statement".

**MANUSCRIPT PREPARATION**

The corresponding author should be identified (include E-mail address, Phone/Mobile number). Full affiliation and postal address must be given for all co-authors.

**Abstract:**

An abstract of not more than 300 words must be included.

**Text:**

The manuscript should be structured to include a front page containing the title, Author(s) name, affiliation and address of the institute where the work was carried out, a short title, and 5-to-6 index terms/Key words. Author(s) present address, if different from the above mentioned address, may be given in the footnote. The corresponding author should be identified with an asterisk and his/her email ID should be provided. This page should be followed by the main text consisting of Abstract, Introduction, Methods/ Techniques/ Area description, Results, Discussion, Conclusions, Acknowledgements, and References. Tables and Figures with captions should be inserted in the main text of the manuscript at appropriate places.

**Figures/ Illustrations:**

All figures should be provided in camera-ready form, suitable for reproduction (which may include reduction) without retouching. Figures in high-resolution (at least 300 dpi) standard formats (*.jpg, *.tiff, *.bmp) are acceptable. Figures should be numbered according to their sequence in the text. References should be made in the text to each figure. Each figure should have a suitable caption.

**Tables:**

Authors should take note of the limitations set by the size and layout of the journal. Table should not exceed the printed area of the page. They should be typed on separate sheets and details about the tables should be given in the text. Heading should be brief. Large tables should be avoided and may be provided as supplementary information, if required.

**Equations:**

Equations should be numbered sequentially with Arabic numerals and cited in the text. Subscripts and Superscripts should be set off clearly. Equation writing software that presents each equation as an object in MS Word will be accepted. Style and convention adopted for the equations should be uniform throughout the paper.

References:

All references to publications cited in the main text should be presented as a list of references following the text and all references in the list must be cited in the text. References should be arranged chronologically, in the text. The list of references should be arranged alphabetically at the end of the paper.

References should be given in the following form:

Kaila, K.L., Reddy, P.R., Mall, D.M., Venkateswarlu, N., Krishna, V.G., and Prasad, A.S.S.S.R.S., 1992. Crustal structure of the west Bengal Basin from deep seismic sounding investigations, Geophys. J. Int., v.111, no., pp: 45-66.

REVIEW PROCESS:

All manuscripts submitted to the journal are peer-reviewed. It is advisable to send the contact details of **4 potential reviewers** along with the manuscript to expedite the review process. Editor has the option to select reviewers from the list or choose different reviewers. The review process usually takes about 3 months. All enquiries regarding the manuscript may be addressed to the Editor.

GALLEY PROOF:

Technical editing of manuscripts is performed by the editorial board. The author is asked to check the galley proof for typographical errors and to answer queries from the editor. Authors are requested to return the corrected proof **within two days** of its receipt to ensure uninterrupted processing. The editor will not accept new material in proof unless permission from the editorial board has been obtained for the addition of a "note added in proof". Authors are liable for the cost of excessive alterations to galley proof.

PUBLICATION CHARGES:

There are no page charges for publication and printing charges for b/w figures. However, in view of substantial cost involved in printing of color figures, author will be charged for printing of pages containing color figures @ Rs. 2,500/- per page. The charges may be revised at any time based on cost of printing and production. Author will receive an estimate/ invoice of the color figures reproduction cost along with the galley proof. It is the responsibility of the author to remit the color figures reproduction cost **within one month** of the receipt of the estimate/invoice.

The corresponding author will receive a soft copy (pdf format) of his/her published article. Should the author desire to purchase reprints of his/ her publication, he/she must send the duly signed Reprint Order Form (accompanies the galley proof and contains price details) along with the corrected galley proof to the Editor. The reprint charges must be paid **within one month** of sending the Reprint Order Form.

Any payment related to printing of color figures and/or purchase of reprints should be made in the form of a Demand Draft in the name of **Treasurer, Indian Geophysical Union**, payable at **Hyderabad**.

You may download the pdf file here: Guide for Authors